Development and application of NMR-based metabolomics techniques

By

James J. Ellinger

A dissertation submitted in partial fullfillment of

the requirements for the degree of

Doctor of Philosophy

(Biochemistry)

at the

UNIVERSITY OF WISCONSIN-MADISON

2012

Date of final oral examination: 7/24/2012

The dissertation is approved by the following members of the Final Oral Committee:

John Markley, Professor, Biochemistry
Michael Sussman, Professor, Biochemistry
Patricia Kiley, Professor, Biomolecular Chemistry
Richard Amasino, Professor, Biochemistry
Richard Eisenstein, Professor, Nutritional Sciences

Table of Contents

Acknowledgments

First and foremost, I would like to thank Dr. John Markley for his guidance, open-mindedness and patience. I would also like to thank Dr. Ian Lewis for taking me under his wing and training me upon my arrival in the group. A large thanks goes to Dr. Milo Westler for his patience and willingness to explain NMR theory (for the upteenth time!) and for providing broad scientific feedback. I would like to thank all of my lab mates and NMRFAM staff, especially Dr. Roger Chylla, Dr. Marco Tonelli, Dr. Arash Bahrami, Dr. Mark Anderson and Dr. Kaifeng Hu. I also thank Dr. Jun Kikuchi for providing an excellent research opportunity and cultural experience during my time in Japan. A very large thanks to my family and all my friends, especially those I met in Madison. Finally I would like to thank my committee for their continual patience and input.

Funding for my research was provided by: The Great Lakes Bioenergy Research Center, The Sam C. Smith graduate fellowship, The National Magnetic Resonance Center at Madison, The National Science Foundation East Asia and Summer Pacific Institute and the Japan Society for the Promotion of Science.

Chapter 1

Introduction

Metabolite \mə-ˈta-bə-ˌlīt\ – a small-molecule that may be a starting component, intermediate or product of metabolism; may be contained within an organism or in the surrounding environment.

Metabolome \mə-ˈta-bə-ˌlōm\ – the complete set of metabolites that are found within a biologically derived sample.

Metabolomics \ mə-ˈta-ˌbə-ˈlō-miks\ – the systematic and comprehensive study of the metabolome.

1.1 Brief history and the role of metabolomics in society

Science fiction often portrays a future in which human health or identity can be monitored and diagnosed in real-time. We can readily infer that this is typically accomplished by taking a snapshot of an individual's molecular makeup, that is to say, all the chemicals that define the individual. This could include DNA, RNA, proteins or *metabolites*, although this snapshot could potentially include the molecular makeup of microbes present in said individual. For example, in the movie *Gattacca* a miniscule drop of blood or small urine sample can instantly and accurately identify an individual based on their unique molecular makeup. The same information is also used to predict an exceptionally accurate timeline of the individual's future health.

Although current technology does not allow such a rapid *and* global analysis of our molecular makeup, scientific progress within the last few decades has brought us within striking-distance of such science fiction. For instance, a recently developed technique

called nanostructure-initiator mass spectrometry (NIMS) has been used to perform spatial mapping of metabolites in dissected brain tissue (Patti et al., 2010). In other words, scientists are pioneering the ability to determine the localized molecular makeup of living tissue. Technology such as NIMS is beginning to truly blur the line that separates reality from science fiction.

Currently, several fields of study attempt to provide insight into the molecular makeup of an organism: genomics, transcriptomics, proteomics and metabolomics. Although metabolomics as a *defined* field of study is the youngest and appeared as recently as 1998 CE (Oliver, Winson, Kell, & Baganz, 1998), its origins can likely be traced to sometime between 1000-2000 BCE.

Hindu physicians practicing Āyurveda medicine recognized that the status of one's health could be determined by analyzing bodily fluids and developed early biological screening assays based on these principles: if flies swarm to a place where a person urinated, then the urine must be sweet, which we can infer indicated high glucose concentration and hence that the patient was diabetic. Similarly, ants swarming to the body indicated that the sweat was sweet, another indication of high glucose content. (Srikanthamurthy, 1983). Āyurvedic physicians may have also used ants to detect toxins in breast milk, which was fed to ants to see if they would die after consumption (Nichter, 1981).

A practitioner of traditional Chinese medicine, Wang Shou published his work *Collection of Diseases* in 752 CE in which he provided a simple method to diagnose

diabetes: have the patients urinate on a wide, flat brick. Then place it near an ant colony. If ants gathered at the spot of urination, then the patient was diabetic (Cohen, 2012).

The beginning of the modern era of quantitative metabolomics is often attributed to two-time Nobel laureate Linus Pauling. In 1971 CE Pauling et al. published on the use of gas chromatography for quantitative analysis of urine vapor and breath. Using this method, they were able to quantify 280 substances in urine vapor (Pauling, Robinson, Teranishi, & Cary, 1971). This was a major step forward analytically and Pauling noted:

> "Information about the genetic nature of an individual human being, as reflected in the rates of various chemical reactions that take place in his body, usually catalyzed by enzymes, could be obtained by the thorough quantitative analysis of body fluids. Moreover, the thorough quantitative analysis of body fluids might permit differential diagnosis of many diseases in a more effective way than is possible at the present time."

As result of Pauling's pioneering work, metabolomics is currently used in a variety of ways to study human health. For example, a recent study has illustrated a mechanism by which insulin resistance, and ultimately type-2 diabetes, can arise via dysregulation of certain metabolites, specifically branched-chain amino acid metabolism (C. B. Newgard et al., 2009). This information has provided the basis for a metabolomics method that could allow physicians to predict the risk of diabetes nearly a decade before onset (C. Newgard, 2012; T. J. Wang et al., 2011).

In other research, metabolomics has been used to identify a novel biomarker for some types of brain cancer and acute myeloid leukemia (AML) (Dang et al., 2009; P. S.

Ward et al., 2010). Patients with these types of cancer can harbor a mutant isoform of the enzyme isocitrate dehydrogenase (IDH), which results in significantly elevated levels of the metabolite 2-hydroxyglutarate (2HG). The 2HG levels are consistently 10 to 100-fold higher in samples that harbor IDH mutations than in those without mutations. Initial testing showed that screening for elevated levels of 2HG can provide a robust and rapid diagnostic method in the detection of cancer associated with IDH mutations (P. S. Ward et al., 2010).

Metabolomics has also proven to be an effective way to study metabolic signatures found during acute (~10 min treadmill or stationary bicycle) and prolonged (marathon running) exercise (G. D. Lewis et al., 2010). Exercise induced metabolic signatures showed positive correlations between fitness and glycerol, glutamine, pantothenate and niacinamide. All of these data have the potential for development of novel biomarker screening assays relevant to cardiovascular health from a minimally invasive approach.

Studying metabolic interactions within microbial communities is another area with great potential for metabolomics. For example, Nakanishi et al. recently observed a commensal relationship between *Bifidobacterium longum* and *Escherichia coli* O157:H7 (O157) using a real-time metabolomics approach (Nakanishi et al., 2010). Specifically they observed that aspartate and serine produced by *B. longum* was consumed by *E. coli* O157:H7. In a similar study, the same group highlighted a symbiotic relationship between host and microbe. Pre-inoculation of mice with *B. longum* prior to infection with *E. coli* O157:H7prevented their death from Shiga toxin produced by *E. coli* O157:H7

(Fukuda et al., 2011). Through a combination of metabolomics and transcriptomics Fukuda et al. showed that BL produces high levels of acetate, which in turn activates anti-inflammatory and anti-apoptotic genes in epithelial cells thereby preventing the negative effects of Shiga toxin.

A metabolomics approach was also used to study metabolic cooperation between *Bacillus megaterium* and *Ketogulonicigenium vulgare* (Zhou et al., 2011). These organisms have been co-cultured to synthesize 2-keto-gulonic acid (2KGA), which is a precursor to vitamin C. However, the mechanism of their interaction was poorly understood. Co-culturing on agar plates showed that amino acids secreted by *K. vulgare* were capable of functioning as chemoattractants for *B. megatarium* and induced swarming toward *K. vulgare*. Furthermore, *B. megatarium* was shown to secrete erythrose, erythritol, guanine and inositol, which were consumed by *K. vulgare*. Consumption of these metabolites correlated to an increase in the concentration of 2KGA produced by *K. vulgare*.

Another promising area in which metabolomics can be applied is metabolic engineering. A recent study probed the effects of acetate and formate on xylose metabolism and ethanol production in an engineered strain of *Saccharomyces cerivisiae* (Hasunuma et al., 2011). In the presence of relatively high levels of acetate, *S. cerevisiae* struggled to consume xylose and showed decreased ethanol production, which is of interest because hydrolysates used for fermentation to biofuels often contain relatively high levels of acetate. A metabolomics analysis showed a positive correlation

between the accumulation of non-oxidative pentose phosphate pathway (PPP) metabolites and increased acetate concentrations in the growth medium. Overexpression of a PPP-related transaldolase or transketolase was able to reduce the levels of accumulated PPP metabolites during acetate stress, restored some ability for xylose consumption and increased ethanol production. This kind of approach demonstrates the use of metabolomics to develop rational strategies to confer stress tolerance through genetic engineering.

In another application of metabolomics to metabolic engineering, Chong et al. found that Chinese hamster ovary (CHO) cells overexpressing recombinant monoclonal antibody (IgG) grown in a standard culture medium effluxed significant quantities of malate (Chong et al., 2010). Using a pulse-chase experiment, they showed that excess malate was produced from aspartate incorporated from growth medium. Eventually, cells released accumulated malate into the external environment, which potentially negatively affected cell viability. To counter the accumulation of malate, CHO cells were transfected with a vector containing malate dehydrogenase II (MDH II). The result was a dramatic reduction in malate efflux accompanied by increased cell viability and higher IgG titer.

Metabolomics has come a long way since its simple origins in the early days of Āyurveda medicine. And as one can see, metabolomics is a tool that can guide research in a broad spectrum of disciplines. In fact, in the last decade the number of metabolomics publications per year has skyrocketed from approximately 200 to nearly

900 (Ellis & Goodacre, 2012). Given this trend, we can likely expect metabolomics to be a driving force that bridges the gap between science fiction and reality.

1.2 The right tools for the job

The ideal tool for metabolomics is one that can detect all metabolites at any concentration, meanwhile analyzing hundreds of samples per day. Although such an Eye of Providence does not exist, nuclear magnetic resonance (NMR) spectroscopy and mass spectrometry (MS) have become the mainstay tools for metabolomics. Both tools are strongly rooted in analytical and organic chemistry for their ability to allow the user to determine chemical structure or discriminate between chemicals in a mixture. For example, organic chemists routinely need to distinguish between the main product of an organic synthesis and unwanted side-products.

While both methods are highly regarded for their ability to discriminate across a breadth of metabolite classes as well as their quantitative reliability (Fiehn, 2002; Pan & Raftery, 2007; Patti, Yanes, & Siuzdak, 2012), the major advantage of MS is its superior sensitivity. For example, zmol (10^{-21} mole or <1000 molecules) quantities of metabolites have been measured by MS (Salehpour, Possnert, & Bryhni, 2008). Although in practice, limits of detection seem to fall more in the pmol to fmol range (10^{-12}-10^{-15} mole) (Bennett et al., 2009; Lu et al., 2010). This is in contrast to NMR, in which we have found practical limits of detection to be in the in the low μmol to high nmol (10^{-6}-10^{-9} mole) range for routine metabolomics experiments.

Recent advances in NMR probe design allow for experiments to be conducted on samples of 10-20 μl, which stands contrast to typical volumes of 500-600 μl (Brey et al., 2006; Grimes & O'Connell, 2011; Olson et al., 2004). These so-called microcoil probes show mass sensitivity increases up to 10-fold. This design shows a lot of promise for sample limited conditions, such as when working with murine serum where one can procure only 25 μl of serum. Furthermore, larger samples can be concentrated into a smaller volume in order to improve signal detection.

Despite the advantage of sensitivity, MS does hold some disadvantages. For example, it is usually necessary to fractionate samples by gas chromatography (GC) or liquid chromatography (LC) prior to analysis by MS. In contrast, NMR does not require sample fractionation due to the ability to excite and observe all NMR active nuclei at once.

Other advantages of NMR are that it is non-destructive, and sample preparation does not require chemical alteration of precious samples. For example, metabolomics analysis by GC-MS often requires chemical derivatization in order to produce a volatile compound for GC. This could lead to quantitative errors if derivatization is incomplete. Furthermore, once a sample is derivatized it is most likely unsuitable for other types of experiments. While LC-MS does not require chemical derivatization, accurate quantitation could be compromised by incomplete chromatographic elution or ion suppression.

Another advantage of NMR is that it can provide direct discrimination between different types of stereochemistry. For example, glucose and mannose have the exact same mass and are essentially the same molecule except for the three-dimensional arrangement of H and OH at C2. Unless they can be fractionated by chromatography, MS will lack the necessary discriminatory power to distinguish between these two molecules. Potentially even more complicated is the case of α- and β-glucose. In both of these examples, NMR can easily discriminate between the diastereoisomers.

A final word on these two powerful tools and their utility in metabolomics. At the end of the day, they should not be regarded as competing tools, but as complementary methods in metabolomics. With the constant discovery of new metabolites, both tools will be required to make progress, and recent developments in synergizing MS and NMR portend a bright future for metabolomics (Godejohann, 2007; Tang, Xiao, & Wang, 2009).

1.3 NMR, a Swiss Army knife for metabolomics

Nuclear magnetic resonance was first described in 1938 by Isidor Rabi (Rabi, Zacharias, Millman, & Kusch, 1938) and its use in liquid and solids was developed independently in 1946 by Felix Bloch and Edward Purcell (Bloch, Hansen, & Packard, 1946; Purcell, Torrey, & Pound, 1946). The first use of NMR for what can be construed as metabolomics appears to be that of Hoult et. al when they developed an assay for ^{31}P NMR to study metabolites in biological tissue (Hoult et al., 1974). Jeremy Nicholson pioneered the use of NMR for modern, systems-level metabolomics throughout the late 1990's.

I have not delved into the theory behind NMR here, because this information has been covered exhaustively by numerous texts and reviews. Instead I have chosen to focus on presenting recent and relevant techniques used for NMR-based metabolomics data collection.

The most common method for NMR-based metabolomics data collection is one-dimensional proton (1D ^{1}H) NMR. This method has several advantages: 1) the ^{1}H nucleus is very sensitive to magnetic induction, 2) the natural abundance of the ^{1}H nucleus is 99%, 3) ^{1}H nuclei are ubiquitous in metabolites and 4) data collection is relatively rapid.

Unfortunately, the dispersion of chemical shift values in 1D ^{1}H is limited to a narrow range. A survey of metabolites with spectral data stored in the Biological Magnetic Resonance Data Bank (BMRB) showed 4561 assigned ^{1}H chemical shifts

corresponding to 906 metabolites. The chemical shifts range from 0 to 11.5 ppm, with 71% between 0 to 5 ppm (http://www.bmrb.wisc.edu/metabolomics/ accessed June 2012). As a result, 1D ^{1}H spectra suffer from severe signal overlap as samples become more complex. This in turn negatively affects one's ability to accurately identify and quantify metabolites.

One practical approach to overcome this barrier is to collect NMR spectra that disperse signals into multiple dimensions. For example, a ^{1}H-^{13}C heteronuclear single quantum coherence (HSQC) experiment correlates chemical shifts of proton nuclei covalently bound to ^{13}C (Figure 1.1). First, this method is actually more sensitive than attempting to directly detect ^{13}C due to the natural abundance and relative high concentration of ^{1}H nuclei. Second, this allows one to take advantage of the ^{13}C nucleus' much wider chemical shift range. For example, the ^{13}C data stored in the BMRB for the 906 metabolites mentioned above spans a chemical shift range from 0 to 223 ppm, with 55% between 0 and 100 ppm.

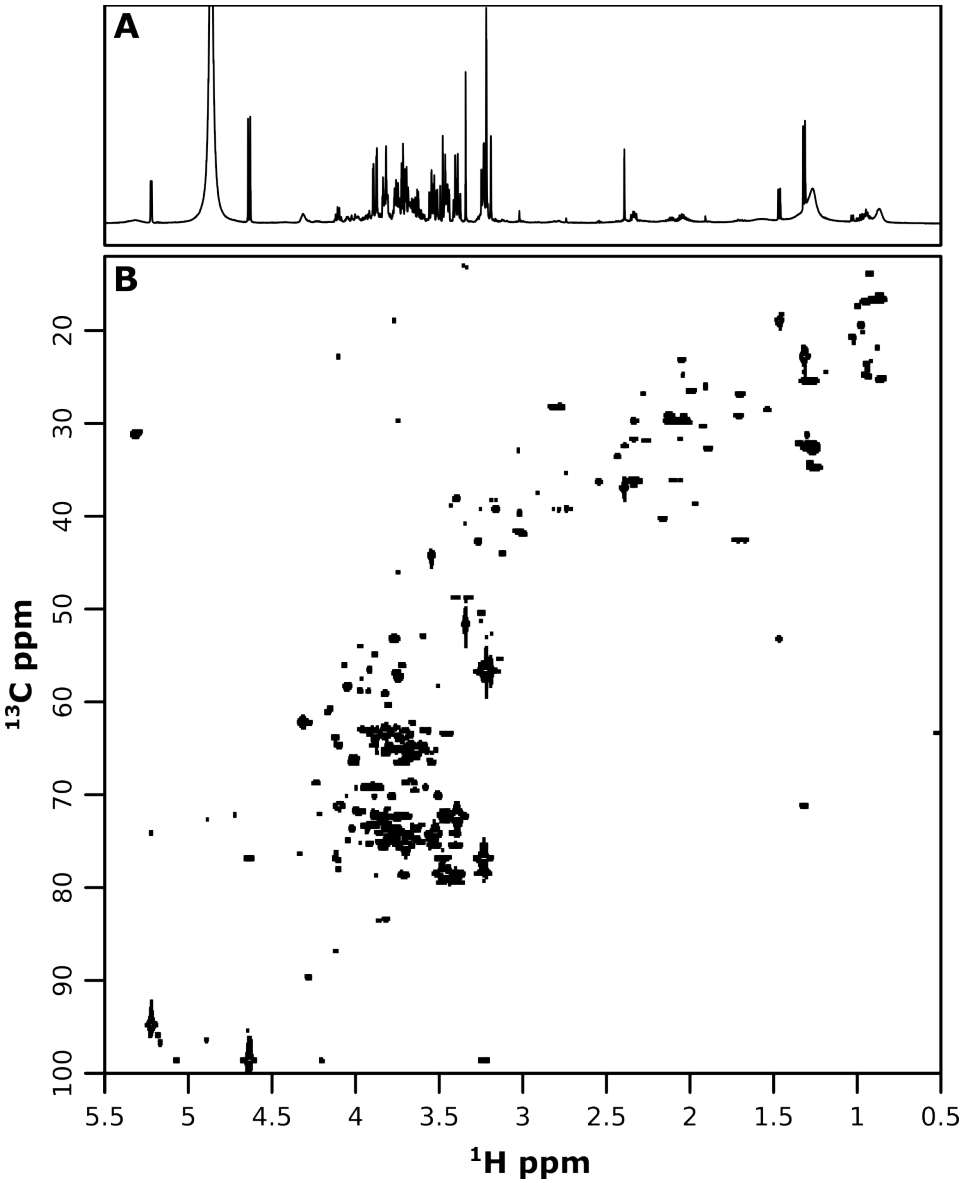

Figure 1.1. Comparison of (A) the 1D ^{1}H spectrum and (B) the ^{1}H-^{13}C HSQC spectrum of a bovine liver extract. Note the greater dispersion along the ^{13}C dimension.

A general and practical method for relatively quick data collection by ^{1}H-^{13}C HSQC was developed in our laboratory by Ian Lewis. This method, dubbed Fast Metabolite Quantification by Nuclear Magnetic Resonance (FMQ by NMR) (I. A. Lewis et al., 2007), is the main method that I used in my studies, and its application is shown in greater detail in Chapters 2-4.

Using this method on an instrument equipped with a cryogenic probe, it is possible to observe 40 metabolites in a sample using only 12 min of data acquisition. However, in order to be observed and accurately quantified, a metabolite generally needs to be present in the NMR tube at concentrations greater than 0.5 mM. It should be noted that the true limits of detection and amount of time for data collection are dictated by the number of protons found in a given H–C functional group (for a given metabolite) as well as the sample matrix. Quantification is achieved by relating peak intensities in samples to peak intensities in standard mixtures. Furthermore, it was shown by Lewis at al. and others (Gronwald et al., 2008; I. A. Lewis et al., 2007) that the multidimensional approach provides better quantitative accuracy over a wider range of metabolite concentrations than 1D ^{1}H experiments.

There are some drawbacks to this method however. First, all metabolites of interest must be pre-identified before a mixture of standard compounds can be generated. Another drawback of FMQ by NMR is that metabolites for which a known standard does not exist cannot be accurately quantified. This is also the case when metabolites have been isotopically enriched and equivalently enriched standard cannot be purchased.

Due to experimental factors such as relaxation times, mixing time, evolution time and uneven excitation profiles that occur during the HSQC experiment, traditional peak integration relative to an internal standard is unreliable for accurate quantification.

One recently developed method overcomes this limitation by applying a correction factor to measured peaks (Rai, Tripathi, & Sinha, 2009). Experimentally determined T_1^H, T_2^H, delay times and J_{CH} values were used to correct for errors introduced during the HSQC pulse sequence. After correction, metabolites are quantified by comparing the peak volume to an internal standard of known concentration. This method has been successfully applied to analysis of human urine samples.

The drawback for this method is the time required to determine the parameters for the correction factor. The authors demonstrate that within a given set of urine samples only slight deviation in the parameters for the correction was observed. Therefore it is feasible that in a particular experiment the correction parameters only need to be determined at the onset. However, if switching to a different instrument or the sample matrix changes significantly (i.e. time-course data), then parameter calibration will probably need to be repeated.

A method developed by Kaifeng Hu in our laboratory called extrapolated time-zero HSQC ($HQSC_0$) is another alternative (Hu, Westler, & Markley, 2011), which does not require determining correction parameters. By measuring the peak volumes of successive HSQC experiments, it was possible to extrapolate back to a signal that was devoid of errors generated by the HSQC pulse sequence. This method was successfully

applied to metabolomics analysis of murine liver (Hu, Ellinger, Chylla, & Markley, 2011). The major drawback is that these experiments can require significantly longer data acquisition than FMQ by NMR. Therefore, this method is not well suited for high-throughput metabolomics.

One disadvantage of using ^{1}H-^{13}C HSQC for samples that are not enriched with ^{13}C is reduced sensitivity compared to 1D ^{1}H experiments. An alternative is to use ^{1}H-^{1}H total correlation spectroscopy (TOCSY) experiments. This experiment correlates the chemical shifts of all the protons in a given molecule. The result is a spectrum that is dispersed into two proton dimensions. The sensitivity of the experiment is essentially equivalent to that of a standard 1D ^{1}H experiment, and it has been successfully applied to study metabolites in insect venom (Zhang, Dossey, Zachariah, Edison, & Bruschweiler, 2007), colorectal cancer cells (C. Ludwig et al., 2009) and *Caenorhabditis elegans* (S. L. Robinette et al., 2011). However, ^{1}H-^{1}H TOCSY spectra can still display significant signal overlap, and from these studies it is apparent that simpler complex mixtures are better suited for ^{1}H-^{1}H TOCSY.

One specific application where the ^{1}H-^{1}H TOCSY experiment is useful is isotope-tracing studies in metabolomics. For a given functional group, protons coupled to ^{13}C nuclei split into distinct peaks from protons coupled to ^{12}C nuclei (Figure 1.2). The integral of the ^{13}C coupled peaks relative to the total signal indicates the percentage of ^{13}C present in that functional group.

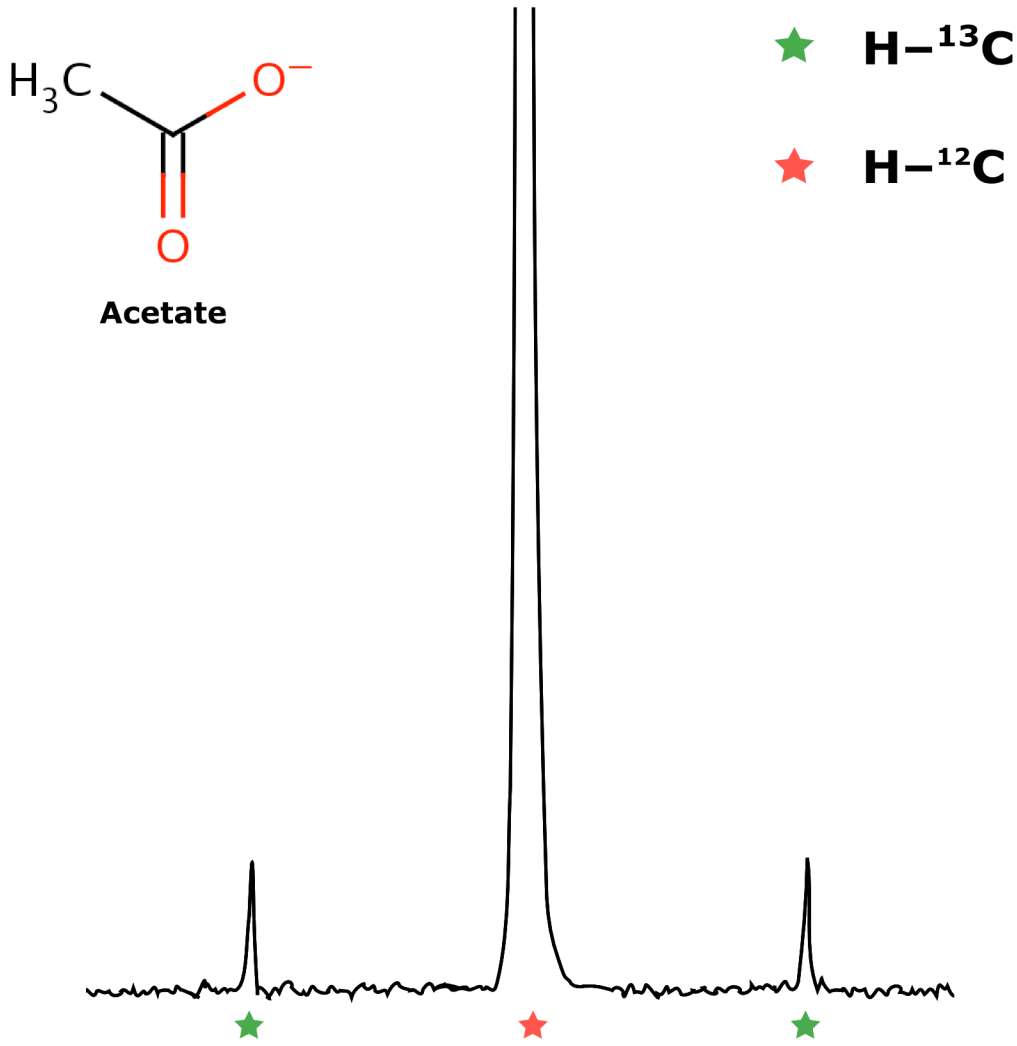

Figure 1.2. Example of ^{13}C-^{1}H coupling from the methyl group of the acetate anion at natural abundance ^{13}C (1.1%) from a 1D ^{1}H spectrum. The central peak (red star) represents all protons coupled to a ^{12}C and the flanking peaks (green start) represent protons coupled to a ^{13}C. The integral of flanking peaks relative to the total integral for the methyl signal indicates the abundance of ^{13}C.

Measurement of ^{13}C enrichment in metabolites using ^{1}H-^{1}H TOCSY has been shown to be quantitatively equivalent to measurements traditionally obtained by 1D ^{1}H NMR experiments (Massou, Nicolas, Letisse, & Portais, 2007a; Massou, Nicolas, Letisse, & Portais, 2007b). The ^{1}H-^{1}H TOCSY experiment has the advantage of some added dispersion from the second ^{1}H dimension. A recent method developed by Ian Lewis in our laboratory, called isotope-edited TOCSY (ITOCSY), filters two-dimensional ^{1}H-^{1}H TOCSY spectra from ^{12}C- and ^{13}C-containing molecules into separate, quantitatively equivalent spectra (I. A. Lewis et al., 2010). All of these methods have been successfully employed to characterize metabolites in *E. coli*.

Not all methods for reducing spectral complexity require multiple dimensions. Often times one metabolite may dominate the spectrum. For example, serum is a common biofluid studied using metabolomics, but its NMR spectrum is dominated by glucose, which is present at levels nearly an order of magnitude higher than other metabolites. This leads to two problems, 1) identifying other metabolites becomes problematic due to spectral overlap, especially in the 3.2 to 4.0 ppm range where the majority of the glucose signals reside and 2) non-targeted metabolomics generally uses multivariate statistical analysis, which can miss important changes in low concentration metabolites when one signal such as glucose dominates the spectrum.

Ye et al. recently investigated methods for background subtraction in 1D ^{1}H spectra (Ye et al., 2011). In conventional background subtraction, a signal is removed from a sample by subtracting the same signal generated by a pure standard. While common in

ultraviolet or infrared spectroscopy, the sample matrix can have significant effects on signals in an NMR spectrum. Consequently, signals align poorly (or not at all!), which produces significant artifacts after subtraction. Instead, Ye et al. collected 1D ^{1}H spectra of serum or urine samples and then spiked the same sample with a small volume of highly concentrated glucose standard to use for background subtraction. The key is that the spectrum used for background subtraction contains identical chemical shifts and lineshapes as the original spectrum. When compared to subtraction using a pure standard or computer modeled glucose signals, their "Add to Subtract" method was capable of reducing glucose signals by 98% while producing virtually no artifacts.

Finally, recent developments in chemoselective isotope tagging have proven to be an effect method for simplifying spectra while increasing sensitivity of low abundance compounds. Methods have been developed for ^{13}C acetylation (Shanaiah et al., 2007) or formylation (Ye et al., 2010) of amine-, ^{31}P phosphorylation of lipid- (DeSilva et al., 2009) and ^{15}N amidation (Ye et al., 2009) of carboxyl-containing metabolites. In particular, isotope tagging of amino acids shows a lot of promise as the sensitivity enhancement was shown to be nearly an order of magnitude and this technique has been applied to investigate amino acid profiles from individuals with phenylketonuria, tyrosinemia, homocystinuria, or arginosuccinic aciduria (Shanaiah et al., 2007).

Although NMR often is chosen for metabolomics because one can avoid chemical derivatization, these methods appear to be highly reproducible with high yields of derivatization (85-100%) (Shanaiah et al., 2007). Furthermore, the costs of reagents

and labor are minimal and, given the appropriate instrumentation, derivatization could be conducted in an automated, high-throughput fashion.

In summary, a myriad of approaches for NMR-based metabolomics are currently available. These methods allow one to overcome spectral complexity as well as sensitivity issues all while maintaining the ability to characterize metabolites across multiple classes of compounds. Taken together, this truly allows NMR to be a Swiss Army knife for metabolomics.

1.4 Primer for metabolomics sample preparation

Although NMR is amenable to *in situ* studies, for most metabolomics studies the initial steps are to isolate molecules from cells or tissues and separate small molecule metabolites from macromolecules. This serves a number of purposes: 1) improved spectral quality by removing cell membrane and macromolecular components, 2) control of sample pH, 3) concentration of low abundance metabolites, and 4) exchanging the solvent with a deuterated counterpart if necessary.

Metabolite isolation can most simply be arranged into three phases: 1) homogenization, 2) extraction and 3) filtration (Figure 1.3). Homogenization serves to increase the available surface area of biomass that can be exposed to solvent during the extraction phase. Common laboratory methods that can be employed to homogenize samples include mortar and pestle, blender, or ball milling, all of which result in pulverization of biomass into a fine powder (Weckworth, 2006; Charlton et al., 2004; Lin, Wu, Tjeerdema, & Viant, 2007; Sobolev, Brosio, Gianferri, & Segre, 2005).

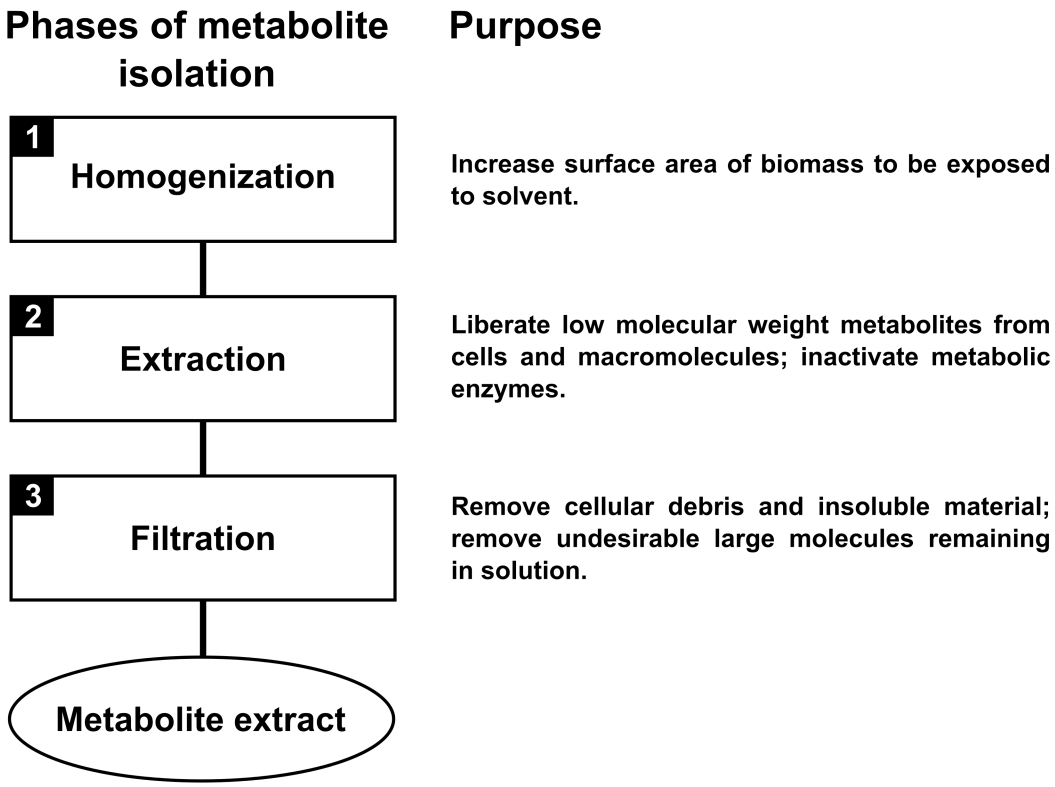

Figure 1.3. Schematic representation of the process of metabolite isolation.

The next step is to separate low molecular weight molecules from cells and macromolecules. It is also imperative that enzymes, specifically those involved in metabolism, are inactivated. The extraction phase is accomplished using a wide variety of methods, but mainly relies on solvents of varying polarity to lyse cells and separate metabolites from macromolecules (Belle, Harris, Williams, & Bhakoo, 2002; Gromova & Roby, 2010; Lin et al., 2007; Rabinowitz & Kimball, 2007; Sekiyama, Chikayama, & Kikuchi, 2011). The method chosen for the extraction phase will depend primarily on the species of metabolites that one intends to study.

The final step, filtration, is intended to remove cellular debris and other insoluble material from the extracted metabolite solution. Furthermore, the filtration phase can also be used to remove undesirable macromolecules remaining in solution. The simplest method involves high speed centrifugation, but the use of molecular weight cutoff filters affords more stringent separations (Chae et al., 2010; Hallows et al., 2011; I. A. Lewis et al., 2010).

Chapter 2 focuses on a novel device we developed to integrate the aforementioned steps into one process. The whole process shown in Figure 1.3 is streamlined and multiple samples can be prepared in parallel. This greatly reduces the labor and time required to isolate metabolites from cells or tissue.

In general, biofluids are easier to prepare than tissues or cells. The extraction step is often skipped because metabolites are already present in a relatively ‘clean’ aqueous solution. In Chapter 4 I highlight a protocol for preparing spent cell media for NMR

analysis. In this straightforward method, the only requirements for sample preparation are the addition of D_2O (to maintain a lock signal) and adjustment of the pH.

However, the specific demands of the analysis and sample will dictate whether an extraction step is necessary. For example, lipids and proteins present in serum samples generate broad peaks that overlap with smaller, more polar metabolites, which can lead to quantitation errors. Lipids are easily separated by the use of strong non-polar solvents.

While proteins can be removed through extraction, it was recently shown that filtering samples through a 3 kDa molecular weight cutoff filter provides the most reliable and reproducible method for preparing serum samples (Tiziani et al., 2008). It was also shown that lipids can be extracted from the serum component that does not pass through the filter. The major disadvantage to filtering is the relatively long amount of time required to completely filter a sample.

Once a metabolite extract is produced, the major remaining concern is to control the pH of the sample. Some metabolites such as histidine or citrate are very sensitive to pH whereas others such as glucose are not. However, the databases listed below in Table 1.1 contain NMR spectra collected under standardized pH conditions, and for this reason it is essential that biological extracts are as similar as possible. The most common approach is to add pH 7.4 phosphate buffer to samples. Phosphate buffer has the advantage of not adding a signal to the NMR spectrum. However, too much phosphate buffer has been shown to degrade spectral quality (Asiago et al., 2008).

Other buffers we have explored are MES and HEPES (which has the advantage of serving as an internal pH indicator) prepared to pH 7.4. These buffers produce signals that overlap with metabolites, but perdeuterated versions that are available from Cambridge Isotope Laboratories do not. It should be noted that we find adding buffer does not always produce the desired pH in our samples, and we often must adjust the pH of samples by reference to a pH meter.

One of the most important principles of metabolomics is the ability to accurately and reproducibly quantify data to produce meaningful results. Therefore, while it is important to choose a robust method to extract metabolites, ultimately one needs to strive for consistency with sample preparation.

1.5 Databases and software for NMR metabolomics

Traditional methods for identifying even one compound in solution by NMR are time intensive, and from my experience, a typical metabolomics sample will have a minimum of 15-20 metabolites observable by NMR. Furthermore, even a small dataset will have more than 10 samples in order to account for controls and biological replication. This becomes a major bottleneck when one considers potential applications of metabolomics that produce hundreds of samples a day, such as clinical research.

Two approaches are used for analyzing metabolomics data: chemometric and quantitative approaches. Using chemometrics, only spectral pattern and intensities are analyzed, which are then compared statistically for only relevant features that differ and distinguish sample classes. After statistical anlaysis, metabolites are then identified.

This has the advantage of reducing the amount of work required because only the important metabolites are identified. Using the quantitative approach, all detectable metabolites are formally identified and quantified prior to subsequent analysis. Although the quantitative approach yields better results (Weljie, Newton, Mercier, Carlson, & Slupsky, 2006), the chemometric approach is still the most commonly employed mode of analysis. This is likely due to ease of use and speed.

Regardless of which method is used, metabolites must still be identified. To accomplish this in a time-efficient manner, we and others have chosen to take a bioinformatics-like approach. The chemical shifts observed in NMR are stable under standardized conditions. As a result standardized data can be stored in freely accessible databases such as those listed in Table 1.1 or purchased with commercial software (discussed below). The basic approach is to collect data that matches the standardized conditions and compare the chemical shifts to those found in a database. More advanced search algorithms can also try to take advantage of metabolite specific information such as *J*-coupling or peak multiplicity and relative intensity.

Table 1.1. Major databases housing spectral data useful for NMR-based metabolomics. Each database allows metabolite searching by name as well as by chemical shift.

Database	Reference
Madison-Qindao Metabolomics Consortium Database (MQMCD)	Cui et al., 2008
Human Metabolome Database (HMDB)	Wishart et al., 2007
Platform for RIKEN Metabolomics (PRIMe)	Akiyama et al., 2008
Biological Magnetic Resonance Bank (BMRB)	Markley et al., 2007
Magnetic Resonance Metabolomics Database (MRMD)	Lundberg et al., 2005
NMRShiftDB	Steinbeck, Krause, & Kuhn, 2003

Several commercial software packages are available for analysis and manipulation of NMR-based metabolomics data. Chenomx NMR Suite (Chenomx Inc.) is by and large the most widely used software for NMR-based metabolomics data analysis, although other commercial options include dataChord Spectrum Miner (One Moon Scientific, Inc.), KnowItAll Metabolomics Edition (Bio-Rad Laboratoires, Inc.) and the AMIX tool-kit for TopSpin (Bruker BioSpin). Each package is capable of spectral processing (only Chenomx and AMIX handle 2D data), automated chemometric analysis and metabolite quantification. Furthermore, Chenomx and KnowItAll also allow automated peak assignment through their provided standard spectral libraries and proprietary databases. Chenomx further distinguishes itself through a myriad of features such as a model compound simulator and a spectral library spanning metabolite data collected at multiple NMR field strengths and multiple pH values.

The main advantage of commercial software is feature richness. Because they have been extensively developed and are backed by teams of full time software developers, a large effort is poured into meeting customer satisfaction and usability. On the other hand, commercial software can be very expensive. For example, a single one year license for dataChord Spectrum Miner is $900 (USD) and the price for Chenomx NMR Suite is by inquiry only, implying a hefty cost.

A wide range of free software is also available and is summarized in Tables 1.2 and 1.3. All of the software listed in Table 1.2 functions as standalone packages that allow

the user to directly interact with and manipulate NMR spectra. In contrast, the software listed in Table 1.3 is web-server based and provides graphical or text output.

One of the major disadvantages of free software is that updates may not routinely occur. For example, MetaboMiner (Table 1.2) has not received an update since June 2008. As a result, software may not always be up to date with current analytical methods.

Automated peak picking and matching (finding related peaks across multiple spectra) are the major hurdles that all software has yet to overcome. Many of the software packages listed in Tables 1.2 and 1.3 attempt to address these problem, but ultimately fall short. Automated peak picking algorithms continue to struggle to distinguish noise from real signals as well as poorly resolved peaks in regions containing spectral overlap. Although it should be noted that the user can improve automated peak picking results by ensuring that spectra have high signal-to-noise, good phasing, minimal baseline distortion and elimination of spectral artifacts. Peak matching continues to struggle with overcoming chemical shift drift in biological samples. Once these obstacles are reliably cleared, we will likely be able to usher in an era of real-time data analysis, which will greatly improve the high-throughput nature of metabolomics.

Table 1.2. Freely available standalone software for NMR-based metabolomics data analysis. For software that performs automated metabolite identification, data are from HMDB, BMRB or PRIMe.

Name	Data input	Features
rNMR (I. A. Lewis, Schommer, & Markley, 2009)	1D and 2D processed spectra for any NMR active nuclei	• Batch analysis by region of interest • Customizable analysis functions • Use R's chemometric functions
Newton (Chylla, Hu, Ellinger, & Markley, 2011)	1D and 2D processed spectra for any NMR active nuclei	• Peak reconstruction to handle spectral overlaps • Robust signal recognition handles chemical shift drift • Batch quantification
MetaboMiner (J. Xia, Bjorndahl, Tang, & Wishart, 2008)	Peaks lists; ^{1}H-^{1}H TOCSY and ^{1}H-^{13}C HSQC processed spectra stored as high resolution PNG files	• Semi-automated metabolite identification from 2D spectra • Improved compound identification by searching bio-fluid specific libraries

MetaboAnalyst 2.0 (J. Xia, Mandal, Sinelnikov, Broadhurst, & Wishart, 2012)	Peak lists with peak intensities (1D or 2D for ^{1}H and ^{13}C) ; Concentration tables	• Produces graphical output for common chemometric anlyses • Pathway identification tools
Automics (T. Wang et al., 2009)	1D ^{1}H raw spectra	• Automated spectral processing and chemometric analysis
The CCPN Metabolomics Project (Chignola et al., 2011)	Processed 1D and 2D spectra	• Spectrum visualization for compound annotation • Contains built-in metabolite library
MetaboLab (C. Ludwig & Günther, 2011)	1D and 2D raw spectra	• Automated spectral processing • Semi-automated assignment of 2D spectra

Table 1.3. Freely available web-based software for NMR-based metabolomics data analysis. For software that performs automated metabolite identification, data is from HMDB, BMRB or PRIMe.

Name	Data input	Features
MetaboAnalyst (J. Xia, Psychogios, Young, & Wishart, 2009)	Peak lists with peak intensities (1D or 2D for ^{1}H and ^{13}C) ; Concentration tables	• Produces graphical output for common chemometric analyses • Pathway identification tools
PRIMe: SpinAssign (Akiyama et al., 2008; Chikayama et al., 2010)	Peak lists (1D or 2D for ^{1}H and ^{13}C)	• Automated peak assignment and annotation.
COLMAR Metabolomics Web Portal (S. L. Robinette, Zhang, Bruschweiler-Li, & Bruschweiler, 2008)	^{1}H-^{1}H TOCSY raw spectra	• Decompose TOCSY into 1D cross sections • Identify metabolites using 1D traces
MetaboHunter (Tulpan, Léger, Belliveau, Culf, & Čuperlović-Culf, 2011)	Processed ^{1}H spectra or peak lists	• Automated peak assignment

All of my work has been conducted using software developed in-house. For the most part I have used rNMR (I. A. Lewis et al., 2009) which was developed by Ian Lewis and for which I conducted extensive beta-testing. This was the first software package designed for large scale quantitative metabolomics. While the focus was 2D NMR, rNMR also handles 1D data.

The key principle behind rNMR is that analysis is performed by drawing a box around a region of interest (ROI). The ROI is then applied to all spectra in the dataset which allows the user to view all the NMR data within the ROI boundary.

Because peaks shift to some degree across multiple samples or may be slightly overlapped, algorithms used for determining related peaks across multiple samples are prone to failure. Using ROIs eliminates this problem by allowing the user to rapidly inspect the data inside the ROIs. This approach allowed us to greatly reduce the amount of time required for data analysis.

The latest software from our laboratory is Newton (Chylla et al., 2011), which is being developed by Roger Chylla and for which I have also conducted extensive beta-testing. Newton borrows many ideas from rNMR, such as batch analysis and ROIs, but also introduces new concepts such as peak modeling by fast maximum likelihood reconstruction. These improvements allow for better peak picking in regions of spectral overlap, reliable peak matching and improved metabolite quantitation. Future enhancements will allow better metabolite identification by matching metabolite specific

spectral patterns in samples to database standards. Newton can be used for 1D and 2D data analysis.

As both commercial and free software continue to mature, the ability to rapidly and accurately analyze complex mixtures of metabolites will improve. Databases are constantly expanding metabolite coverage and software used for analysis implements for rigorous algorithms for peak picking and matching. These improvements are essential for the long term success of metabolomics.

1.6 Continuing application and development of metabolomics

The application of metabolomics-based research has seen an explosion in the last decade. Consequently, a tremendous effort has been placed on continued methods development and improvement. In the following chapters I present various projects I have undertaken that involved applications of NMR-based metabolomics or the development of new research methods.

Chapter 2

Semi-automated device for batch extraction of metabolites from tissue samples

Adapted from**:**

Ellinger J, Miller D, Lewis I, Markley J (2012) *Semiautomated Device for Batch Extraction of Metabolites from Tissue Samples*. Analytical Chemistry 84, 1809-1812

My role in this project: I helped design and refine the apparatus, tested it thoroughly, and wrote the first draft of the manuscript.

2.1 Abstract

Metabolomics has become a mainstream analytical strategy for investigating metabolism. The quality of data derived from these studies is proportional to the consistency of the sample preparation. Although considerable research has been devoted to finding optimal extraction protocols, most of the established methods require extensive sample handling. Manual sample preparation can be highly effective in the hands of skilled technicians, but an automated tool for purifying metabolites from complex biological tissues would be of obvious utility to the field. Here, we introduce the semi-automated metabolite batch extraction device (SAMBED), a new tool designed to simplify metabolomics sample preparation. We discuss SAMBED's design and show that SAMBED-based extractions are of comparable quality to extracts produced through traditional methods (13% mean coefficient of variation from SAMBED versus 16% from manual extractions). Moreover, we show that aqueous SAMBED-based methods can be completed in less than a quarter of the time required for manual extractions.

2.2 Introduction

Metabolomics sample preparation methods can be divided into three main phases, 1) homogenization, 2) metabolite extraction, and 3) sample filtration. Each of these steps plays a direct role in the overall yields and error rates associated with metabolite isolation from biological tissues. Given the paramount importance of consistent sample preparation to metabolomics (Weckworth, 2006; Lin et al., 2007; Rabinowitz & Kimball, 2007; Sekiyama et al., 2011), surprisingly few tools are available for automating sample preparation and ensuring consistent metabolite extraction. This is particularly problematic for nuclear magnetic resonance (NMR) spectroscopic studies, which require large sample sizes and substantial volumes of solvents.

Several commercial devices are currently available to automate sample preparation. The Precellys 24 (Bertin Technologies), gentleMACS® Dissociator (Miltenyi Biotec) and Tissuelyser (Qiagen). Furthermore, recent studies have shown that these devices are effective for medium to high throughput preparation of metabolite extracts (Geier, Want, Leroi, & Bundy, 2011; Römisch-Margl et al., 2011; H. Wu, Southam, Hines, & Viant, 2008; J. Wu, An, Yao, Wang, & Tang, 2010). However, these devices focus on automating the homogenization process, while addition of extraction solvents and sample filtration has not been fully streamlined.

In this report, we introduce the semi-automated metabolite batch extraction device (SAMBED). SAMBED is a new tool that supports the parallel extraction of metabolites from NMR-scale samples. Our goal in designing SAMBED was to integrate all of the

requisite steps of sample preparation into a single platform while maintaining flexibility with respect to a range of extraction solvents. Consequently, SAMBED was constructed from autoclavable materials that are tolerant of both water and organic solvents and operates effectively at temperatures ranging from 4 to 100° C. Our prototype accommodates six parallel extractions and is designed for processing large samples (0.05 – 1 g of tissue). Although SAMBED's scale makes it most appropriate for NMR-based metabolomics, the design could be rescaled for smaller samples, such as those used in mass spectrometry.

SAMBED is composed of six integrated components: (1) milling chamber, (2) vibrational shaker, (3) solvent reservoir, (4) homogenization platform, (5) filtration chamber and (6) filtration platform (Figures 2.1-6). The system is powered by compressed air supplied from a conventional air compressor. Biological tissues are placed in the milling chamber and are homogenized by ball milling in the vibrational shaker. Our custom milling chamber (Figure 2.2) has a pneumatically-controlled plunger in its base that allows extraction solvents to be injected directly into the chamber and raw extracts to be transferred to the downstream filter chambers (Figure 2.6). A pre-allocated volume of extraction solvent flows from the solvent reservoir into the milling chamber by gravity. Homogenate is then transferred via the fluid delivery system to a filtration chamber, where metabolites are separated from cellular debris and macromolecules by ultrafiltration.

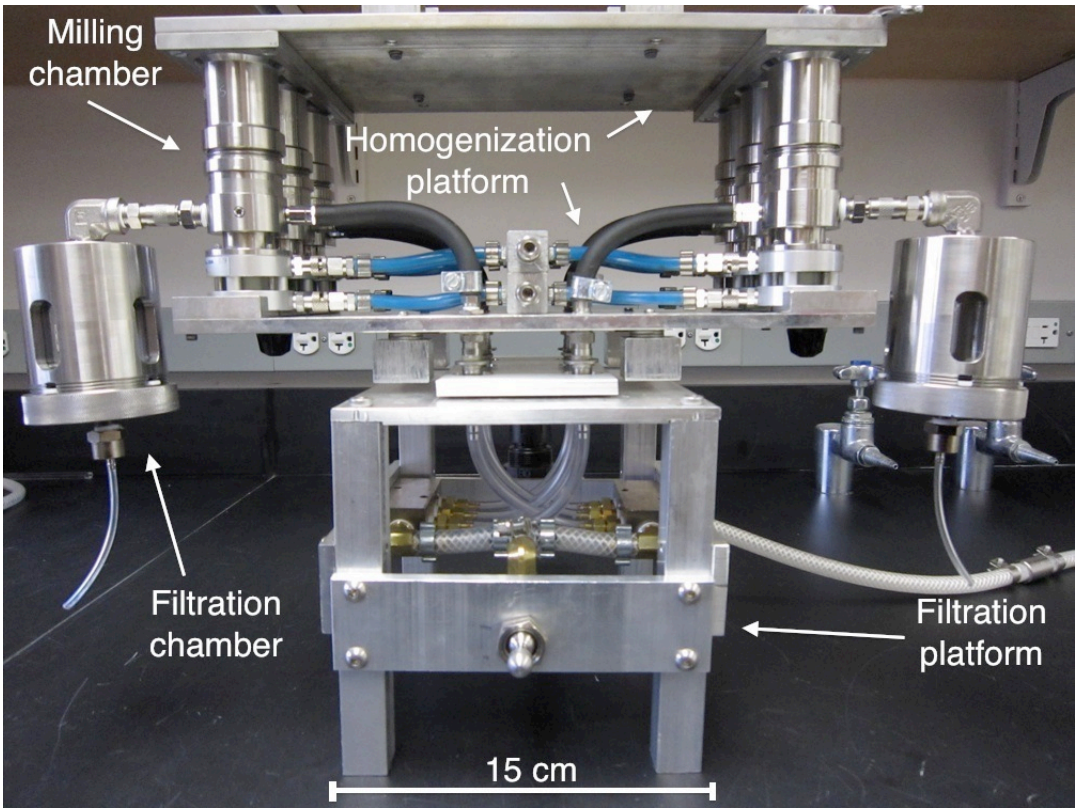

Figure 2.1. Photograph of the major components of the assembled SAMBED. The air compressor and vibrational shaker are not shown.

Figure 2.2. Photograph of a deconstructed milling chamber.

Figure 2.3. Photograph of the solvent reservoir attached to the filtration platform. The solvent reservoir consists of 6 canisters, each of which delivers a pre-allocated volume of extraction solvent to a single milling chamber.

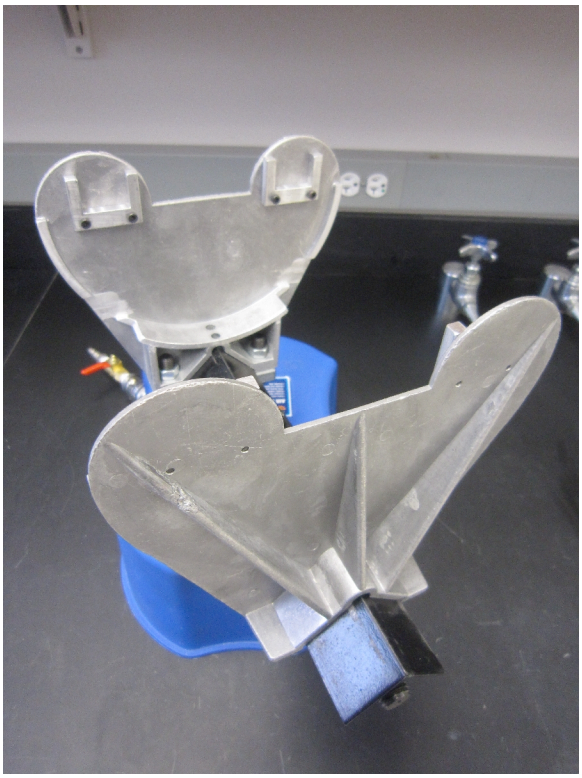

Figure 2.4. Photograph of the vibrational shaker.

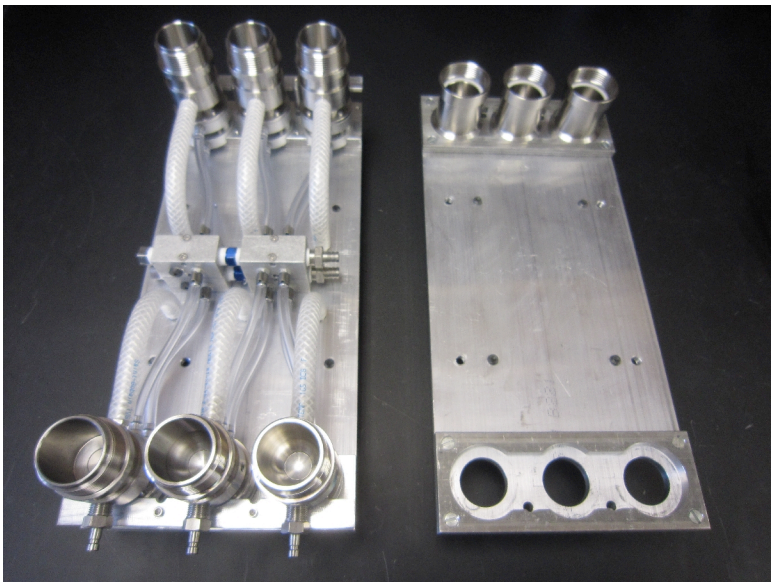

Figure 2.5. Photograph showing milling chambers resting on the homogenization platform.

Figure 2.6. Photograph of a deconstructed filtration chamber.

2.3 Experimental Section

Manual sample processing

Bovine liver was obtained from a local grocery store. The liver was frozen, lyophilized, and aliquoted into 500–600 mg (large samples) or 100–150 mg (small samples) portions. Metabolites were extracted by following established aqueous (I. A. Lewis et al., 2010) (Chae et al., 2010) (Hallows et al., 2011) or organic protocols (Rabinowitz & Kimball, 2007) (Bennett et al., 2009). Briefly, dry liver samples (large samples for aqueous extractions and small samples for organic extractions) were homogenized with a rounded glass rod, then suspended in either 16 ml of 95° C deionized water (aqueous extraction) or 3 ml of -20° C 40:40:20 Acn:MeOH:H_2O (organic extraction). Aqueous extractions were vortexed and incubated in a 95° C water bath for 7.5 min then placed on ice for 10 min to cool. Organic extractions were vortexed and stored at 4° C for 15 min. Following extraction, all samples were vortexed and centrifuged at 10,000 RPM for 10 min (4° C). Supernatants from aqueous extracts were transferred to pre-washed centrifugal microfilters (3000 Da cutoff, Sartorius Biolab Products) and centrifuged at 4100 RPM for 10.5 h. The long centrifuge time was necessary for passing the entire sample through the filter membrane (excluding the 200 μl dead volume). Supernatants from organic extracts were decanted into a fresh tube, and the pellet was re-extracted twice with 2 ml of Acn:MeOH:H_2O, incubated for 5 min at 4° C, and centrifuged. Supernatants from the two organic wash steps were combined with the original extract to yield a single 7-mL extract from each sample. All

metabolite extracts were frozen, lyophilized, and stored dry at -80° C until NMR analysis.

Sample processing by SAMBED

SAMBED was kept at room temperature for aqueous extractions and was conducted in a 4° C cold room for organic extractions. Lyophilized liver samples (large and small samples for aqueous extractions and small samples for organic extractions) were placed in each of the six milling chambers along with a 1.8 mm diameter grinding ball. Dry samples were milled on the shaker platform for 30 s, and either 17 mL of 95° C ddH_2O (aqueous extractions) or 8 ml of -20° C 40:40:20 Acn:MeOH:H_2O (organic extractions) were injected from the solvent reservoir into each chamber. Samples were wet-milled for an additional 30 s. For aqueous extractions, the homogenization platform was submerged in a 95° C water bath for 7.5 min. The homogenization platform was coupled to the filtration platform, and six filtration chambers (pre-chilled for one hour to 4° C) containing pre-washed ultrafiltration membranes (3000 Da cutoff, Millipore) were attached. The contents of each milling chamber were transferred to the downstream filter chamber under compressed air at 35 psi. The pressure was increased to 70 psi, and filtration was allowed to progress until most of each sample had passed through the filtration membrane. Each milling chamber was flushed with 5 ml ddH_2O, and filtration was allowed to progress until outflow from the filter chambers ceased. Aqueous extracts

were collected in tubes placed on ice. All metabolite extracts were frozen, lyophilized, and stored at -80° C until NMR analysis.

NMR analysis. All dry metabolite extracts were dissolved in 800 μl (large samples) or 200 μl (small samples) D_2O containing 1 mM 2,2-dimethyl-2-silapentane-5-sulfonate(DSS, chemical shift standard) and 500 μM NaN_3 (microbial growth inhibitor). The resulting solution was titrated with concentrated DCl or NaOD as needed to achieve a glass electrode pH reading of 7.40 ± 0.01. NMR data were collected at the National Magnetic Resonance Facility at Madison on a 600 MHz Bruker Avance III spectrometer equipped with a triple-resonance (^{1}H, ^{13}C, ^{15}N, ^{2}H lock) 1.7 mm cryogenic probe. The probe was tuned, matched, and locked to deuterium for the first sample. Each sample was shimmed, and the 90° pulse width was determined. A 2D ^{1}H-^{13}C HSQC spectrum (Bruker sequence hsqcetgpsisp2.2) was then collected for each sample. Data were processed using custom NMRPipe (Delaglio et al., 1995) scripts written in-house. Metabolites were identified and quantified using the rNMR software package (I. A. Lewis et al., 2009) following established methods (I. A. Lewis et al., 2007). Briefly, metabolites were identified by submitting peak lists to the Madison-Qingdao Metabolomics Consortium Database (MMCD) (Cui et al., 2008); assignments were verified by overlaying NMR spectra of standards from the BioMagResBank (BMRB) (Markley et al., 2007). Metabolite concentrations were calculated on the basis of calibration curves from metabolite standards prepared at 2, 5 and 10 mM. Peak amplitudes used for

quantitation were obtained by fast maximum likelihood reconstruction as implemented in the Newton software package (Chylla et al., 2011).

Statistical analysis. To measure the relative consistency of manual versus SAMBED-based preparations, we computed the coefficient of variation (CV) observed for each metabolite across the 18 replicates of each sample preparation method. Overall variability was then expressed as the mean CV associated with each method. All calculations were performed using the R statistical software program (www.r-project.org).

2.4 Results and Discussion

One of the primary motivations for developing SAMBED was to make sample preparation more efficient by automating and parallelizing the metabolite purification process. Consequently, we measured the time required to prepare 18 samples (three trials of 6 samples each) via established aqueous (I. A. Lewis et al., 2010) (Chae et al., 2010) (Hallows et al., 2011) and organic extraction methods (Rabinowitz & Kimball, 2007) (Bennett et al., 2009). Sample preparation times were compared between manual and SAMBED-based extractions (Table 2.1). As expected, SAMBED greatly decreased the time required to prepare samples. SAMBED-derived extracts were generated in 21% of the time required for manual preparation of aqueous extracts. Most of the time savings are attributable to the ultrafiltration step, which is 5 times more efficient by SAMBED because of its large surface area filters. For organic extractions, SAMBED-

based extractions required slightly more time than manual preparation (81 versus 89 min). However, these times are not directly comparable because the SAMBED-based organic extractions were subject to microfiltration whereas the manual sample processing method omitted this step. In contrast to the centrifugal microfilters, the filter membranes used by SAMBED are resistant to the Acn:MeOH:H_2O solvent used in this study. Our data show that the additional microfiltration step only adds ~10% to the total processing time and comes with the clear benefit of reduced labor.

Table 2.1. Average times required to prepare metabolite extracts by manual and SAMBED-based protocols [a]

Protocol	Prefiltration time (min)	Filtration Time (min)	Total time (min)
A (Aqueous, manual) [b]	51.14 ± 5.6	630 ± 0.00	681 ± 6.0
B (Aqueous, SAMBED)[b]	17.02 ± 0.5	145 ± 3.0	162 ± 4.0
C (Aqueous, SAMBED)[c]	18.11 ± 0.4	68.0 ± 0.9	86.1 ± 0.5
D (Organic, manual)[c]	51.22 ± 3.8	30.0 ± 0.0 [d]	81.2 ± 3.8
E (Organic, SAMBED)[c]	N/A [e]	N/A [e]	88.7 ± 7.8

[a] Data are reported as the mean of three trials ± the $\frac{range}{2}$

[b] Large sample (500-600 mg per sample)

[c] Small sample (100-150 mg per sample)

[d] Time required for high speed centrifugation

[e] Separating the prefiltration and filtration times was not possible

A second motivation for developing SAMBED was to standardize sample processing by eliminating manual sample manipulation. To measure SAMBED's success in producing consistent metabolite extracts, we measured variations in 29 metabolite levels observed in 18 liver extracts produced via traditional versus our new SAMBED-based protocol. Two established methods, one organic the other aqueous, were evaluated in this study. For each metabolite, we compared the yields per gram of liver and the average variability of metabolite levels associated with the different protocols (Table 2.2). As expected, SAMBED-generated extracts were comparable to those prepared by an experienced technician. Metabolite concentrations observed in SAMBED extracts were linearly related to those observed in manual extractions across multiple orders of magnitude (Figure 2.7). Moreover, the mean CV of metabolites observed in aqueous SAMBED extracts was 12.3% whereas manual sample preparation resulted in a mean CV of 13.6% (N = 522). Manual preparation of organic extracts was the least consistent protocol tested with a mean CV of 18.1%; this variability was reduced to 14.1% when extracts were prepared by SAMBED. We attribute the more consistent performance of the organic SAMBED-based method to microfiltration step, which is not possible via the traditional method due to membrane/solvent incompatibility.

Table 2.2. Average amounts [nmol mg^{-1} dry weight liver ± standard deviation (n = 18)] of various metabolites extracted by manual and SAMBED protocols.

Method used:	Manual	Sambed	Sambed	Manual	Sambed
Extraction:	Aqueous	Aqueous	Aqueous	Organic	Organic
Average dry mass of liver sample (mg):	543.1	534.8	138.2	118.5	127.4
Metabolite [nmol mg^{-1} dry weight liver ± standard deviation][a]					
3HB	0.8 ± 0.09	0.88 ± 0.1	0.9 ± 0.08	0.66 ± 0.13	0.81 ± 0.15
Ace	1.4 ± 0.24	8.33 ± 1.45	10.51 ± 3.15	4.88 ± 0.9	6.1 ± 0.77
Ala	16.68 ± 2.32	22.95 ± 2.53	30.11 ± 2.9	26.49 ± 3.33	21.76 ± 4.12
Asp	2.77 ± 0.33	3.06 ± 0.31	3 ± 0.46	2.53 ± 0.56	3.11 ± 0.74
Bet	0.37 ± 0.05	0.46 ± 0.07	0.57 ± 0.1	0.77 ± 0.23	0.48 ± 0.1
Crn	24.5 ± 3.49	30.84 ± 2.4	35.12 ± 1.66	44.26 ± 8.17	37.79 ± 3.16
Cho	11.2 ± 1.24	16.36 ± 1	18.31 ± 1.03	20.34 ± 2.71	19.8 ± 1.94
Crt	4.75 ± 0.62	5.85 ± 0.83	6.41 ± 0.6	6.16 ± 0.87	5.02 ± 0.59
Fru	11.09 ± 0.74	14.51 ± 1.14	17.89 ± 1.38	17.82 ± 2.27	16.03 ± 1.57
Gln	3.55 ± 0.33	3.78 ± 0.52	4.79 ± 0.42	3.89 ± 0.52	3.89 ± 0.88
Glu	21.56 ± 4.61	18.32 ± 1.7	19.5 ± 1.53	31.71 ± 2.2	34.26 ± 2.02
Glc	344.8 ± 27.85	357.17 ± 27.06	396.64 ± 28.61	383.42 ± 21.1	387.07 ± 18.95
Gly	35.67 ± 3.12	37.53 ± 2.25	40.12 ± 1.96	39.06 ± 1.66	43.25 ± 5.12
Ile	2.61 ± 0.4	3.2 ± 0.39	3.31 ± 0.42	3.22 ± 0.35	3.44 ± 0.25
Lac	63.95 ± 7.35	54.33 ± 6.35	70.33 ± 7.48	78.21 ± 11.91	72.73 ± 5.39
Leu	6.37 ± 0.89	8.32 ± 0.94	8.46 ± 1.11	7.64 ± 0.87	8.11 ± 0.57
Lys	5.84 ± 0.79	7.65 ± 0.81	8.31 ± 1.1	4.22 ± 0.58	6.43 ± 1.31
Man	3.21 ± 0.36	3.42 ± 0.39	4.64 ± 0.67	3.16 ± 0.84	3.06 ± 0.84
Met	1.69 ± 0.3	1.93 ± 0.28	1.83 ± 0.43	0.87 ± 0.38	1.48 ± 0.27
Orn	3.97 ± 0.42	3.89 ± 0.48	4.51 ± 0.42	1.42 ± 0.3	3.65 ± 0.66
Pan	0.48 ± 0.05	0.84 ± 0.22	0.79 ± 0.04	0.67 ± 0.23	0.66 ± 0.08
Phe	2.86 ± 0.41	3.34 ± 0.4	3.43 ± 0.58	2.72 ± 0.42	3.36 ± 0.32
Pro	4.27 ± 0.38	6.08 ± 0.62	6.73 ± 0.62	5.97 ± 1.49	5.58 ± 0.59
Ser	5.81 ± 0.75	7.68 ± 0.85	8.15 ± 1.04	7.95 ± 0.83	7.86 ± 0.67
Suc	22.35 ± 2.68	24.67 ± 1.95	28.74 ± 1.77	31.82 ± 2.4	33.99 ± 1.13
Tau	4.04 ± 1.02	3.63 ± 0.71	4.7 ± 0.72	3.18 ± 1.03	2.67 ± 0.77
Thr	4.39 ± 0.74	4.78 ± 0.55	4.45 ± 0.39	3.98 ± 0.67	4.16 ± 0.71
Ura	2.24 ± 0.57	2.52 ± 0.6	2.89 ± 0.69	2.69 ± 1.03	2.56 ± 0.62
Val	4.76 ± 0.64	6.1 ± 0.72	6.22 ± 0.77	5.73 ± 0.59	6.34 ± 0.61
Mean CV	13.6	12.3	11.9	18.1	14.1

[a]All amino acids are represented by their standard three-letter code; 3HB, 3-hydroxybutrytate; Ace, acetate; Bet, betaine; Crn, carnitine; Cho, choline; Crt, creatine; Fru, fructose; Lac, lactate; Man, mannose; Orn, ornithine; Pan, pantothenate; Suc, succinate; Tau, taurine; Ura, uracil.

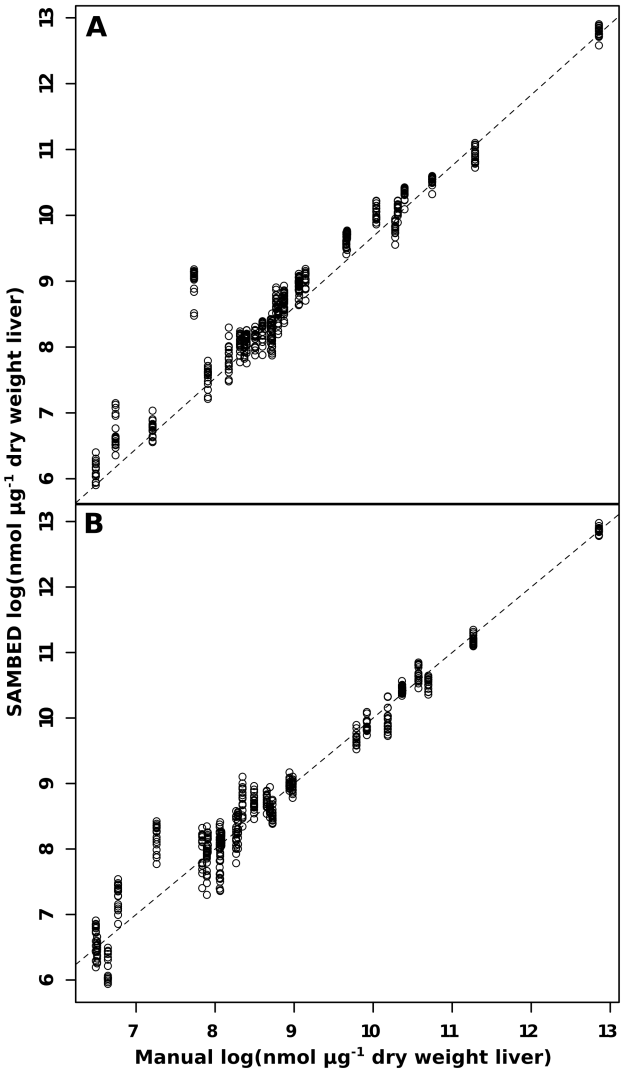

Figure 2.7. Linear relationship of the metabolite levels measured by manual or SAMBED processing for A) aqueous and B) organic extractions. SAMBED-derived metabolite levels ($n = 522$) are plotted relative to the mean abundance for each metabolite observed in the manual-derived extracts. The dotted black line indicates the theoretical ideal regression (slope = 1). In the case of aqueous extractions, only data from large samples are shown.

Previous research has shown automated sample preparation is feasible and can produce consistent results (Geier et al., 2011; Römisch-Margl et al., 2011; H. Wu et al., 2008; J. Wu et al., 2010). Minimizing technical error is a critical design feature of automated sample preparation tools. The mean CV values for SAMBED-based extracts reported here (12 - 14%) compare favorably to those reported for other automated tools (15 - 30%)(Geier et al., 2011; Römisch-Margl et al., 2011).

2.5 Conclusions

We have developed and tested SAMBED, a new device that streamlines and automates the isolation of metabolites from biological tissues. SAMBED consistently generates metabolite extracts that are of comparable, or slightly better, quality than those generated by traditional methods. Our design allows aqueous extractions to be completed in a fraction of the time required for manual sample processing, and the materials used in SAMBED support a wide range of extraction conditions. In summary, SAMBED simplifies one of the most laborious aspects of metabolomics studies without affecting data quality.

2.6 Acknowledgments

This work was supported by NIH grant RR02301 and by the DOE Great Lakes Bioenergy Research Center (DOE BER Office of Science DE-FC02-07ER64494 GLBRC). This study made use of the National Magnetic Resonance Facility at Madison, which is supported by National Institutes of Health grants P41RR02301 and 3P41RR002301-26S1 from the Biomedical Research Technology Program, National

Center for Research Resources. Equipment in the facility was purchased with funds from the University of Wisconsin, the National Institutes of Health (P41GM66326, P41RR02301, RR02781, RR08438), the National Science Foundation (DMB-8415048, OIA-9977486, BIR-9214394), and the U.S. Department of Agriculture.

Chapter 3

Role of aminotransferases in glutamate metabolism of human erythrocytes

Adapted from:

Ellinger J, Lewis I, Markley J (2011) *Role of aminotransferases in glutamate metabolism of human erythrocytes*. Journal of Biomolecular NMR 49, 221-229

My role in this project: With Ian Lewis, I co-designed and conducted experiments as well as co-wrote the manuscript. We shared responsibility for NMR data analysis, but I handled all MS analysis.

3.1 Abstract

Human erythrocytes require a continual supply of glutamate to support glutathione synthesis, but are unable to transport this amino acid across their cell membrane. Consequently, erythrocytes rely on *de novo* glutamate biosynthesis from α-ketoglutarate and glutamine to maintain intracellular levels of glutamate. Erythrocytic glutamate biosynthesis is catalyzed by three enzymes, alanine aminotransferase (ALT), aspartate aminotransferase (AST), and glutamine aminohydrolase (GA). Although the presence of these enzymes in RBCs has been well documented, the relative contributions of each pathway have not been established. Understanding the relative contributions of each biosynthetic pathway is critical for designing effective therapies for sickle cell disease, hemolytic anemia, pulmonary hypertension, and other glutathione-related disorders. In this study, we use multidimensional ^{1}H-^{13}C nuclear magnetic resonance (NMR) spectroscopy and multiple reaction mode mass spectrometry (MRM-MS) to measure the kinetics of *de novo* glutamate biosynthesis via AST, ALT, and GA in intact cells and RBC lysates. We show that up to 89% of the erythrocyte glutamate pool can be derived from ALT and that ALT-derived glutamate is subsequently used for glutathione synthesis.

3.2 Introduction

Glutathione (GSH) plays a central role in repairing oxidative damage to red blood cells (RBCs). Alterations in glutathione levels have been linked to a variety of human disorders, including sickle cell disease, hemolytic anemia, and pulmonary hypertension

(G. Wu, Fang, Yang, Lupton, & Turner, 2004). Although all of the enzymes required for synthesizing glutathione from its component amino acids (glutamate, cysteine, glycine) are present in erythrocytes (Majerus, Brauner, Smith, & Minnich, 1971; Minnich, Smith, Brauner, & Majerus, 1971), the RBC membrane is essentially impermeable to glutamate (Sass, 1968; Winter & Christensen, 1964; D. J. Young et al., 1987). Consequently, RBCs rely on *de novo* glutamate biosynthesis to maintain intracellular levels of this amino acid.

RBCs contain three enzymes for synthesizing glutamate: alanine aminotransferase (ALT; EC 2.6.1.2), aspartate aminotransferase (AST; EC 2.6.1.1), and glutamine aminohydrolase (GA; EC 3.5.1.2). ALT and AST synthesize glutamate from α-ketoglutarate whereas GA synthesizes glutamate from glutamine (Figure 3.1). Since RBC membranes are permeable to both α-ketoglutarate and glutamine (Griffith, 1981; Sass, 1968; J. D. Young, Wolowyk, Jones, & Ellory, 1983) all three mechanisms can potentially influence intracellular glutamate levels. However, GA is generally thought to be the main contributor to RBC glutamate biosynthesis (Ellory, Preston, Osotimehin, & Young, 1983; Griffith, 1981; Morris et al., 2008; Niihara, Zerez, Akiyama, & Tanaka, 1997).

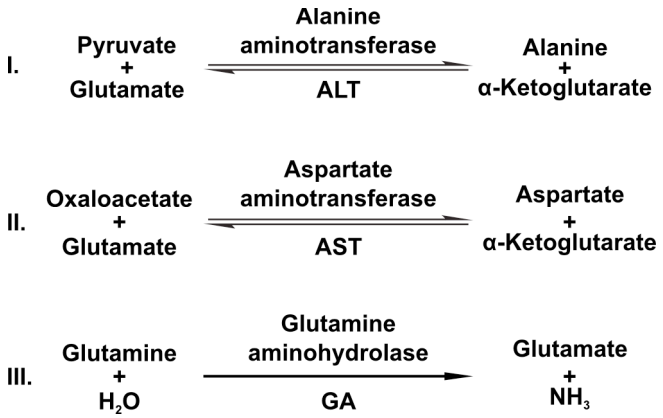

Figure 3.1 Reaction mechanisms for I) alanine aminotransferase (ALT) and II) aspartate aminotransferase (AST). Unlike glutamate, both alanine and α-ketoglutarate cross the RBC membrane; ALT and AST provide a mechanism for *de novo* glutamate production that could support glutathione biosynthesis.

We recently reported that roughly one percent of the glucose consumed by RBCs incubated in an amino acid free medium is devoted to *de novo* alanine production (I. A. Lewis, Campanella, Markley, & Low, 2009). Since ALT is the only enzyme for synthesizing alanine in RBCs, this result suggests that ALT activity can have a significant impact on steady-state glutamate levels. Given that ALT and AST reactions are readily reversible, and that the substrates for the ALT and AST reactions are normally present in the serum (Wishart et al., 2007), we reasoned that aminotransferase reactions may be playing a significant, and currently underappreciated, role in RBC glutamate biosynthesis *in vivo*.

Although most of the transport and enzymatic kinetics associated with RBC glutamate metabolism are known (Griffith, 1981), the relative biosynthetic capacities of ALT, AST, and GA have not been directly evaluated in intact cells. Understanding the relative contribution of each pathway is important for designing effective therapies for diseases related to glutathione deficiencies. In this study, we apply modern metabolomics techniques to measure the biosynthetic capacities of AST, ALT, and GA in intact cells and hemolysates. Using multidimensional ^{1}H-^{13}C nuclear magnetic resonance (NMR) spectroscopy and multiple reaction mode mass spectrometry (MRM-MS) we show that ALT can contribute up to 89% of the intracellular glutamate pool and that ALT-derived glutamate is incorporated into glutathione. These data argue that aminotransferase reactions are more significant than GA in influencing steady-state levels of glutamate *in vivo*.

3.3 Methods

Preparation of RBCs and lysates

Fresh blood was collected by venipuncture from healthy human volunteers ($n = 3$) into heparinized vacutainers. RBCs were isolated by centrifugation (10 min at 3,000 × g), and the buffy coat was discarded. Samples were washed three times in isotonic HEPES buffer (25 mM HEPES, 1 mM NaH_2PO_4, 106 mM NaCl, 19 mM KCl, 1 mM $CaCl_2$, pH 7.4), combined into a single pool, and resuspended at 20% hematocrit in HEPES buffer containing 20 IU/mL Penicillin/Streptomycin (Gibco). Lysates were prepared from washed RBCs suspended at 36% hematocrit. RBCs were hemolyzed by sonication for 1 min and the resulting lysates were diluted to the equivalent of 25% hematocrit with isotonic HEPES buffer containing metabolite standards (see aminotransferase activity assays in RBC lysates). All sample preparations were conducted at 4 °C to minimize metabolic activity.

Metabolic activity assays in intact RBCs

Washed RBCs were prepared in isotonic HEPES buffer containing either (i) 5 mM [U-^{13}C]-glucose (Isotec), (ii) 5 mM glucose, 5 mM alanine, and 5 mM [$^{13}C_{1,2,3,4}$]-α-ketoglutarate (Cambridge Isotope Laboratories) or (iii) 5 mM glucose and 1 mM [U^{13}C-^{15}N] glutamine. Each RBC suspension was split into three replicate samples, which were incubated at 37 °C over periods of (i, iii) 12 h or (ii) 21 h. Aliquots (1 mL) were collected from samples after incubation times of 0, 1.5, 3, 6, 12, and 21 h (only ii) and

flash frozen in liquid nitrogen. Metabolites were then extracted from each sample (as described below) and analyzed by NMR spectroscopy and MS for the presence of isotopically enriched molecules. Enriched metabolites were identified and quantified by NMR, and the isotopic enrichments were determined by MS. Samples containing [U-^{13}C]-glucose (i) provided information about glycolytically-related metabolism; samples containing [$^{13}C_{1,2,3,4}$]-α-ketoglutarate (ii) provided information on aminotransferase reactions; and samples containing [U^{13}C-^{15}N] glutamine (iii) provided information on glutamine aminohydrolase activity.

Aminotransferase activity assays in RBC lysates

RBC lysates were incubated at 37 °C for 6–12 h in isotonic HEPES buffer containing 200 μM pyridoxal-5′-phosphate (PLP; the cofactor required by aminotransferases) and one of the following pairs of substrates (5 mM each): pyruvate + glutamate for alanine aminotransferase (ALT) assays, alanine + α-ketoglutarate for reverse ALT assays, oxaloacetate + glutamate for aspartate aminotransferase (AST) assays, aspartate + α-ketoglutarate for reverse AST assays, and pyruvate plus one of each of the amino acids listed in Figure 3.3 for aminotransferase screening assays. Aliquots (900 μL) of each sample were collected after 0, 1, 3, 6 and 12 h of incubation and flash frozen in liquid nitrogen. Metabolites were then extracted (as described below) and analyzed by NMR.

Metabolite extraction

Samples were placed in a boiling water bath for 7.5 min to lyse cells and halt enzymatic activity. Boiled lysates were spun at 16,000 × g to pellet cellular debris. For samples to be analyzed by LC-MS/MRM, a 200 µL aliquot of each supernatant was transferred to a fresh tube and stored at -80 °C until analysis. For samples to be analyzed by NMR, an 800 µL aliquot of each supernatant was dried in a SpeedVac Concentrator (Thermo Scientific), and the resulting residue was dissolved in 800 µL D_2O containing 500 µM NaN_3 and 500 µM 3-trimethylsilylpropane-1-sulfonate(DSS).

NMR spectroscopy

NMR data were collected at the National Magnetic Resonance Facility at Madison. Two-dimensional sensitivity enhanced ^{1}H-^{13}C HSQC spectra were collected on a Varian 600 MHz spectrometer equipped with a cryogenic probe. Spectra were collected, following 16 transients to achieve steady state, as four averaged transients with 128 increments in the second dimension (50 increments for the *in vivo* labeling studies). The acquisition time was 300 ms (3,000 data points), following an initial delay of 1 s; the carbon spectral width was 70 ppm. Time-domain data were Fourier transformed with a shifted exponential sine-bell window function, phased, and chemical shift referenced to DSS using custom nmrDraw (Delaglio et al., 1995) scripts written in-house.

Our methods for identifying and quantifying metabolites by ^{1}H-^{13}C NMR have been described elsewhere (I. A. Lewis et al., 2007; I. A. Lewis et al., 2009). Briefly, metabolites were identified using the Madison Metabolomics Consortium Database

(MMCD) (Cui et al., 2008); assignments were verified by overlaying NMR spectra of standards from the BioMagResBank (BMRB) (Markley et al., 2007); metabolite concentrations were calculated from peak intensities on the basis of calibration curves from metabolite standards prepared at 2, 5, and 10 mM. The rNMR software package (I. A. Lewis et al., 2009) was used in performing all NMR data analyses.

Mass spectrometry

Mass spectra were collected at the University of Wisconsin Biotechnology Center Mass Spectrometry Facility. An aliquot (5 μL) of each metabolite extract was analyzed by liquid chromatography (LC) MS on an Applied Biosystems 3200 Q TRAP LC-MS/MS system equipped with an Agilent 1100 series capillary LC pump and an electrospray ionization (ESI) source. Online LC used a 4.6 mm × 150 mm Phenomenex Luna hydrophylic interaction chromatography (HILIC) column (200-Å pore size, 5-μm particle size) with a constant flow rate of 200 μL/min. Samples were eluted over a 48-min ammonium formate (50 mM, pH 5.4; buffer A) to acetonitrile gradient. The elution gradient was constructed as follows: 90% A at time zero, 70% A at 20 min, holding at 70% A for 2 min, 10% A at 22 min, holding at 10% A for 1 min, back to 90% A at 23 min, and isocratic at 90% A until 48 min. ESI-MS was performed in positive ion multiple reaction mode (MRM). Peak picking and integration were accomplished with Analyst software (Applied Biosystems). Metabolite identification, retention times, and ion fragment patterns, were verified by reference to standard compounds. The Kombyonyx

isotope calculator (www.kombyonyx.com) was used to calculate isotopomer distributions.

Regression analyses and statistics

Rates of metabolite consumption and production were calculated by linear regression of metabolite concentration as a function of time. Regression analyses were based on all time points, except for samples incubated with aspartate + α-ketoglutarate and oxaloacetate + glutamate. Kinetics observed in the latter samples were nonlinear because of spontaneous decarboxylation of oxaloacetate to pyruvate (Hatch & Heldt, 1985). For these samples, initial rates were determined from the time points between 0 and 1 h. Samples incubated with [$^{13}C_{1,2,3,4}$] α-ketoglutarate contained contaminating [$^{13}C_{1,2,3,4}$] glutamate, which was determined from the 0 h time points and used as a baseline for subsequent measurements. Glutamate kinetics from cells incubated with [$^{13}C_{1,2,3,4}$] α-ketoglutarate were derived from linear regression of the first three time points. All of the *p* values presented here were derived from a two-tailed equal variance *t*-test.

3.4 Results

Reports of *de novo* alanine synthesis by intact RBCs (I. A. Lewis et al., 2009; Manuel y Keenoy et al., 1991) suggest an active role for aminotransferases in maintaining intracellular glutamate levels. We confirmed these reports by incubating RBCs in 5 mM [U-^{13}C] glucose and measuring the appearance of ^{13}C enriched alanine

by ^{1}H-^{13}C NMR (Figure 3.2). The rate of ^{13}C alanine production we observed (0.022 ± 0.001 μmol mL^{-1} RBC h^{-1}) is consistent with our previous findings and accounted for 1.1% of the total ^{13}C output (Table 3.1). LC-ESI-MS analyses indicated that 35% of the total alanine pool was uniformly ^{13}C labeled after 12 h of incubation with [U-^{13}C] glucose, whereas samples harvested at 0 h showed natural abundance ^{13}C levels (Table 3.2).

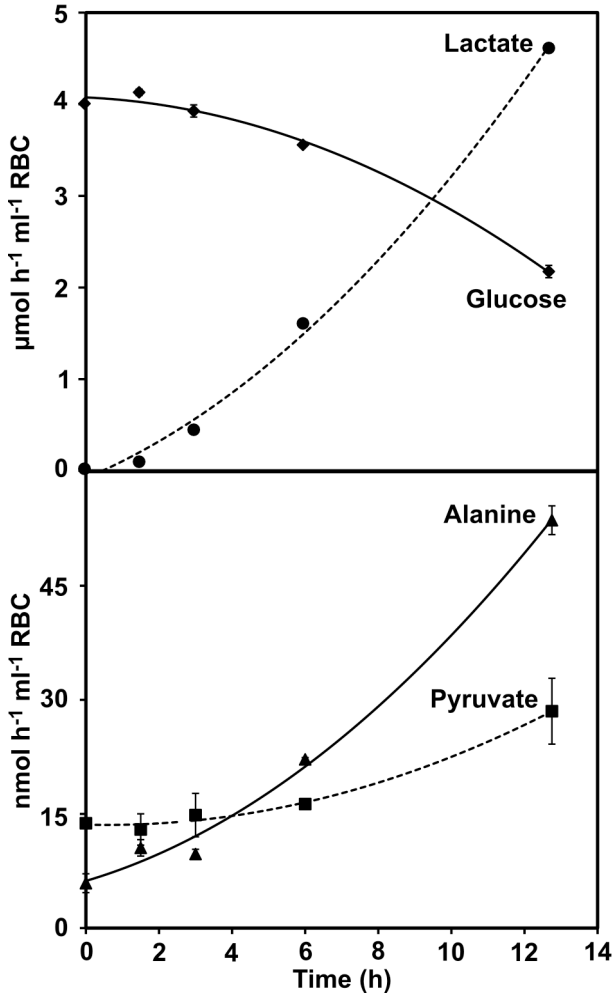

Figure 3.2 Glucose, lactate, alanine, and pyruvate metabolism observed in human RBCs. Samples were incubated with 5 mM [U-^{13}C] glucose and metabolites were quantified by ^{1}H-^{13}C NMR. Error bars represent S.E.M. (n = 3).

Table 3.1 Rates of glucose, lactate, alanine, pyruvate and glutamate metabolism observed in intact RBCs

	Observed rates of biosynthesis from the labeled substrate ($\mu mol\ ml^{-1}\ RBC\ hr^{-1}$)[a]					
Metabolite(s) added	Glucose	Lactate	Alanine	Pyruvate	Glutamate	α-Ketoglutarate
[U-$^{13}C_6$] glucose	-0.78±0.03	1.89± 0.01	0.02±0.001	0.01±0.002	n.o.[b]	n.o.[b]
[$^{13}C_{1,2,3,4}$] α-ketoglutarate glucose alanine	-0.80± 0.01[c]	1.35±0.02[c]	-0.11±0.07[c]	0.57±0.04[c]	0.17 ±0.01[c]	-0.16±0.06[c]
[U^{13}C-^{15}N] glutamine glucose	-0.9±0.03	2.13±0.04	n.o.[b]	n.o.[b]	0.004±0.001	n.o.[b]

[a] Means and S.E.M. for $n = 3$

[b] n.o. = not observed

[c] 21 h time point was excluded in the rate calculation

Table 3.2 Isotopomer distribution of alanine in RBCs incubated with [U-^{13}C] glucose

	Percent mass isotopomer distribution (alanine)[a]				
Time (h)	Monoisotopic	M+1	M+2	M+3	M+4
0	95.6±0.4	2.43±0.63	n.d.[b]	1.94±0.51	0
12	60.6±1.1**	4.04±0.04*	n.d.[b]	35.4±1.1**	0
Expected distribution due to natural abundance	95.92	3.62	0.44	0.01	0

[a] Means and S.E.M. for $n = 3$

[b] n.d. = not determined

* $p < 0.05$; ** $p < 0.001$

Aminotransferase activity in RBC lysates

To screen for alanine synthesis reactions, we incubated RBC lysates for 6 h in HEPES buffered saline containing 5 mM pyruvate, 200 μM pyridoxal-5′-phosphate (PLP), and 5 mM target amino acid. ^{1}H-^{13}C NMR analysis of the lysates showed significant alanine and α-ketoglutarate production in the sample incubated with glutamate as the target amino acid (Figure 3.3).

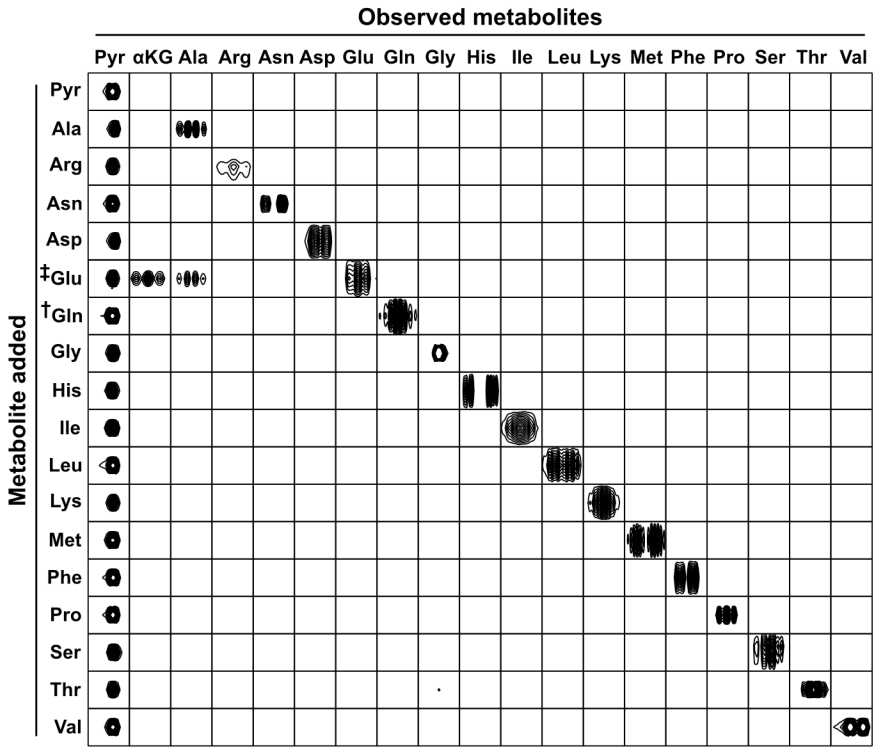

Figure 3.3 Aminotransferase screening assay used to determine the alanine biosynthetic route in human RBCs. Cell lysates were incubated with 200 μM pyridoxal-5′-phosphate, 5 mM pyruvate, and 5 mM of a target amino acid. Each square shows the unique ^{1}H-^{13}C NMR sub-spectrum used to identify and quantify each metabolite observed in the RBC lysates. Row labels denote the compounds added to samples, and column labels denote metabolite signals observed by ^{1}H-^{13}C NMR. In the first row, no amino acid was added in addition to pyruvate; in subsequent rows, the indicated amino acid was added in addition to pyruvate. Abbreviations: Pyr, pyruvate; αKG, α-ketoglutarate; amino acids are represented by standard three letter code. ‡The samples prepared with glutamate showed signals from both the substrate (glutamate) and the two products (alanine and α-ketoglutarate). †Samples incubated with glutamine showed no detectable levels of GA activity. However, GA activity was detectable by MS.

Conversion of glutamate + pyruvate to α-ketoglutarate + alanine in the presence of PLP is consistent with the established alanine aminotransferase (ALT) reaction mechanism (Figure 3.1) and is indicative of aminotransferase activity in the lysates. However, ALT is present in serum, and contaminating enzyme from the wash medium could influence our results. To control for contaminating ALT, both serum and the final RBC wash buffer were assayed for ALT activity using the method we applied to the RBC lysates. Although ALT activity was observed in serum samples (2.82 ± 0.32 μmol alanine produced over 12 h), the final RBC wash buffer showed no detectable ALT activity (Figure 3.4). These findings demonstrate that our assay is sufficiently sensitive to detect serum levels of ALT and that the ALT activity observed in RBC lysates did not result from extracellular ALT.

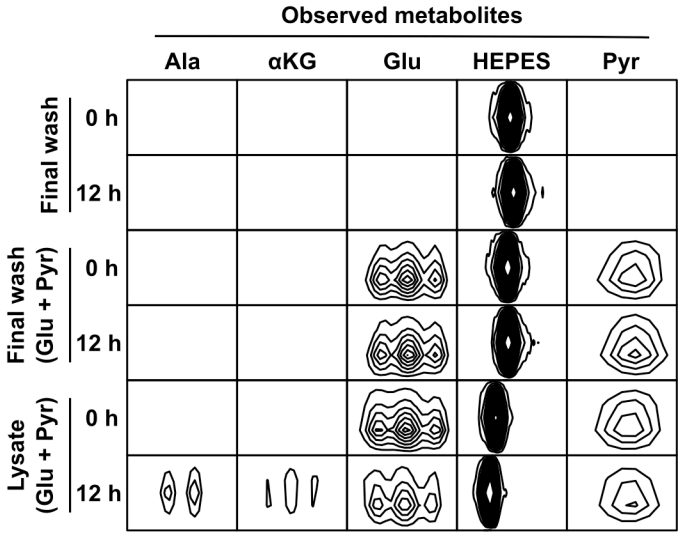

Figure 3.4. Metabolic activity of final wash buffer used for RBC preparation. ^{1}H-^{13}C NMR signals indicating no detectable aminotransferase activity after 12 h of incubation. Abbreviations: αKG, α-ketoglutarate; Pyr, pyruvate; amino acids are represented by their three letter codes.

Glutamate biosynthesis via aminotransferase reactions can be limited by either transport or reaction kinetics. To determine the maximum enzymatic rates of the AST and ALT reactions under physiologically-relevant conditions with naturally-occurring levels of enzymes, we incubated RBC lysates for 12 h with 200 μM PLP and saturating levels of substrates for the two aminotransferases (Figure 3.1). We determined both the forward and reverse reaction rates for each aminotransferase. ^{1}H-^{13}C NMR analysis of the lysates showed efficient conversion of α-ketoglutarate to glutamate in the presence of either aspartate or alanine (5.32 ± 0.45 and 0.42 ± 0.03 μmol mL^{-1} lysate $hour^{-1}$, respectively), indicating that RBCs have a high enzymatic capacity for both AST and ALT reactions. Similarly, glutamate was efficiently converted to α-ketoglutarate in the presence of either pyruvate or oxaloacetate (Figure 3.5). As expected, rate constants observed for the forward and reverse reactions were comparable (Table 3.3).

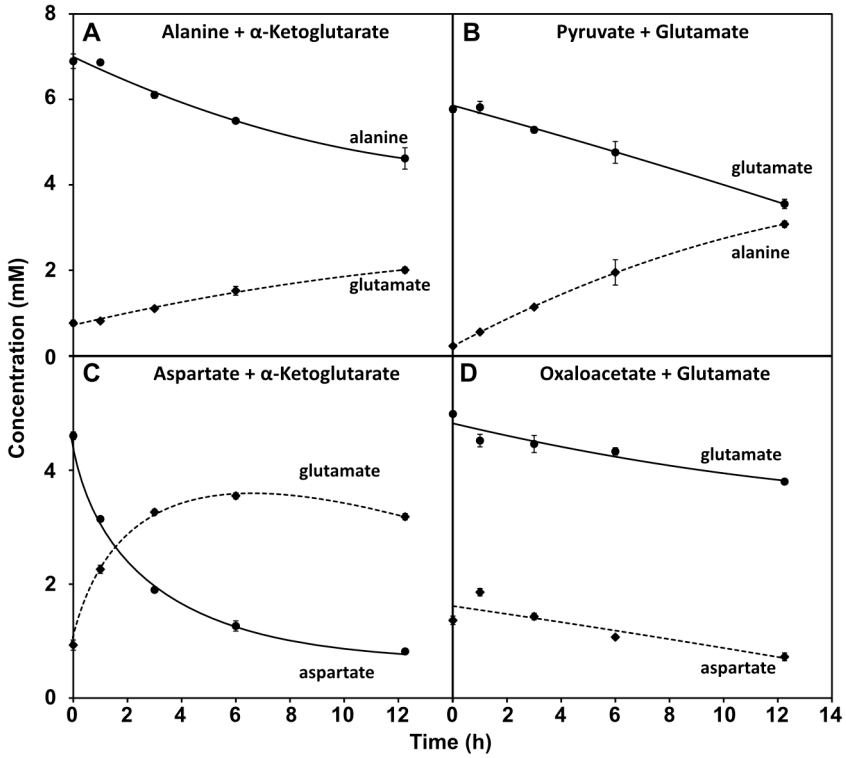

Figure 3.5. Aminotransferase reactions catalyzed by (A,B) alanine aminotransferase and (C,D) aspartate aminotransferase observed in human RBC lysates. Samples were incubated with 5 mM of each substrate and analyzed by ^{1}H-^{13}C NMR. The title of each plot indicates which substrates were added. Error bars represent S.E.M. ($n = 3$).

Table 3.3. Rates of ALT and AST aminotransferase reactions observed in RBC lysates.

	Observed rates (μmol mL^{-1} lysate $hour^{-1}$)[a]				
Metabolites added	Alanine	α-Ketoglutarate	Aspartate	Glutamate	Pyruvate
alanine+α-ketoglutarate[e]	-0.78±0.11	-0.77±0.08	n.o.[b]	0.42±0.03	0.46±0.03
glutamate+pyruvate[e]	0.94±0.03	0.57±0.01	n.o.[b]	-0.76± 0.04	-0.46±0.06
aspartate+α-ketoglutarate[f]	0.49±0.17	-3.23±0.75[c]	-5.85±0.30[c]	5.32±0.45[c]	0.73±0.05
glutamate+oxaloacetate[f]	-0.73±0.05	2.13±0.54[c]	1.98±0.53[c]	-1.87±0.28[c]	-0.18±0.04

[a] Means and S.E.M. for $n = 3$

[b] n.o. = not observed

[c] rate was calculated using the first two time points

[e] ALT pathway

[f] AST pathway

Interpretation of the AST reaction is complicated by the rapid spontaneous degradation of oxaloacetate to pyruvate (Hatch & Heldt, 1985). RBC lysates incubated with aspartate + α-ketoglutarate showed rates of alanine production comparable to samples incubated with pyruvate + glutamate (Table 3.3). This non-intuitive result is caused by a three-part coupled reaction involving conversion of aspartate to oxaloacetate via AST, spontaneous degradation of oxaloacetate to pyruvate (Hatch & Heldt, 1985), and the subsequent conversion of pyruvate to alanine via ALT.

Glutamate and glutathione synthesis in intact RBCs

GA is generally considered to be the main glutamate biosynthesis pathway in RBCs (Ellory et al., 1983; Griffith, 1981; Morris et al., 2008; Niihara et al., 1997), but the high levels of ALT and AST activity we observed in RBC lysates suggest that aminotransferases can have a significant impact on steady-state glutamate levels. However, the extent to which aminotransferases contribute to glutamate biosynthesis in intact cells is limited by the transport rates for the various substrates. Aspartate transport previously has been shown to be low (5 μM h^{-1}) (Fincham, Mason, Paterson, & Young, 1987; Maede, Inaba, & Taniguchi, 1983), and thus is a limiting factor in AST-derived glutamate production. However, the substrates of the GA and ALT reactions previously were shown to be efficiently transported at similar rates (108 and 256 μM h^{-1}, for glutamine and alanine respectively) (Ellory et al., 1983; Niihara et al., 1997), which argues that both GA and ALT reactions contribute to the glutamate pool. To determine

the relative contributions of ALT and GA to the total glutamate pool of intact cells, we incubated RBCs with ^{13}C labeled precursors of the ALT and GA reactions and measured the appearance of ^{13}C in glutamate and glutathione by ^{1}H-^{13}C NMR and LC-MS/MRM.

Rates of ALT-derived glutamate were derived from RBCs incubated for 21 h with glucose, alanine, and [$^{13}C_{1,2,3,4}$] α-ketoglutarate (5 mM each). Intact RBCs produced ^{13}C-enriched glutamate at an average rate of 0.17 μmol mL^{-1} RBC h^{-1} and consumed alanine at a rate of 0.11 μmol mL^{-1} RBC h^{-1} (Table 3.1). MS analysis showed that 89% ($p < 0.001$ relative to natural abundance) of the RBC glutamate pool was [$^{13}C_{1,2,3,4}$] labeled after 21 h (Table 3.4), indicating active *de novo* glutamate synthesis by intact cells. Although ALT-derived glutathione biosynthetic rates were below the NMR detection limit, MS analysis showed significant ($p < 0.05$ relative to natural abundance) $^{13}C_{1,2,3,4}$ isotopic enrichment in the glutamate moiety of glutathione at the 21 h time point and time-dependent enrichment of glutathione over the course of the experiment (Table 3.5). Rates of GA-derived glutamate production were derived from RBCs incubated in glucose (5 mM) and [U^{13}C-^{15}N] glutamine (1 mM). GA-derived glutamate was produced at a rate 30 times lower (0.0039 ± 0.00065 μmol mL^{-1} RBC h^{-1}) than rates observed for ALT-derived glutamate (Table 3.1).

Table 3.4. Isotopomer distribution of glutamate in RBCs incubated with [$^{13}C_{1,2,3,4}$] α-ketoglutarate, alanine, and glucose.

	Percent Mass isotopomer distribution (glutamate)[a]				
Time (h)	Monoisotopic	M+1	M+2	M+3	M+4
0	95.3±1.7	4.66±1.66	0	0	0
6	15.9±0.7**	0.72±0.08**	0.10±0.10	2.52±0.37*	80.8±0.3**
12	10.4±0.7**	0.41±0.01**	0	3.08±0.55*	86.1±0.9**
21.25	7.47±0.24**	0.24±0.01**	0	2.82±0.14*	89.4±0.3**
Expected distribution due to natural abundance	93.40	5.64	0.91	0.05	0.00

[a]Means and S.E.M. for $n = 3$

* $p < 0.05$; ** $p < 0.001$

Table 3.5. Isotopomer distribution of GSH in RBCs incubated with [$^{13}C_{1,2,3,4}$] α-ketoglutarate, alanine, and glucose.

	Percent Mass isotopomer distribution (GSH)[a]				
Time (h)	Monoisotopic	M+1	M+2	M+3	M+4
0	85.6±2.5	11.4±2.9	1.47±0.86*	1.59±0.81	0
6	86.6±1.1	7.99±0.19*	1.67±0.45*	0.33±0.33	3.42±0.33**
12	80.9±0.8	8.08±0.60	2.11±0.34*	0.80±0.42	8.09±0.15**
21.25	78.4±0.9*	7.96±0.67	1.03±0.52*	1.38±0.18*	11.3±1.2*
Expected distribution due to natural abundance	82.93	10.90	5.43	0.62	0.10

[a]Means and S.E.M. for $n = 3$

* $p < 0.05$; ** $p < 0.001$

3.5 Discussion

Human erythrocytes require a continual supply of glutamate to support glutathione synthesis, but are unable to transport this amino acid across their cell membrane (Sass, 1968; Winter & Christensen, 1964; D. J. Young et al., 1987). Although glutamine aminohydrolase is often cited as the main contributor to intracellular glutamate levels (Ellory et al., 1983; Griffith, 1981; Niihara et al., 1997), rates of glutathione biosynthesis are considerably higher than the maximum capacity of GA to produce glutamate. Even by conservative estimates (Griffith, 1981), demand from glutathione biosynthesis is nearly 8 times higher than the rates of GA-derived glutamate production observed in this study (Figure 3.6). The discrepancy between glutamate demand and GA's biosynthetic capacity argues that GA is a minor contributor to the glutamate pool.

In contrast to our GA findings, we found that up to 89% of the intracellular glutamate pool of intact cells can be attributed to alanine aminotransferase. ALT activity observed in this study exceeded GA activity by 30 fold and was considerably greater than demand from glutathione synthesis. As expected, ALT-derived glutamate is ultimately incorporated into glutathione. These findings clearly demonstrate that ALT can be a major contributor to steady-state glutamate levels of intact RBCs and argue that *in vivo* glutamate synthesis is predominantly attributable to ALT.

The biological significance of the high aspartate aminotransferase activity we observed in this study is unclear. Although RBC membranes are essentially impermeable to aspartate (Fincham et al., 1987; Maede et al., 1983), the intracellular

machinery for converting aspartate to glutamate is nearly 13 times more efficient than ALT. Since mature erythrocytes lack the enzymes required for oxaloacetate synthesis, the presence of AST cannot be attributed to aspartate biosynthesis. One possible explanation for the presence of AST is that the enzyme is a developmental holdover from reticulocytes, which synthesize oxaloacetate as a part of the tricarboxylic acid cycle (Gasko & Danon, 1972).

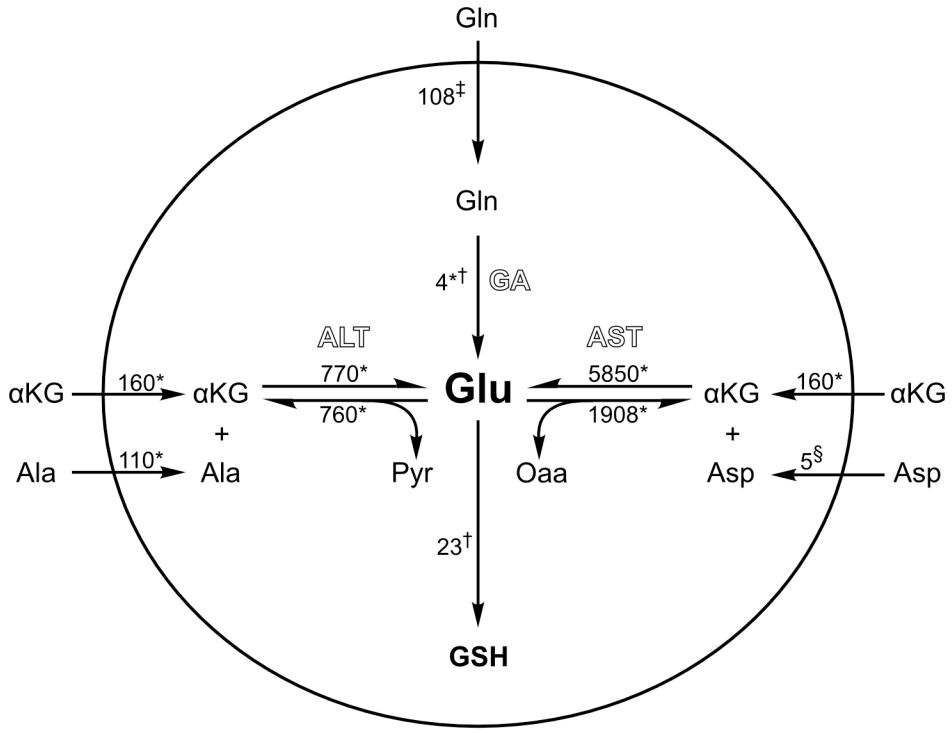

Figure 3.6. Three pathways for *de novo* glutamate synthesis in RBCs. Rates (μM h^{-1}) indicate NMR, MS and literature values for transport kinetics, alanine aminotransferase, aspartate aminotransferase, glutamine aminohydrolase, and glutathione biosynthesis. Abbreviations: Pyr, pyruvate; αKG, α-ketoglutarate; Oaa, oxaloacetate; amino acids are represented by their three letter codes. *Data from the current study; †data from (Griffith, 1981); ‡data from (Niihara et al., 1997); §data from (Fincham et al., 1987; Maede et al., 1983). Because of rapid kinetics of the aminotransferase reactions, alanine and α-ketoglutarate transport rates were assumed to be equivalent to the overall rates at which intact cells consumed these compounds.

In summary, we evaluated three possible pathways for glutamate production in RBCs using ^{1}H-^{13}C NMR and MS metabolomics techniques. Of these pathways, only ALT provides a plausible mechanism for supporting glutathione synthesis in intact cells. Given that human RBCs are readily permeable to cysteine and glycine (Harvey & Clive Ellory, 1989), and that all of the glutathione biosynthetic steps are well characterized (Majerus et al., 1971; Minnich et al., 1971), the ALT mechanism presented here provides a simple explanation for the sole unresolved step in glutathione biosynthesis.

3.6 Acknowledgments

We thank Dr. Philip S. Low and M. Estela Campanella (Purdue University) for collecting the blood used in this study. This work was supported by NIH grant P41 RR02301; I.A.L. was the recipient of a fellowship from the NHGRI 1T32HG002760; NMR data were collected at the National Magnetic Resonance Facility at Madison (NMRFAM) funded by NIH grants (P41 RR02301 and P41 GM GM66326).

Chapter 4

Targeted metabolite screening in AFEX-treated corn stover hydrolysates

4.1 Background

Conversion of lignocellulosic biomass to fuels has become a major goal for many scientists and nations. Currently, a large effort is underway to push the limits of ethanol production from *Saccharomyces cerevisiae* as well as to engineer ethanologenic *Escherichia coli*. I have collaborated with scientists at the Great Lakes Bioenergy Research Center (GLBRC) to provide metabolite data relevant to the development of these organisms.

To keep these studies in the context of real world biofuel production, engineered microbes are grown in ammonia fiber expansion pretreated corn stover hydrolysates (AFEXCSH) (Teymouri, Laureano-Pérez, Alizadeh, & Dale, 2004). Ammonia fiber explosion (AFEX) pretreatment is one of several processes that makes lignocellulosic material more susceptible to enzymatic hydrolysis; corn stover is residual leaves and stalks of corn (*Zea mays*) that remain in the field after harvest. Corn stover was treated by AFEX and then mixed with commercial mixtures of cellulase and hemicellulase enzymes. This final mixture, which contains glucose, xylose and other metabolites liberated from plant cells, is used as a growth media.

In this chapter I will present:

1) A general workflow for preparation, data collection and analysis of AFEXCSH samples.

2) An evaluation of automated shimming. One of the most important parameters for ensuring high quality NMR data is shimming. Automating this process has been

available for many years, and is especially useful within the metabolomics community. However, the performance of automated shimming for high-throughput metabolomics has not been reported in the literature. All data collected for AFEXCSH spent media samples was performed using automated shimming and we evaluated the performance using common metrics.

3) Data from two collaborations with GLBRC scientists.

4.2 Protocol for AFEXCSH sample preparation and data collection

Materials and reagents

Syringe filters (0.45 micron) were from Nalgene. Sodium azide (NaN_3, microbial growth inhibitor) was from Sigma-Aldrich. The following reagents were from Cambridge Isotope Laboratories: deuterated water (D_2O) and 2,2-dimethyl-2-silapentane-5-sulfonate (DSS, chemical shift reference standard). A micro pH combination electrode (part number: Z113441) from Sigma-Aldrich was used for titrating samples.

Sample collection and preparation

Samples were collected from continuous growth fermenters using AFEXCSH as the growth medium. At designated time points, 1 ml of sample was collected from the fermenter and centrifuged to clear *S. cerevisiae* or *E. coli* from the AFEXCSH spent media. Then the sample was filtered using a 0.45 micron syringe filter. Filtering served to remove large particles and residual microbial cells. Samples were frozen at -20 °C until further processing.

The samples were thawed, briefly vortexed, centrifuged at 12,000 RPM for 5 min and prepared for NMR as follows: 560 μl of AFEXCSH sample, 100 μl of D_2O containing 6.6 mM 2,2-dimethyl-2-silapentane-5-sulfonate(DSS) and 3.3 mM NaN_3 (H_2O:D_2O = 85%:15%). The resulting solution was titrated with concentrated HCl or NaOH as needed to achieve a glass electrode pH reading of 7.40 ± 0.05. If samples were not immediately used for data collection, they were frozen at -20 °C until data collection. For each sample, 550 μl was pipetted into a Bruker SampleJet 5 mm NMR tube and placed in a 96-tube rack. Occasionally samples formed precipitates, in those instances the sample was centrifuged at 12,000 RPM for 5 min prior to loading into an NMR tube.

NMR data collection, processing and analysis

NMR data were collected at the National Magnetic Resonance Facility at Madison on a Bruker Avance III spectrometer operating at 600 MHz for ^{1}H and equipped with a triple-resonance (^{1}H, ^{13}C, ^{15}N, ^{2}H lock) 5 mm cryogenic probe and SampleJet. The probe was tuned and matched for the first sample. Samples were maintained at 298 K. For each sample, data were collected as 1D ^{1}H (with water suppression) and 2D ^{1}H-^{13}C HSQC spectra. The T_1 inversion recovery experiment was used to determine an optimal interscan delay time for 1D ^{1}H experiments. All preset experimental parameters are listed in Table 4.1.

Table 4.1. Table of recommended experimental parameters used for data collection.

	Bruker pulse sequence	
	1D ^{1}H	2D ^{1}H-^{13}C HSQC
Parameter	*zgpr*	*hsqcetgpsisp2.2*
Spectral width (ppm)	10.5	10.5 (^{1}H), 70 (^{13}C)
Number of scans	32	4
Steady-state scans	0[†]	16
Number of data points	25,250	2524
Number of increments	not applicable	368
Interscan delay (s)	25	1.75
Presaturation power (W)	2.9×10^{-6}	not applicable
Data collection time (min)	15	49

[†]We originally chose to set this value to 8 scans. However with such a long interscan delay time (25 s), there is no reason to perform steady-state scans. By removing steady-state scans, we decreased data collection time by 3.3 minutes. The data presented below used the original value of 8 scans.

The entire data collection process was automated using a Python script written in-house by Dr. Larry Clos (NMRFAM staff scientist). Briefly, the script performed the following tasks prior to acquiring data: 1) sample switching, 2) sample temperature equilibration, 3) sample locking to D_2O, 4) automated 3D shimming using TopShim, 5) automatic calibration of the 90° pulsewidth and the transmitter offset frequency for ^{1}H, 6) automatic adjustment of receiver gain.

Data from 1D ^{1}H experiments were processed as follows using TopSpin 3.1: 1) phase-corrected, 2) zero-filled to 65,536 points, 3) application of squared cosine window function and 4) automatic baseline correction. Data from 2D ^{1}H-^{13}C were processed as follows with nmrPipe (Delaglio et al., 1995): 1) phase-corrected 2) a squared cosine window function was applied in both dimensions, 3) zero-filled to 4096 and 512 points in the ^{1}H and ^{13}C dimensions, respectively, 4) the ^{13}C dimension was shifted 27.5 ppm to the right by applying a circular shift. Initially 2D data were not processed using TopSpin because we were unaware of a function that could perform the circular shift, however we recently discovered the existence of a TopSpin AU program called '2df1shift', which performs a circular shift. 2D data are also correctly referenced in TopSpin using the macro 'Xnucref' written by Dr. Larry Clos.

Metabolites were identified using the Madison Metabolomics Consortium Database (MMCD) (Cui et al., 2008); assignments were verified by overlaying NMR spectra of standards from the BioMagResBank (BMRB) (Markley et al., 2007); All data were analyzed using rNMR (I. A. Lewis et al., 2009). For metabolites quantified by 1D ^{1}H,

peak volumes were calibrated to DSS. For metabolites quantified by 2D ^{1}H-^{13}C HSQC, peak intensities were calibrated to standards of known concentration from metabolite mixtures prepared at 3 different concentrations (Table 4.2). The standard mixtures were prepared in H_2O:D_2O (85%:15%) containing 1 mM DSS and 0.5 mM NaN_3. Each mixture was titrated to a glass electrode pH reading of 7.40 ± 0.05. The contents and high concentration value for each metabolite was chosen to reflect estimations from a pilot study. Concentrations measured in the NMR tube for each AFEXCSH sample were multiplied by 0.85^{-1} to account for dilution after addition of D_2O. I recommend repeated measures of the standard mixtures at regular intervals (i.e. every 20 samples) when a large number of samples are collected.

Table 4.2. Metabolite standard mixtures used for calibration. Each mixture was prepared in H_2O:D_2O (85%:%15) containing 1 mM DSS and 0.5 mM NaN_3. Each mixture was titrated to a glass electrode pH reading of 7.40 ± 0.05.

Metabolite	High mix (mM)	Mid mix (mM)	Low mix (mM)
Acetamide	21.08	10.54	4.22
Acetate	31.03	15.51	6.21
Alanine	3.29	1.64	0.66
Arabinose	49.99	25.00	10.00
Arginine	2.06	1.03	0.41
Asparagine	2.05	1.03	0.41
Aspartate	1.94	0.97	0.39
Betaine	8.30	4.15	1.66
Carnitine	2.00	1.00	0.40
Cellobiose	2.02	1.01	0.40
Choline	2.18	1.09	0.44
Citrate	2.40	1.20	0.48
Fructose	12.35	6.18	2.47
Galactose	5.21	2.61	1.04
Glucose	200.60	100.30	40.12
Glutamate	2.01	1.01	0.40
Glutamine	2.07	1.04	0.41
Glycine	2.38	1.19	0.48
Isocitrate	2.48	1.24	0.50
Isoleucine	2.01	1.01	0.40
Lactate	20.93	10.46	4.19
Leucine	2.18	1.09	0.44
Lysine	2.13	1.07	0.43
Malate	2.38	1.19	0.48
Mannose	5.02	2.51	1.00
Methionine	1.94	0.97	0.39
Phenylalanine	2.11	1.05	0.42
Proline	1.95	0.98	0.39
Serine	2.24	1.12	0.45
Succinate	10.55	5.28	2.11
Threonine	2.10	1.05	0.42
Valine	2.27	1.14	0.45
Xylose	199.90	99.95	39.98

4.3 Evaluation of automated shimming for AFEXCSH spent media samples

When a sample is inserted into an NMR spectrometer, inhomogeneities develop between the local magnetic field of the sample and the static field produced by the spectrometer. Perturbations arise from different sources such as solvent, tube quality, sample composition or ionic strength. These inhomogeneities lead to broad, low signal-to-noise peaks that compromise resolution and metabolite detection.

Shimming, in the modern day sense, is the process of correcting these inhomogeneities by altering the electric current flowing through specialized sets of coils that lay in the vicinity of the sample. Altering the current in turn affects the induction of the local magnetic field. The various coils are manipulated in an iterative fashion until the local magnetic field matches that of the field generated by the spectrometer. Although tedious, an experienced NMR spectroscopist should be able to shim a sample for metabolomics within 5 minutes. However, manual shimming presents a bottleneck for high-throughput data collection, because the spectroscopist must rest eventually.

Automated shimming is routinely used for collecting metabolomics data (Beckonert et al., 2007; Gronwald et al., 2008; Ward Jane et al., 2010; Mercier, Lewis, Chang, Baker, & Wishart, 2011; Verwaest et al., 2011). However, the performance of automated shimming for high-throughput metabolomics has not been reported.

For this study I utilized automated shimming and evaluated its performance toward data collection for AFEXCSH spent media. The data were collected on a 600 MHz

Bruker Avance III spectrometer running TopSpin 3.1 and shimming was conducted using TopShim with spectrum optimization (Weiger, Speck, & Fey, 2006).

A common strategy for shimming is to choose an isolated peak in the spectrum and manipulate the shim coils until the chosen peak is symmetric about a Lorentzian shape and the non-weighted linewidth (peak width at 50% of maximum intensity) reaches a predetermined value.

2,2-dimethyl-2-silapentane-5-sulfonate(DSS, Fig. 4.2A) is routinely added to samples as a chemical shift reference (set to 0 ppm) and internal standard. Furthermore, the peak observed from the degenerate trimethyl protons ($DSS(CH_3)_3$) is isolated from other peaks that arise from common metabolites. Therefore, I chose to use DSS for shimming.

When manually shimming, I try to shim the sample so that the non-weighted linewidth for the $DSS(CH_3)_3$ (Figure 4.2A) is 1.0 Hz or better. This is accomplished by employing what I will refer to as real-time Fourier transform shimming (RTFT shimming). This process involves continuously collecting a free induction decay, Fourier transformation and observing the resulting 1D ^1H spectrum zoomed into $DSS(CH_3)_3$. In this manner one can manipulate the shim coils while observing a real-time response. A linewidth of 1.0 Hz is sufficient to resolve key signals in a targeted assay, and this value is also less than most coupling constants, which can be useful when confirming metabolite assignments.

It is also good practice to use peak symmetry as another criterion for evaluating the quality of shimming. If a sample has been shimmed well, then the $DSS(CH_3)_3$ is symmetric and approximates a Lorentzian shape (Fig 4.2B). Furthermore, peaks due to coupling of ^{29}Si and ^{1}H will appear on both sides of the $DSS(CH_3)_3$ peak (Fig 4.2B). Achieving a high degree of symmetry and Lorentzian shape is important because all signals in a sample will show systematic errors if the shimming is bad. This may lead to signal overlap, unambiguous assignment and may negatively impact the accuracy of quantification.

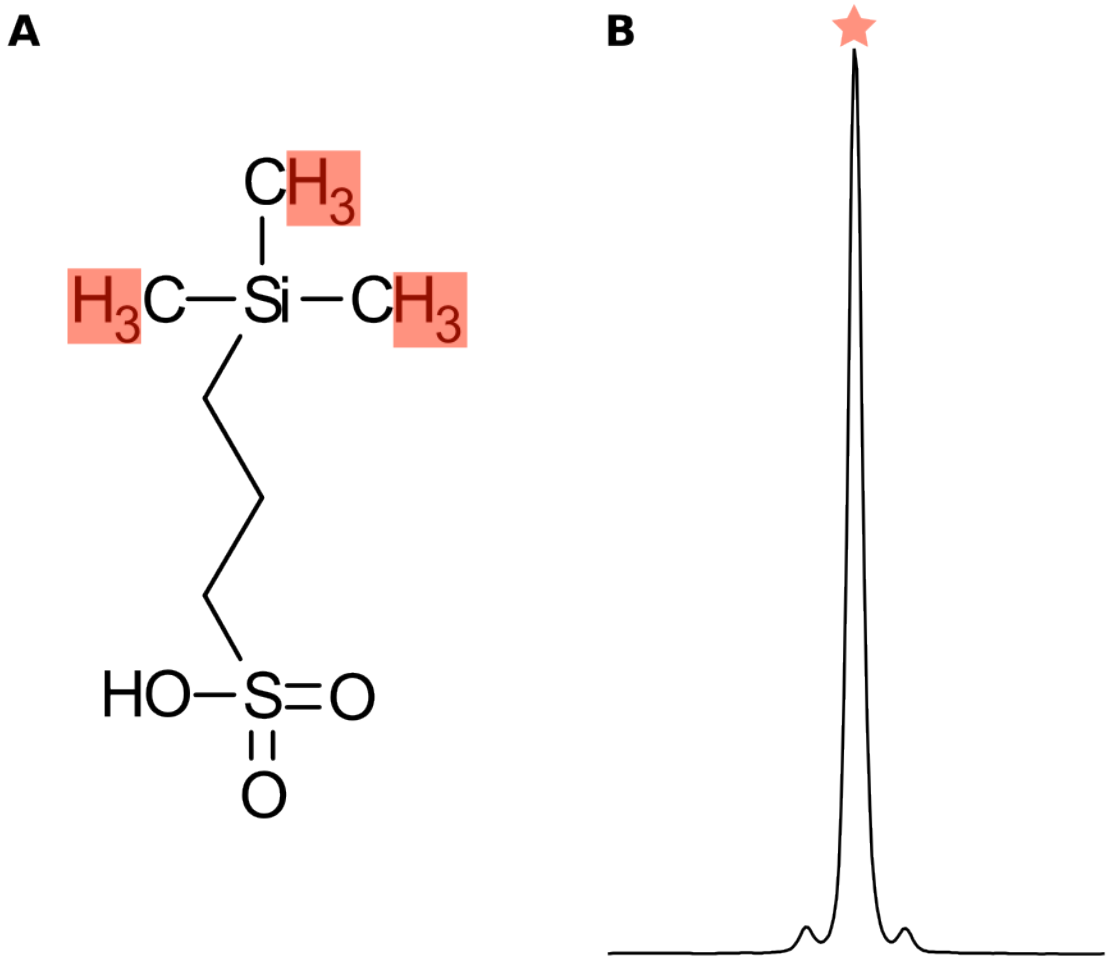

Figure 4.2. A) Structure of DSS. B) DSS-$(CH_3)_3$ peak found at 0 ppm. The three methyl groups appear as a single peak. The two flanking peaks represent coupling between ^{1}H and ^{29}Si ($^{2}J_{H\text{-}Si}$ = 3.3 Hz).

I evaluated the quality and reproducibility of automated shimming by first comparing the linewidth and peak shape of the $DSS(CH_3)_3$ signal from 97 spectra. I collected data for 82 AFEXCSH spent media samples over two data collection sessions. The three standard mixtures were collected in duplicate for the first session and in triplicate during the second session resulting in 15 spectra total.

Using automated shimming I found the average non-weighted linewidth for all samples to be 0.846 ± 0.104 Hz (mean ± standard deviation, $n = 97$). For AFEXCSH spent media samples the average was 0.864 ± 0.096 Hz ($n = 82$). For the standards the average was 0.749 ± 0.098 Hz ($n = 15$). A histogram displaying the range of values obtained is shown in Figure 4.3. These values indicate that automated shimming performed well and was reproducible for AFEXCSH spent media samples.

However, linewidth alone is not the only criterion for assessing shim quality. I also evaluated the quality of automated shimming by judging the peak symmetry of $DSS(CH_3)_3$. Table 4.3 describes our grading scheme. Figure 4.4 shows examples of grades described in Table 4.3. All spectra were weighted with a squared cosine function to remove sinc wiggles.

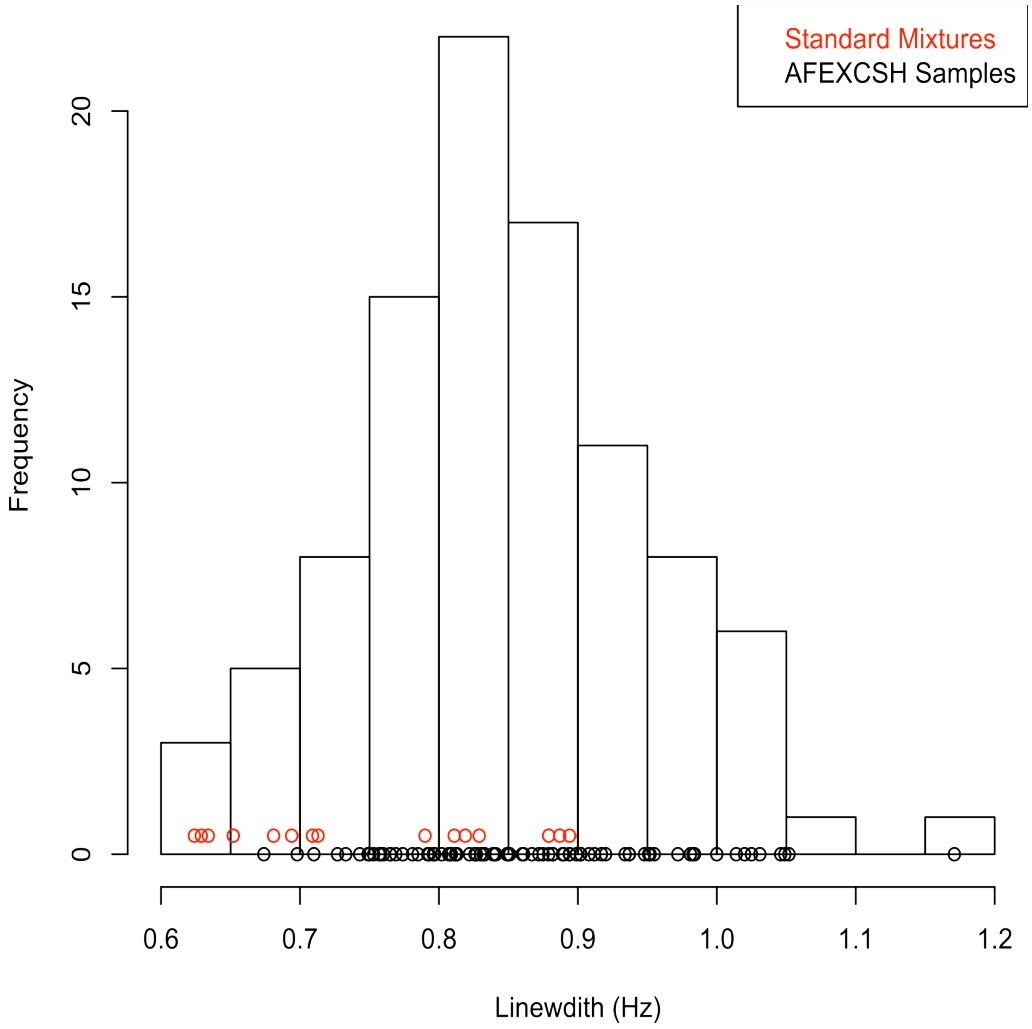

Figure 4.3. Histogram of linewidths obtained from automated shimming. Circles overlaid on histogram represent observed values.

Table 4.3. Shim grading visual analysis criteria.

Grade	Description	Example
A	Peakshape is symmetric with well-resolved ^{29}Si peaks; Completely acceptable for data collection.	Fig. A.3A
B	Slight or noticeable asymmetry; ^{29}Si peaks are evident but less well resolved; Acceptable, although provided adequate experimental time, fix shim problems and recollect data.	Fig. A.3B
C	Large asymmetry; One or both ^{29}Si peaks absent; Unacceptable for data collection, must fix shim problems and recollect data.	none

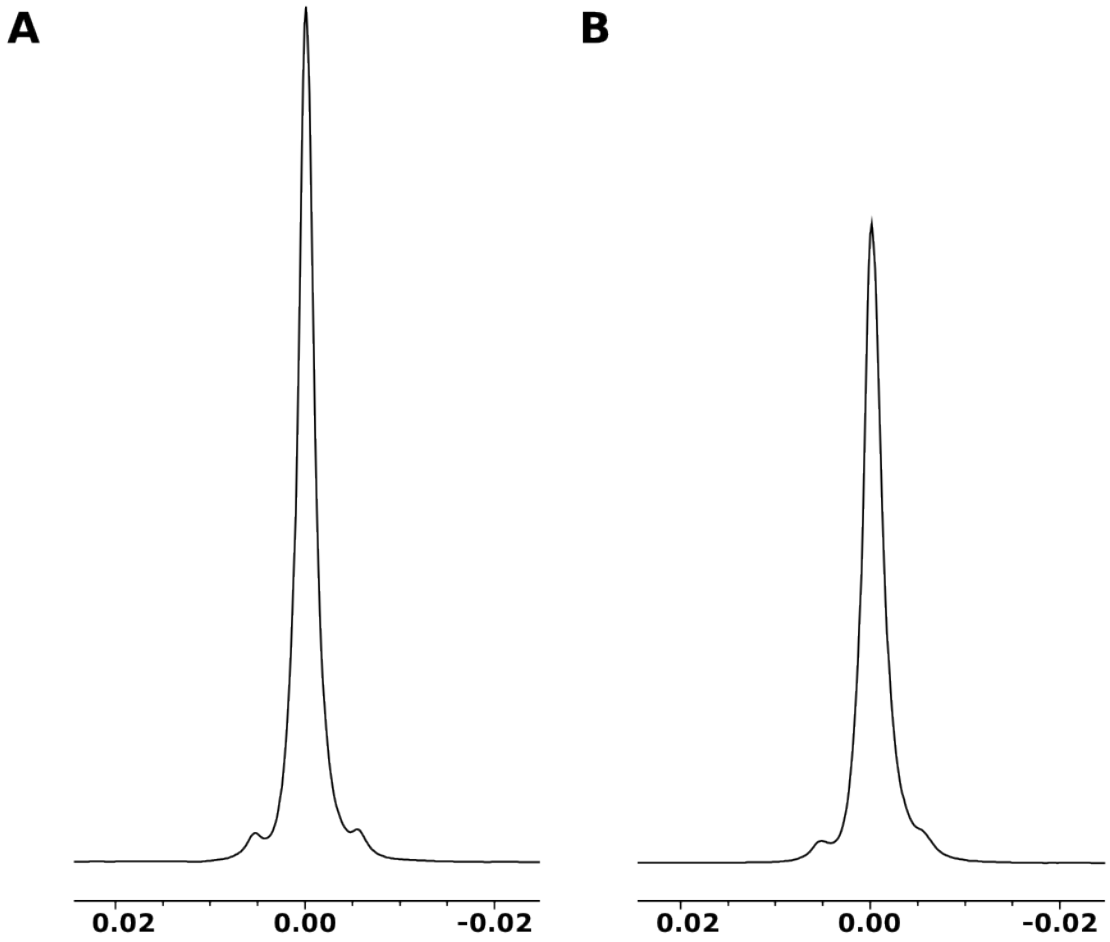

Figure 4.4. Examples of grades A and B peak shapes for $DSS(CH_3)_3$ in AFEXCSH spent media samples. Data are from AFEXCSH spent media samples. Both spectra had the same receiver gain and were weighted with a squared cosine function to remove sinc wiggles.

Based on my grading scheme, 82% of the spectra received an A rating while 18% received a B rating. No samples received a C rating! These results provide further indication that automated shimming for AFEXCSH spent media samples is of high, reproducible quality.

An important aside to point out is that while I shim using 1D NMR, our assay is primarily based 2D NMR. As a result, some of the resolution gained from good shimming is lost because of limitations in the amount of data that can be digitally recorded during a multidimensional experiment, although that loss of resolution is replaced by a gain in peak dispersion by having two dimensions of data. Most importantly though, good shimming effectively increases signal-to-noise, even within the context of a 2D ^{1}H-^{13}C HSQC experiment, and, therefore, good shimming is rewarded.

In conclusion I found that automated shimming using TopShim on a Bruker Avance III 600 MHz spectrometer yields high quality, reproducible shimming for AFEXCSH spent media samples. The quality of shimming was more than adequate for assaying by 2DFMQ and is very promising for conducting NMR-based metabolomics within the framework of 1D NMR.

4.4 Effect of sample rotation on AFEXCSH samples

In order to conduct targeted analyses within the framework of 1D NMR, further improvements in shimming and even higher reproducibility may be desirable. A well-established method for improving shimming is to rotate the sample in the bore during data collection. By providing this motion to the molecules within the sample, the

effective homogeneity of the magnetic field can be improved. However, using this method is undesirable for methods such as 2DFMQ due to the use of pulsed field gradients in the HSQC pulse sequence.

One potential drawback of sample rotation is the generation of spinning side bands, which arise from poor shimming in the axes perpendicular to the axis of rotation (off-axis shims). The spinning sidebands are signals that flank the signal of interest and they occur at integer multiples of the sample rotation rate.

I investigated the effects of sample rotation using one standard mixture (Mid mix from Table 4.2) and one AFEXCSH sample. The protocol was modified slightly from that listed above in that sample rotation was turned on after the automated shimming followed by a second round of automated shimming in which only the axis of rotation was shimmed. The second shimming procedure only requires about 30 seconds.

Sample rotation speeds of 8, 12, 16 and 20 Hz were all capable of improving the linewidth of $DSS(CH_3)_3$ (Figure 4.5) Sample rotation of the standard mix only improved linewidth by 0.180 Hz (at 12 Hz rotation and above), whereas an AFEXCSH sample that only achieved a B grade autoshim was reduced by 0.524 Hz (at 16 Hz rotation) and reassigned to a grade A shim based on lineshape (Figure 4.6).

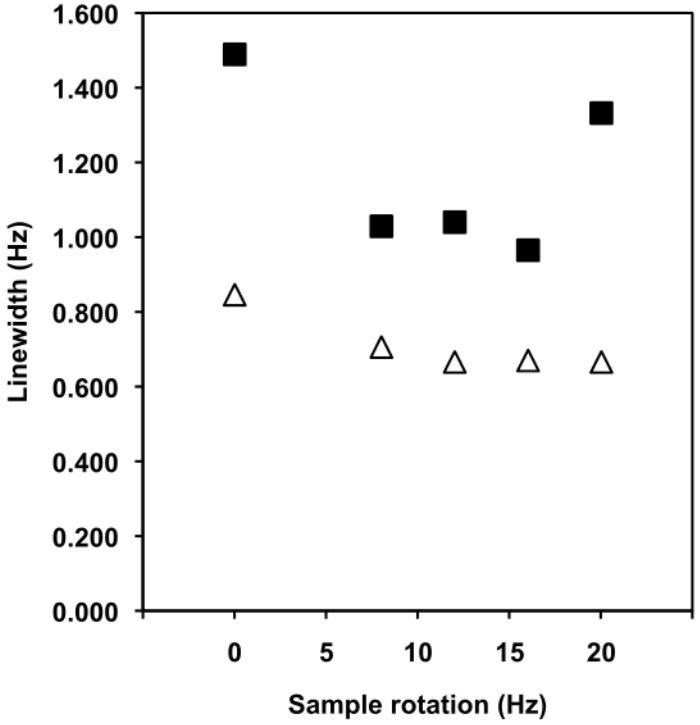

Figure 4.5. Effect of sample rotation rate on linewidth of $DSS(CH_3)_3$. Filled squares represent an AFEXCSH sample, and triangles represent a standard mixture (Mid mix, Table 4.2). The minimum (instrument limited) sample rotation rate was 7 Hz.

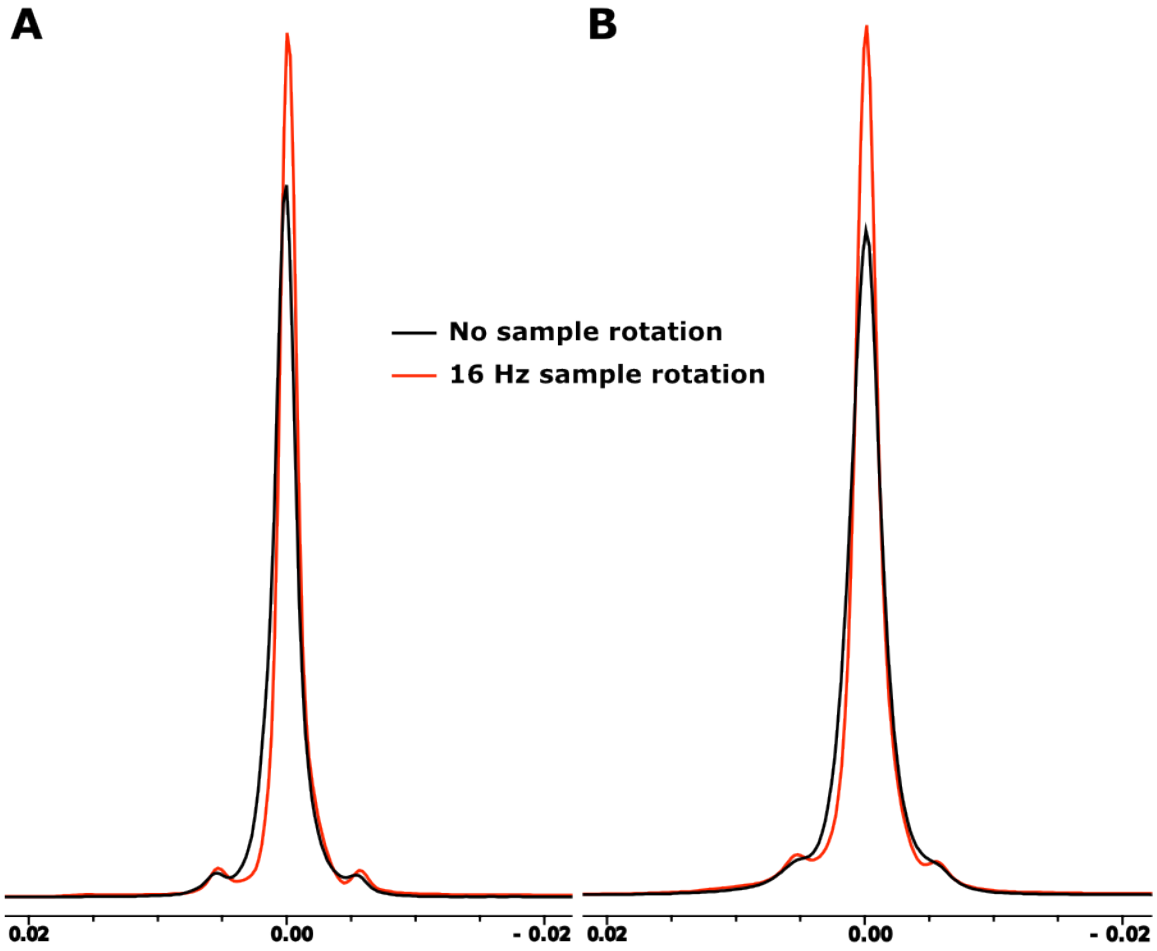

Figure 4.6. Lineshape comparison of (A) a standard mixture (Mid mix, Table 4.2) and (B) an AFEXCSH sample during sample rotation. Spinning noticeably improved the lineshape of the AFEXCSH sample.

From this preliminary investigation it appeared that sample rotation provided only a modest improvement in shimming for a standard mixture that already achieved high quality shimming. In contrast, sample rotation significantly improved the lineshape of an AFEXCSH sample which initially achieved mediocre shimming. Furthermore, no spinning sidebands were present, indicating that even in the AFEXCSH sample off-axis shims were correctly determined during the first round of automated shimming.

A more thorough analysis should be conducted on a larger dataset to ensure reproducibility, but sample rotation does appear offer an approach to improved shimming for 'troublesome' samples when conducting 1D ^{1}H NMR assays.

4.5 Analysis of AFEXCSH in ethanologenic *E. coli* fermentations

The following data are adapted from:

Schwalbach M, Keating D, Tremaine M, Marner W, Zhang Y, Bothfeld W, Higbee A, Grass J, Cotton C, Reed J, da Costa Sousa L, Jin M, Balan V, Ellinger J, Dale B, Kiley P, Landick, R (2012) *Complex physiology and compound stress responses during fermentation of alkaline-pretreated corn stover hydrolysate by an Escherichia coli ethanologen*. Applied and Environmental Microbiology 78(9), 3442-3457

My role in the project: I carried out NMR analyses of the concentrations of a set of metabolites present in AFEXCSH at the beginning and end of a 124-hour fermentation.

The goal of this study was to characterize how ethanologenic *E. coli* responds metabolically and transcriptionally to concentrated hydrolysates derived from alkali-pretreated lignocellulose, with ACSH as the test case. The study was conducted using an ethanologenic *E. coli* K-12 strained developed by the GLBRC. The results of one of my analyses are presented in Table 4.4.

Table A.4. NMR analysis of AFEXCSH at the beginning and end of fermentation.

Compound	0 hours (mM)	124 hours (mM)
Glucose	358.2	17.6
Xylose	198.5	176.4
Arabinose	33.7	16.4
Fructose	8.2	0
Galactose	6.4	5
Mannose	2.6	0
Malate	9.3	0
Acetamide	75.8	70.4
Acetate	33.3	41.5
Succinate	0.3	62
Ethanol	55	273
Betaine	0.7	0.6
Choline	0.7	0.7
Carnitine	0.2	0.1
Alanine	0.8	1.1

In this study, gene expression experiments were conducted using a synthetic hydrolysate (SynH) and glucose minimal media for comparison with AFEXCSH. SynH was a defined medium that was based on metabolites and micronutrients characterized in AFEXCSH.

My analysis, which was conducted after SynH formulation, showed that several metabolites were missing from SynH. By NMR I identified the following metabolites that were not characterized by other methods: acetamide, fructose, choline, betaine, carnitine and malate. Acetamide was of particular interest due to its high concentration and potential implication in osmotic stress. Malate and fructose may also be of interest because they were completely consumed by *E. coli*, which could have implications toward understanding inefficient use of other carbon sources, such as xylose, for energy. I expect that one of the major contributions of my analysis will be toward improved future formulations of SynH.

4.6 Analysis of AFEXCSH in *S. cerevisiae* fermentations

The following data were generated from a collaboration with Dr. Trey Sato in the GLBRC. His group is interested in using comparative multi-omic analyses (transcriptomics, metabolomics, etc.) of engineered *S. cerevisiae* to identify bottlenecks in biofuel fermentation. One of the goals of their work was to compare evolved and unevolved strains with different abilities to ferment xylose.

We evaluated four strains of *S. cerevisiae*: 1) GLBRC2YA was wild-type *S. cerevisiae* engineered with *Pichia stipitis* XYL1-3; 2) GLBRCY79 and GLBRCY73 were substrains evolved from GLBRCY2A on yeast lab media + 2% xylose for 36 generations; 3) GLBRCY4A was wild-type *S. cerevisiae* engineered with *Clostridium phytofermentans* XylA, *P. stipitis* XYL3 and *S. cerevisiae* TAL1.

I provided time-course analyses for metabolites present in AFEXCSH spent media samples at the beginning and end of 120 hour fermentations (in one data set the fermentation lasted 148 hours). All time-course data are presented in Table 4.5 through Table 4.8.

Table 4.5. Metabolite data for strain GLBRC2YA (wild-type *S. cerevisiae* engineered with *Pichia stipitis* XYL1, 2 and 3). Data are reported in mM as mean ± SEM (n = 3 unless otherwise indicated). Timepoints were not exactly the same for all experiments, so the average was taken for similar time points, n = 3 unless otherwise indicated.

	GLBRCY2A Time(hrs)							
Metabolite	**0**	**12.74**	**22.19†**	**24.83‡**	**27.22†**	**47.81**	**119.72**	**143.88‡**
Ace	32.77±0.94	31.16±0.77	28.13±0.53	28.29	27.69±0.51	28.40±0.69	27.31±0.97	29.60
Ala	0.78±0.01	0.53±0.02	0.27±0.07	0.38	0.34±0.01	0.39±0.03	0.48±0.03	0.51
Amd	70.35±1.74	70.45±1.50	68.46±2.34	70.39	68.28±0.59	69.46±1.74	71.44±2.63	71.84
Ara	32.94±0.73	31.80±1.15	30.16±0.07	30.98	29.40±0.96	30.09±1.23	27.88±1.53	29.86
Bet	0.57±0.00	0.53±0.01	0.51±0.02	0.56	0.51±0.00	0.54±0.01	0.52±0.02	0.57
Cho	0.61±0.04	0.55±0.00	0.39±0.00	0.44	0.41±0.02	0.44±0.03	0.41±0.03	0.45
Crn	0.17±0.01	0.17±0.00	0.16±0.00	0.18	0.16±0.00	0.17±0.01	0.16±0.01	0.18
Eth	0.00±0.00	212.85±7.39	464.26±28.12	520.50	483.53±4.64	466.52±23.90	287.68±52.59	428.23
For	5.66±0.29	5.70±0.18	4.92±0.23	5.02	5.04±0.09	4.89±0.05	4.37±0.08	4.66
Fru	5.68±0.07	4.58±0.17	0.00±0.00	0.00	0.00±0.00	0.00±0.00	0.00±0.00	0.00
Gal	5.54±0.14	5.57±0.21	5.18±0.16	5.98	5.24±0.10	5.39±0.21	5.01±0.13	5.30
Glc	304.61±9.88	181.82±11.13	13.39±0.06	11.14	10.42±0.20	10.39±0.73	8.07±0.26	8.61
Gly	0.38±0.02	0.31±0.03	0.23±0.05	0.28	0.26±0.01	0.27±0.02	0.29±0.03	0.32
Lac	10.48±0.31	10.97±0.22	11.69±0.56	12.12	11.50±0.01	11.52±0.31	11.11±0.54	11.43
Leu	0.43±0.01	0.03±0.03	0.00±0.00	0.00	0.00±0.00	0.00±0.00	0.00±0.00	0.00
Mal	6.44±0.32	6.78±0.23	6.29±0.46	6.34	6.56±0.05	6.29±0.01	6.43±0.03	6.48
Man	2.07±0.02	1.95±0.12	0.00±0.00	0.00	0.00±0.00	0.00±0.00	0.00±0.00	0.00
Ser	0.56±0.02	0.47±0.03	0.53±0.01	0.48	0.44±0.02	0.47±0.06	0.37±0.03	0.35
Suc	0.57±0.03	0.72±0.03	0.78±0.04	0.94	0.74±0.01	0.81±0.05	0.76±0.05	0.91
Val	0.30±0.01	0.08±0.08	0.00±0.00	0.00	0.00±0.00	0.00±0.00	0.00±0.00	0.00
Xyl	198.06±4.82	192.87±6.51	177.79±1.31	187.76	171.12±2.43	163.54±7.08	107.53±4.50	125.00

†Data was only available in duplicate

‡Only single dataset available

Metabolite key code: Ace, acetate; Ala, alanine; Amd, acetamide; Ara, arabinose; Bet, betaine; Cho, choline; Crn, carnitine; Eth, ethanol; For, formate; Fru, fructose; Gal, galactose; Glc, glucose; Gly, glycine; Lac, lactate; Leu, leucine; Mal, malate; Man, mannose; Ser, serine; Suc, succinate; Val, valine; Xyl, xylose.

Table 4.6. Metabolite data for strain GLBRCY79 (GLBRCY2A evolved on yeast lab media + 2% xylose for 36 generations). Data are reported in mM as mean ± SEM (n = 3 unless otherwise indicated). Timepoints were not exactly the same for all experiments, so the average was taken for similar time points, n = 3 unless otherwise indicated.

	GLBRCY79 Time(hrs)							
Metabolite	**0**	**12.74**	**22.19†**	**24.83‡**	**27.22†**	**47.81**	**119.72**	**143.88‡**
Ace	31.83±0.69	31.33±0.85	30.16±0.01	27.32	28.29±0.01	29.21±1.45	29.38±0.97	27.44
Ala	0.74±0.01	0.50±0.01	0.35±0.04	0.34	0.31±0.00	0.40±0.03	0.46±0.02	0.45
Amd	68.33±1.23	69.69±0.99	73.13±0.35	68.05	70.11±1.26	70.38±2.80	72.26±1.89	69.22
Ara	30.97±0.56	31.39±0.47	30.91±0.57	28.24	28.91±0.81	30.16±0.66	27.96±0.49	27.57
Bet	0.54±0.01	0.53±0.01	0.54±0.00	0.53	0.51±0.02	0.54±0.00	0.53±0.02	0.53
Cho	0.60±0.01	0.53±0.01	0.41±0.03	0.45	0.40±0.01	0.41±0.01	0.41±0.01	0.43
Crn	0.17±0.00	0.17±0.00	0.17±0.00	0.17	0.16±0.00	0.17±0.00	0.17±0.00	0.17
Eth	0.00±0.00	213.82±10.31	529.13±8.77	513.01	509.98±17.33	471.65±20.74	365.83±39.29	421.92
For	5.74±0.23	5.82±0.10	5.40±0.03	5.05	4.95±0.14	5.18±0.11	5.06±0.03	4.72
Fru	5.45±0.10	4.48±0.13	0.00±0.00	0.00	0.00±0.00	0.00±0.00	0.00±0.00	0.00
Gal	5.30±0.09	5.26±0.07	5.77±0.06	5.61	5.44±0.14	5.36±0.05	5.07±0.10	5.05
Glc	305.77±3.12	183.39±8.72	12.35±0.01	10.96	10.07±0.29	9.87±0.35	8.08±0.45	7.31
Gly	0.37±0.00	0.31±0.01	0.26±0.01	0.27	0.23±0.01	0.26±0.01	0.28±0.01	0.26
Lac	10.19±0.22	10.83±0.07	12.31±0.24	11.70	11.67±0.09	11.72±0.58	11.44±0.66	11.27
Leu	0.42±0.01	0.00±0.00	0.00±0.00	0.00	0.00±0.00	0.00±0.00	0.00±0.00	0.00
Mal	6.18±0.29	6.76±0.22	6.94±0.09	6.36	6.49±0.15	6.73±0.22	6.78±0.20	6.54
Man	2.15±0.06	1.74±0.00	0.00±0.00	0.00	0.00±0.00	0.00±0.00	0.00±0.00	0.00
Ser	0.60±0.05	0.53±0.07	0.44±0.01	0.34	0.40±0.00	0.45±0.03	0.35±0.03	0.34
Suc	0.54±0.03	0.71±0.03	0.78±0.04	0.85	0.75±0.04	0.82±0.03	0.78±0.06	0.79
Val	0.29±0.02	0.05±0.05	0.00±0.00	0.00	0.00±0.00	0.06±0.06	0.00±0.00	0.00
Xyl	194.20±2.07	190.59±4.55	182.17±3.49	174.34	166.64±4.94	147.93±9.60	92.01±6.86	67.35

†Data was only available in duplicate

‡Only single dataset available

Table 4.7. Metabolite data for strain GLBRCY73 (also from GLBRCY2A evolved on yeast lab media + 2% xylose for 36 generations). Data are reported in mM as mean ± SEM (n = 3 unless otherwise indicated). Timepoints were not exactly the same for all experiments, so the average was taken for similar time points, n = 3 unless otherwise indicated.

	GLBRCY73 Time(hrs)							
Metabolite	**0**	**12.74**	**22.19†**	**24.83‡**	**27.22†**	**47.81**	**119.72**	**143.88‡**
Ace	32.87±0.46	28.86±1.07	29.19±0.71	28.95	27.48±1.67	26.90±0.81	28.21±1.22	27.12
Ala	0.78±0.02	0.48±0.04	0.31±0.03	0.27	0.19±0.02	0.26±0.04	0.31±0.01	0.36
Amd	70.28±1.02	65.26±2.55	70.15±1.00	71.75	69.15±1.64	68.00±0.98	71.01±2.17	67.64
Ara	32.19±0.55	29.51±1.19	30.22±1.23	30.94	28.08±1.09	28.24±0.74	26.32±0.29	28.72
Bet	0.56±0.01	0.52±0.03	0.54±0.01	0.56	0.51±0.02	0.51±0.01	0.51±0.00	0.53
Cho	0.61±0.02	0.50±0.03	0.42±0.00	0.43	0.42±0.00	0.36±0.02	0.39±0.02	0.40
Crn	0.17±0.00	0.16±0.01	0.16±0.01	0.17	0.16±0.00	0.15±0.01	0.16±0.01	0.17
Eth	0.00±0.00	180.49±12.54	488.12±4.32	539.99	493.08±8.13	477.45±17.96	381.25±65.41	459.09
For	5.89±0.03	5.28±0.17	5.23±0.10	5.18	4.79±0.07	4.93±0.13	5.00±0.30	5.01
Fru	5.65±0.09	4.39±0.18	0.00±0.00	0.00	0.00±0.00	0.00±0.00	0.00±0.00	0.00
Gal	5.46±0.07	4.96±0.19	5.46±0.30	5.31	5.15±0.03	5.08±0.07	4.87±0.11	4.67
Glc	307.05±5.06	188.28±4.85	14.14±0.15	11.28	10.04±0.36	9.41±0.27	7.57±0.21	7.20
Gly	0.36±0.01	0.29±0.02	0.25±0.04	0.25	0.18±0.03	0.21±0.03	0.23±0.02	0.25
Lac	10.52±0.11	9.96±0.48	11.66±0.53	12.03	11.34±0.20	11.08±0.01	11.24±0.45	10.77
Leu	0.41±0.00	0.00±0.00	0.00±0.00	0.00	0.00±0.00	0.00±0.00	0.00±0.00	0.00
Mal	6.59±0.01	6.23±0.22	6.87±0.18	6.43	6.25±0.00	6.47±0.04	6.32±0.01	6.55
Man	2.11±0.01	1.76±0.06	0.00±0.00	0.00	0.00±0.00	0.00±0.00	0.00±0.00	0.00
Ser	0.55±0.01	0.43±0.03	0.48±0.09	0.39	0.40±0.02	0.38±0.05	0.37±0.03	0.28
Suc	0.56±0.02	0.71±0.06	0.78±0.01	0.96	0.76±0.02	0.80±0.04	0.76±0.03	0.84
Val	0.30±0.03	0.05±0.05	0.00±0.00	0.00	0.00±0.00	0.00±0.00	0.00±0.00	0.00
Xyl	195.26±4.58	182.12±6.37	187.17±5.24	176.47	163.13±0.49	143.32±5.15	75.88±5.71	63.65

†Data was only available in duplicate

‡Only single dataset available

Table 4.8. Metabolite data for strain GLBRCY4A (wild-type *S. cerevisiae* engineered with *Clostridium phytofermentans* XylA, *P. stipitis* XYL3 and *S. cerevisiae* TAL1.). Data are reported in mM as mean ± SEM (n = 3 unless otherwise indicated). Timepoints were not exactly the same for all experiments, so the average was taken for similar time points, n = 3 unless otherwise indicated.

	GLBRCY4A Time(hrs)							
Metabolite	**0**	**12.74**	**22.19†**	**24.83‡**	**27.22†**	**47.81**	**119.72**	**143.88‡**
Ace	32.81±0.46	31.26±0.55	29.82±0.63	26.49	28.00±0.32	29.59±0.96	32.73±1.33	30.10
Ala	0.78±0.01	0.56±0.00	0.35±0.09	0.40	0.32±0.10	0.38±0.04	0.48±0.02	0.47
Amd	70.70±0.98	70.39±0.91	73.37±4.06	66.71	69.89±3.08	71.12±1.44	72.51±2.18	69.65
Ara	32.92±0.44	31.20±0.90	30.62±1.46	30.50	29.17±1.85	30.02±1.47	29.53±1.40	30.84
Bet	0.56±0.02	0.55±0.01	0.55±0.03	0.57	0.53±0.01	0.54±0.02	0.54±0.02	0.56
Cho	0.62±0.02	0.53±0.03	0.42±0.02	0.45	0.39±0.01	0.41±0.02	0.41±0.03	0.48
Crn	0.18±0.01	0.17±0.01	0.17±0.01	0.17	0.17±0.01	0.17±0.01	0.17±0.01	0.18
Eth	0.00±0.00	200.67±17.94	526.72±35.85	500.09	495.76±21.92	473.33±19.87	311.43±46.79	344.25
For	5.79±0.29	5.86±0.08	5.45±0.09	4.91	4.89±0.34	5.01±0.14	4.47±0.17	4.27
Fru	5.68±0.06	4.71±0.18	0.00±0.00	0.00	0.00±0.00	0.00±0.00	0.00±0.00	0.00
Gal	5.50±0.14	5.49±0.19	5.46±0.56	5.49	5.44±0.28	5.23±0.23	5.32±0.24	5.36
Glc	308.68±8.51	195.65±15.97	12.72±0.12	10.92	10.11±0.64	9.96±0.17	8.82±0.28	8.22
Gly	0.38±0.02	0.34±0.01	0.24±0.02	0.28	0.25±0.02	0.26±0.02	0.27±0.02	0.31
Lac	10.50±0.17	10.88±0.06	12.15±0.54	11.35	11.49±0.52	11.82±0.18	11.55±0.30	10.85
Leu	0.45±0.01	0.00±0.00	0.00±0.00	0.00	0.00±0.00	0.00±0.00	0.00±0.00	0.00
Mal	6.39±0.30	6.97±0.18	6.97±0.33	6.63	6.53±0.48	6.48±0.34	6.66±0.33	6.32
Man	2.07±0.04	2.05±0.07	0.00±0.00	0.00	0.00±0.00	0.00±0.00	0.00±0.00	0.00
Ser	0.62±0.03	0.57±0.03	0.51±0.02	0.35	0.44±0.06	0.42±0.05	0.38±0.04	0.29
Suc	0.57±0.02	0.73±0.03	0.82±0.03	0.86	0.78±0.02	0.85±0.05	0.81±0.03	0.89
Val	0.31±0.01	0.06±0.06	0.00±0.00	0.00	0.00±0.00	0.00±0.00	0.00±0.00	0.00
Xyl	199.37±2.71	195.60±2.44	186.82±11.30	185.91	177.15±5.39	173.90±6.08	148.85±9.26	153.88

†Data was only available in duplicate

‡Only single dataset available

The major goal was to profile carbohydrate usage and ethanol production in AFEXCSH. A time-course showing the relationship between carbohydrate consumption, ethanol production and cell density is shown in Figure 4.7 from a representative dataset. All strains appeared to reach the same cell density at stationary phase. Strain GLBRCY73 was the most successful at utilizing xylose.

Interestingly, ethanol levels peaked at the same time that glucose levels bottomed out, however ethanol levels then dropped even though xylose was consumed. Carbon from xylose is expected to enter glycolysis via the pentose phosphate pathway, at which point the path to ethanol can continue. At this point it is unclear why the ethanol levels dropped. It also is unclear how much xylose was actually converted to ethanol. One way to determine if xylose is converted to ethanol might be to add ^{13}C labeled xylose to the AFEXCSH, or possibly SynH, and measure ^{13}C incorporation into ethanol.

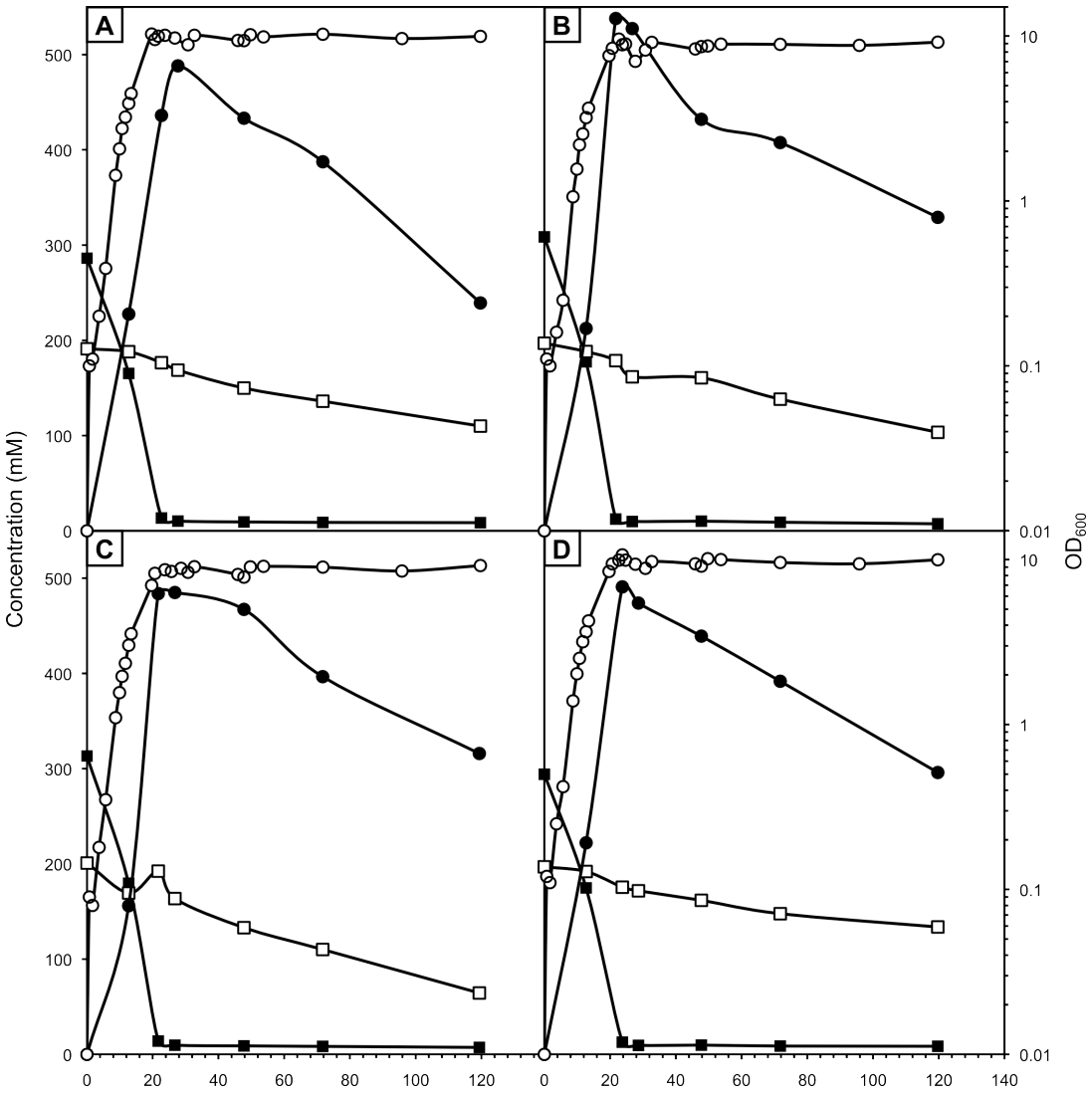

Figure 4.7. Carbohydrate consumption, ethanol production and cell density in AFEXCSH for GLBRCY2A (A), GLBRCY79 (B), GLBRCY73 (C) and GLBRCY4A (D). Symbol key: ○ cell density, ● ethanol, □ xylose, ■ glucose. This data represents one experiment of three that were conducted to evaluate these strains of *S. cerevisiae*. Cell density data was provided by Dr. Trey Sato.

Chapter 5

Conclusions and Outlook

Throughout the course of my Ph.D. training I have had the opportunity to receive world-class NMR training and to apply that knowledge to metabolomics. I have used metabolomics techniques to study basic biochemical mechanisms in human erythrocytes and to profile metabolites in complex media used for engineering improved ethanologenic organisms. Furthermore, I have made a significant contribution toward improving the efficiency and reproducibility of sample preparation for metabolite samples.

I think the major role in the future for NMR in metabolomics will be in synergy with MS. The current push in high throughput metabolomics is to do more with less. To be able to reach the level of science fiction we need the ability to analyze 10-fold as many metabolites as currently possible in a single drop of blood or urine in the blink of an eye. Sadly, NMR cannot accomplish this. However, based on current database knowledge, neither can MS alone solve this problem.

The future for NMR in metabolomics will be its utility in the identification of novel metabolites with which we can continue to populate our databases. This will be in conjunction with integrated LC-MS-SPE-NMR systems (SPE, solid phase extraction). In this setup, metabolites are partitioned by LC and then directed by mass to SPE columns. Collection on the SPE columns will allow metabolites to be concentrated prior to NMR analysis. Over the next decade, I expect to see an explosion in the number of metabolites populating the various databases.

Appendix A

NMR-based study of extracellular metabolites produced by *E. coli* K12 under butanol stress

The following Appendix presents a short project I conducted at the RIKEN Yokohama Institute Plant Science Center during the summer of 2010. I worked in Dr. Jun Kikuchi's Advanced Metabolomics Research Unit. This project was funded by a fellowship jointly awarded by the National Science Foundation East Asia and Pacific Summer Institute (NSP EAPSI) and the Japan Society for the Promotion of Science. The goal of this program is to introduce students to East Asia and Pacific science and engineering in the context of a research setting, and to help students initiate scientific relationships that will better enable future collaboration with foreign counterparts.

A.1 Background

In the search for sustainable forms of energy, there has been a large increase in research to develop microorganisms that can ferment biomass feedstocks into a combustible liquid fuel such as butanol. However, these fermentation products are toxic at the large concentrations required to meet current energy needs. In order for these fuels to be produced at a practical level, solvent-tolerant microorganisms need to be developed.

Microorganisms live in dynamic environments and are constantly adapting in order to handle external stress, such as increased external osmolarity or toxic polar solvents. The primary response to this external stress in many cases is metabolic in nature. For example, in a hyperosmotic environment, cells lose volume and turgor pressure, which leads to disruption of cellular activity. *Escherichia coli* and *Saccharomyces cerevisiae* respond to increased external osmolarity by decreasing overall energy metabolism, leading to higher ATP availability for driving ATP-dependent ion pumps. Furthermore, *E. coli* and *S. cerevisiae* upregulate the production of trehalose and glycerol, respectively which function to reestablish osmotic equilibrium and protein-water interactions (Hohmann, 2002; Rod, Alam, Cunningham, & Clark, 1988).

In contrast, less is known about the primary metabolic response to increased toxic polar solvents in the external matrix. Polar solvents, such as ethanol or butanol, are believed to: a) alter the dielectric properties of the cellular environment, b) disrupt hydrogen bonding interactions between water and other macromolecules, and c)

weaken hydrophobic interactions between the plasma membrane lipid bilayer (Ingram, 1990; Liu & Qureshi, 2009). In both *E. coli* and *S. cerevisiae* exposure to polar solvents results in reduced metabolic activity (Ingram, 1990; Liu & Qureshi, 2009). Prolonged exposure to ethanol results in an increase in fatty-acid chain length in *E. coli* (Dombek & Ingram, 1984), presumably to help maintain plasma membrane integrity. Similarly, *Clostridia acetobutylicum* responds to prolonged butanol exposure by modification of the cell membrane to include increased fatty acid chain length in the plasma membrane (Vollherbst-Schneck, Sands, & Montenecourt, 1984).

Butanol is a promising next generation biofuel. According to the U.S. Department of Energy Alternative Fuels and Advanced Vehicles Data Center, butanol a) has an energy density that is much more comparable to gasoline than ethanol, b) can be produced from the same biomass feedstocks as ethanol and c) is compatible with current automobile design and fuel transportation infrastructure. The engineering of organisms that can produce branched-chain higher chain alcohols is being led by James Liao's group where they have engineered *E. coli* to produce, amongst other alcohols, butanol via exogenous, non-fermentative pathways (Hanai, Atsumi, & Liao, 2007; Atsumi, Hanai, & Liao, 2008); Shen & Liao, 2008).

A recent study investigated changes in intracellular metabolites in *E. coli* during butanol stress. (Rutherford et al., 2010). In general, amino acids were less abundant. Spermidine and agmatine were also noted to decrease under butanol stress.

The experimental goal of the current study was to gain an understanding of the changes in the external metabolite profile of *E. coli* under butanol stress. While most metabolomics studies focus on changes in intracellular metabolites, I think that we can gain valuable information by studying the exometabolome. Furthermore, I also had the goal of learning an in vivo NMR technique developed in Dr. Kikuchi's Advanced Metabolomics Research Unit. Finally, I had the goal of experiencing Japanese culture and language while at the same time establishing international relationships with Japanese scientists.

A.2 Materials and Methods

^{13}C D-glucose (U-13C6, 99%) was from Cambridge Isotope laboratories; ^{13}C/^{15}N and unlabeled Algal Amino Acid mixture Chlorella Industry Co.; ^{13}C D-xylose (U-^{13}C5, 99%) was from Omicron Biochemicals, Inc.; Silantes E. coli OD2 liquid media (^{13}C/^{15}N labeled and unlabeled) was from Silantes GmbH.

Measurement of growth kinetics

Growth kinetics for *E. coli* K12 were evaluated to determine the effect of butanol treatment on doubling rate. Preculture cells were selected by isolating a single colony from an LB agar plate and were grown to saturation in LB liquid media in a 37°C incubator with agitation. Growth analysis was conducted on cells grown in duplicate using Silantes OD2 (unlabeled) media supplemented with natural abundance carbon glucose or xylose (0.5% w/v) and non-^{13}C algal amino acid mixture. The media used for

growth kinetics did not contain potassium phosphate buffered D_2O (see *in vivo* 1D and 2D NMR measurements) Cells were treated with 0%, 0.5%, 1% and 2% butanol (v/v).. Samples for growth kinetics analysis were inoculated from the preculture to an OD_{600} of 0.05, and readings were acquired every 45 min using a benchtop spectrophotometer. The unit growth rate was determined by regressing the linear range of data during exponential growth phase for time versus ln OD_{600}. The doubling time was calculated as:

$$g = \frac{\ln 2}{k}$$

where *k* is the slope determined from regressing time versus ln OD_{600}. The final results are expressed as percent of inhibition relative to the 0% butanol treatment.

in vivo 1D and 2D NMR Measurements

All NMR measurements were recorded on a Bruker DRX-500 spectrometer operating at 500.13 MHz ^{1}H frequency with the temperature of the NMR samples maintained at 310 K. To minimize variance that could arise from different methods of tube production, samples were collected in tubes manufactured from a single source. All samples were collected in 5 mm NMR tubes manufactured by New Era Enterprises, Inc. (NE-UL5). Samples for *in vivo* NMR measurements were grown in Silantes OD2 ($^{13}C/^{15}N$ labeled) media, supplemented with 0.5% ^{13}C D-glucose or 0.5% ^{13}C D-xylose and 0.5% ^{13}C algal amino acid mixture. Each sample also contained 10% D_2O to maintain the lock signal, 1 mM 2,2-dimethyl-2-silapentane-5-sulfonate (DSS) as an

internal chemical shift reference and 100 mM potassium phosphate buffer prepared to pH 7.400.

For *in vivo* NMR, 1D and 2D data were collected by interleaving respective experiments for 10 hours. Each 1D experiment lasted approximately 6 min, and each 2D experiment lasted approximately 24 min. One-dimensional spectra were collected with a total of 1500 complex points, 256 scans, 1.2-s recycle delay, water signals were suppressed using a Watergate pulse sequence and a ^{13}C GARP broadband decoupled proton acquisition to reduce spectral complexity by removal of carbon satellites. Two-dimensional HSQC experiments were collected with a total of 32 complex f1 (^{13}C) and 1024 complex f2 (1H) points, with 8 scans per f1 increment and a ^{13}C GARP decoupling scheme according the method of Kikuchi and Hirayama (Hirayama & Kikuchi, 2007). Samples were collected in triplicate.

NMR data processing and analysis

All spectra were processed using custom NMRPipe (Delaglio et al., 1995) processing scripts. Spectra for 1D proton NMR were zero-filled to 2048 points and Fourier transformed with a squared cosine window function, phase correction and automatic baseline correction. Spectra for 2D HSQC NMR were zero-filled to 1024 points in both the f2 and f1 dimensions. After zero-filling the spectra were Fourier transformed with 10 Hz (f2) and 15 Hz (f1) line broadening, phase correction and

automatic baseline correction. The solvent line was removed during processing for 2D spectra.

Data analysis and statistics were performed using R (http://www.r-project.org) and the rNMR software package (I. A. Lewis et al., 2009). Metabolites were identified using the Platform for RIKEN Metabolomics (PRIMe) (Akiyama et al., 2008) or the Madison Metabolomics Consortium Database (MMCD) (Cui et al., 2008); assignments were verified by overlaying NMR spectra of standards from the BioMagResBank (BMRB) (Markley et al., 2007). Due to the narrow spectral window in f2 for HSQC data, standards were often re-referenced by adding 40 ppm to the assigned f2 value.

A.3 Growth analysis

Previous studies investigating the adaptation to butanol stress in *E. coli* were conducted in minimal and rich media (Knoshaug & Zhang, 2009). These studies have established that *E. coli* can grow in 1% butanol, however the rate of growth was significantly perturbed. Furthermore, other studies have shown that cells display a different metabolic profile (Rutherford et al., 2010). The media used in the current study (Silantes OD2) is a rich medium. I found that media supplemented with glucose and treated with 1% butanol, the doubling rate was inhibited 40% relative to that of the untreated glucose control (Table A.1), which is in agreement with previously published data for cells grown in YPD, a rich medium (Knoshaug & Zhang, 2009). However, I discovered that at the 1% level *E. coli* did not grow in 5 mm NMR tubes. Therefore my NMR experiments were conducted at the 0.5% butanol level.

Previous studies indicate that glycolysis is perturbed by the presence of butanol (Gonzalez et al., 2003; Brynildsen & Liao, 2009; Rutherford et al., 2010), therefore I chose to examine the effects of growth when *E. coli* were supplemented with xylose, which is metabolized through the pentose phosphate pathway. Growth curves for *E. coli* K12 grown in 0.5% glucose or 0.5% xylose supplemented Silantes OD2 (unlabeled) displayed a slight pertubration in the growth profile when cultures were treated with 0.5% butanol (Figure A.1). Interestingly, while all cultures reached stationary phase within 6 hours, *E. coli* K12 grown in glucose supplemented media and treated with 0.5% butanol reached stationary at a lower optical density than other conditions. I did not collect data for *E. coli* grown in xylose supplemented media and treated with 1% BuOH because I found that cells would not grow at 1% BuOH in NMR determines, regardless of carbon source.

Growth kinetics analysis for *E. coli* grown in Silantes OD2 (unlabeled) and supplemented with glucose or xylose show a relative rate of inhibition of 21% and 24%, respectively, when treated with 0.5% butanol (Table A.1). Although cells grown in xylose supplemented media showed an inhibition of 6% relative to glucose supplemented media, it was determined that this difference was not of practical significance.

Table A.1. Data shown is the inhibition of doubling time relative to untreated (0% butanol), Silantes OD2 (unlabeled) supplemented with glucose or xylose. The value in parantheses for the xylose supplement indicates inhibition relative to untreated glucose. Data shown is represented as the average value obtained from duplicates.

	Percent butanol			
Supplement	0%	0.5%	1%	2%
0.5% Glucose	0	.213	.396	n.g.
0.5% Xylose	0 (.06)	.189 (.237)	n.d.	n.g.

n.d. = not determined; n.g. = no growth was observed.

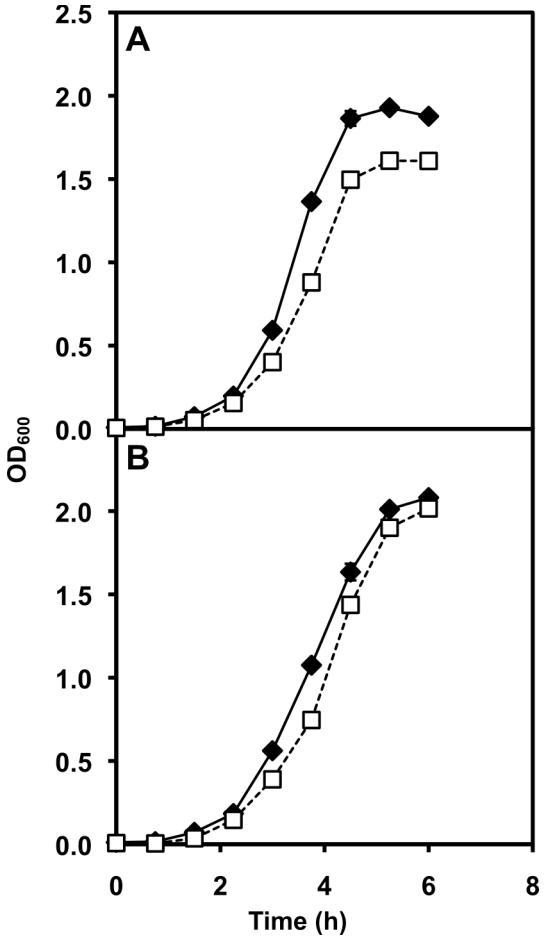

Figure A.1. Growth curves for *E. coli* K12 grown in Silantes OD2 (unlabeled) supplemented with (A) 0.5% glucose and (B) 0.5% xylose. Control samples (0% butanol) are represented as filled diamonds with solid line and treated samples (0.5% butanol) are represented as open squares with dashed line. Values reported are the average of duplicates and error bars represent the range.

In summary, I noted no significant difference in the growth profiles as a function of carbon source. One limitation we noted at the end of the project was that these cultures were grown aerobically with shaking. Whereas the NMR experiments discussed below were conducted under anaerobic conditions without shaking. Therefore, I could not provide a direct comparison of these growth results with the in vivo NMR experiments.

A.4 Analysis of real-time NMR experiments

Previous research showed that *E. coli* display different profiles of intracellular metabolites when exposed to butanol (Rutherford et al., 2010). I hypothesized that *E. coli* would display different extracellular metabolite profiles when provided with different carbon sources, while under butanol stress. To assess time-dependent differences I used *in vivo* NMR techniques, which would allow me to monitor the consumption and production of extracellular metabolites in real-time.

I observed and monitored, in real-time, 17 extracellular metabolites (Figure A.2-5). The following metabolites did not have a significant correlation with respect to time: alanine, arginine, glutamate, glycine, isoleucine, leucine, lysine, valine.

As expected, glucose and xylose were consumed throughout the time-course. Xylose was consumed at a slower rate than glucose. Furthermore, when cultures were treated with 0.5% BuOH, the relative rate of carbohydrate consumption appeared to be slower (Figure A.3). Interestingly, the only amino acid we observed to be consumed was aspartate, which appeared to be slightly inhibited by the 0.5% BuOH treatment. Aspartate consumption was inhibited the most when cultures were supplemented with

xylose and 0.5% BuOH treatment (Figure A.2). The actual rate at which aspartate was consumed qualitatively appeared the same; however, different cultures may have experienced different amounts of time in the lag phase. Other observable amino acids did not change significantly.

Not surprisingly, I observed large accumulation of acetate, ethanol, formate, lactate and succinate, all products of anaerobic metabolism. Acetate and lactate appeared more quickly when glucose was supplied as the carbon source. Hardly any lactate was produced in 0.5% BuOH treated cultures supplemented with xylose. Since these metabolites are derived mostly from pyruvate, this finding was unsurprising since we can expect higher production of pyruvate in the glucose-supplemented samples versus the xylose-supplemented samples. Lower production of these acids under butanol stress in also unsurprising considering that glycolysis is negatively perturbed. Finally, the production of ethanol is also directly tied to pyruvate, and therefore it is reasonable that we observed a greater rate of production in glucose-supplemented samples.

Formate and succinate appeared at relatively similar rates regardless of carbon source; however, from scanning the EcoCyc database it is apparent that their metabolism is complicated by multiple routes of synthesis (Karp et al., 2002).

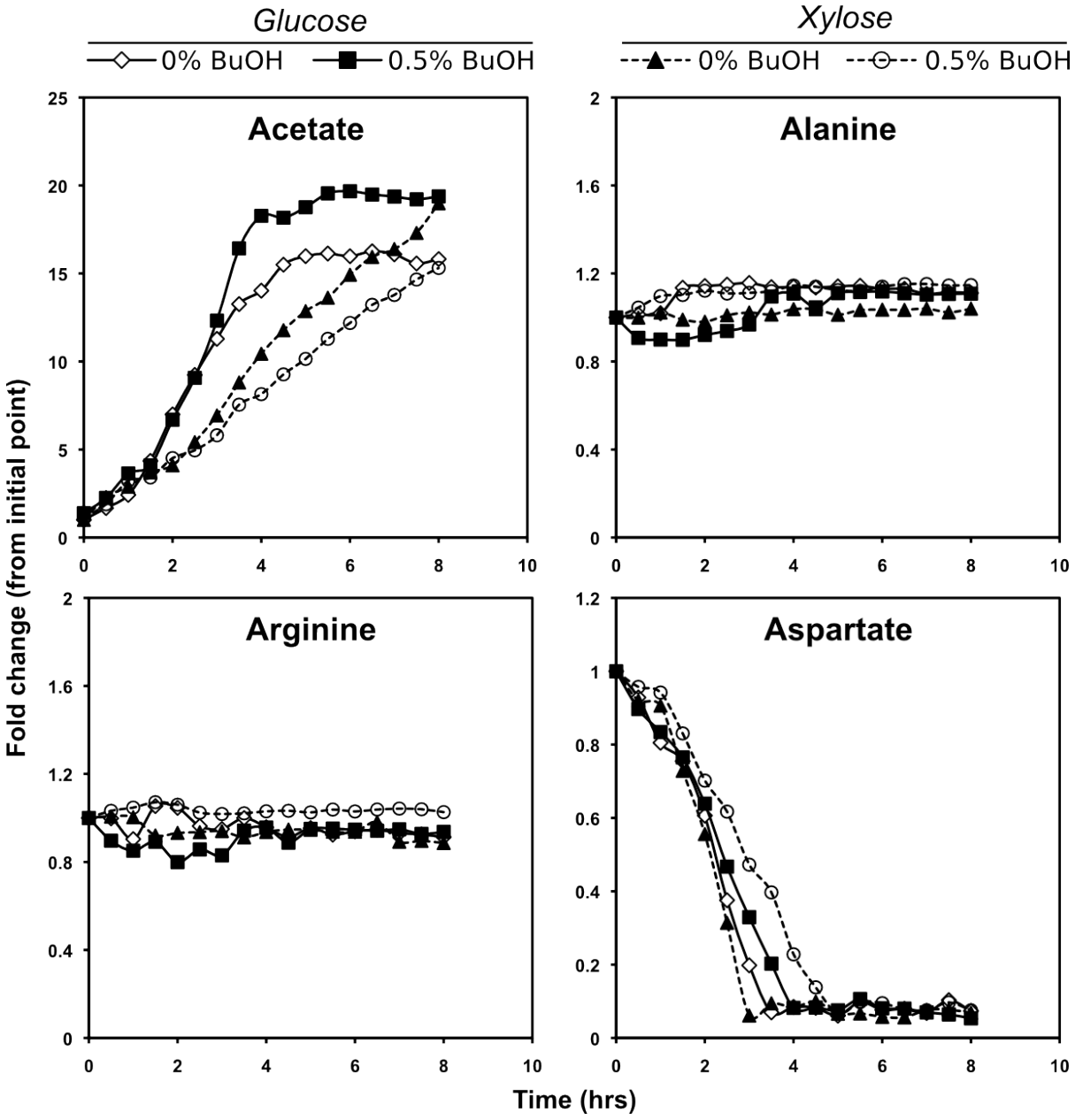

Figure A.2. Time-course profiles for extracellular metabolites observed in NMR tubes of cultures grown in glucose or xylose supplemented media, treated with 0% or 0.5% butanol. Data were normalized to the first time-point where a signal was available.

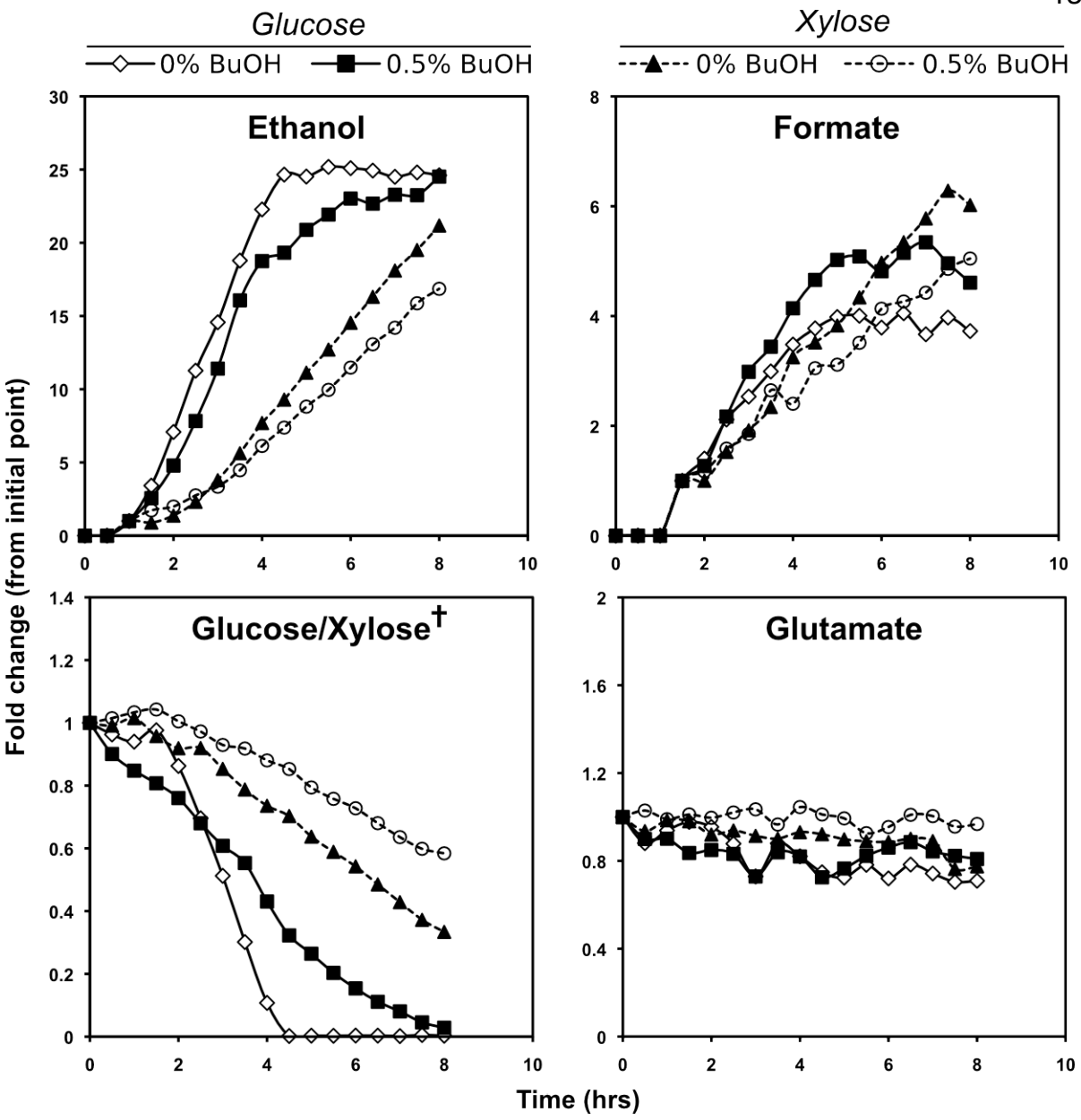

Figure A.3. Time-course profiles for extracellular metabolites observed in NMR tubes of cultures grown in glucose or xylose supplemented media, treated with 0% or 0.5% butanol. Data were normalized to the first time-point where a signal was available. †Glucose was only measured in glucose supplemented samples, likewise for Xylose.

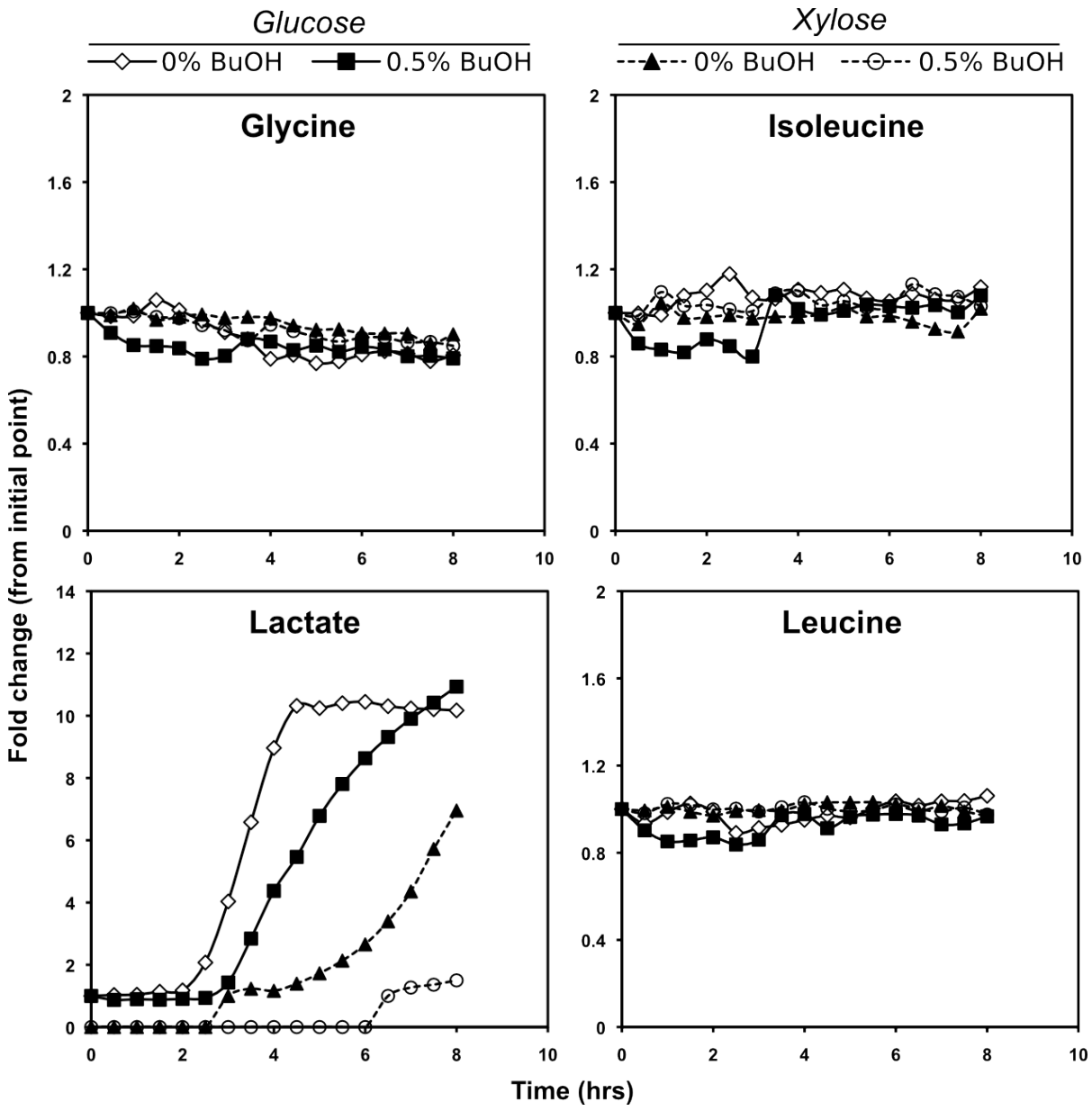

Figure A.4. Time-course profiles for extracellular metabolites observed in NMR tubes of cultures grown in glucose or xylose supplemented media, treated with 0% or 0.5% butanol. Data were normalized to the first time-point where a signal was available.

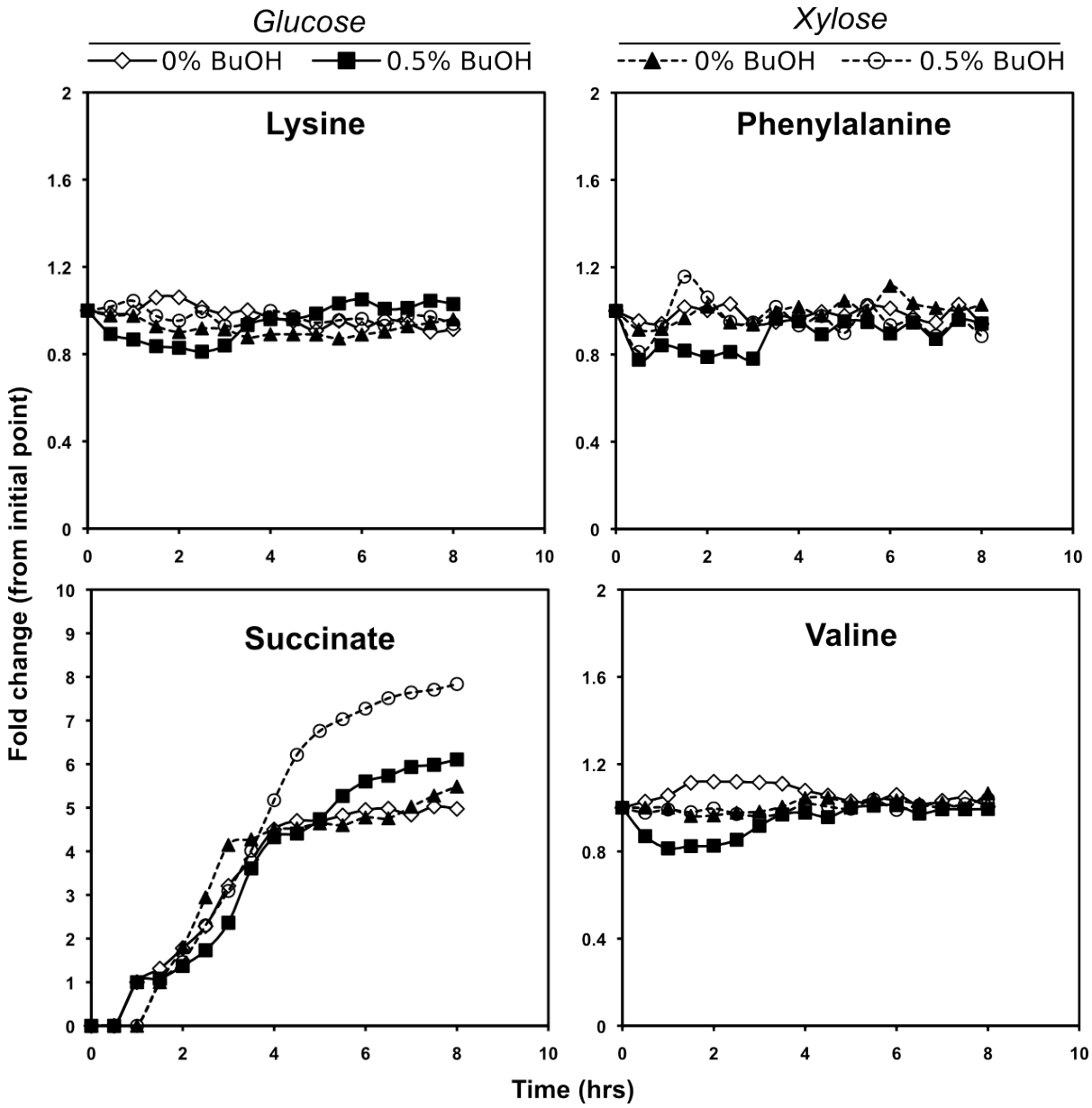

Figure A.5. Time-course profiles for extracellular metabolites observed in NMR tubes of cultures grown in glucose or xylose supplemented media, treated with 0% or 0.5% butanol. Data were normalized to the first time-point where a signal was available.

One of the limitations of this study was that I could not compare relative levels of metabolites between samples. Although I added DSS, which can serve as an internal standard, its signal was not evident in the HSQC spectra. Another limitation was that several replicates failed to grow after inoculating the NMR tube with *E. coli*. Also in one case the supplements added to the media were not ^{13}C-enriched supplements. Therefore, the data could be strengthened by repeating with a higher concentration of DSS and by ensuring that all replicates work.

One insight gained from this study is that ethanol is a byproduct of the metabolic response to butanol stress. This presents a problem for *E. coli* engineered for butanol production. First, any ethanol produced takes away carbon that should go to butanol production. Second, the ethanol is yet another stress with which the organism will have to contend. An interesting follow-up study might be to understand why aspartate was the only amino acid consumed to a significant degree.

A.5 Reflections on my experience abroad

The opportunity to conduct this research was funded through a fellowship awarded jointly by the NSF EAPSI and JSPS. The main objectives of the program are 1) to introduce students to East Asia and Pacific science and engineering in the context of a research setting 2) to help students initiate scientific relationships that will better enable future collaboration with foreign counterparts, 3) to receive an orientation on Japanese culture and research systems and to pursue research under the guidance of host researchers at Japanese universities.

The nearly 3 months spent in Japan was my first significant experience abroad. This opportunity gave me valuable experience and taught me how to set aside pre-conceived notions about another culture, notions that often arise from Hollywood. For example, we often think of the Japanese as a culture addicted to work. Certainly, from my experience I still believe that Japan is a culture of hard work ethic. However I could not have prepared myself for how relaxed the atmosphere became after work hours. The Japanese truly know how to enjoy a nice weekend in the summer. I found that nearly every weekend my newfound friends were eager to attend a baseball game or fireworks display. And more importantly, I discovered that the Japanese love a nice cold beer!

Another pre-conceived notion that I had prior to spending time in Japan pertains to diet. It is no secret that the average Japanese citizen is slimmer than their American counterparts. For some reason, I had assumed this was because the Japanese ate less food. While I found it to be true that the average size of a meal in Japan was certainly smaller than that found in the United States, I equated this with the inability to actually eat a lot of food. But I can say unequivocally that the Japanese are completely capable of mass food consumption. I was put to shame in an eating contest at least once!

What I was able to take away from my experience is that the Japanese in general make better dietary choices. The first thing I noticed at restaurants or at the lunch cafeteria at the RIKEN Yokohama campus is that nobody was drinking beverages laden with high-fructose corn syrup. In fact, as I recall the cafeteria did not serve any Coke, Pepsi, etc.. Instead, everyone drank tea. Therefore, I started drinking a lot of green tea,

a habit I continue even two years later. I also learned about using various types of seaweed for cooking. As it turns out, seaweeds are a rich source of nutrients (perhaps referring to them as ‘weeds’ is a misnomer). Now, I keep my cupboard stocked with various types of seaweed and use them regularly in my cooking.

Another important experience I had was that of being a foreigner in an ethnically homogeneous group. As an American scientist I have routinely worked with international scientists, mainly from East Asia. However, I had never stopped think about their experience upon arriving in America and starting work in a completely new cultural and ethnic setting. It is definitely scary as first; you are surrounded by people who are speaking a different language at a million miles per hour. Even with basic skills in a foreign language, communication at first is challenging. However, I chose to persevere and in the end I gained profound respect for the challenges that many of my current and former international coworkers have experienced.

The main message from my experience in Japan really comes down to learning to respect others and their culture while trying to learn something about yourself. I had the opportunity to establish scientific collaborations with researchers in Japan, but more importantly I made new friends.

一期一会

Appendix B

Schematics and parts list for the SAMBED

The following appendix contains detailed schematics and a parts list used in the contruction of the SAMBED. This work was contributed by Dan Miller, who was the engineer that constructed the SAMBED.

MILLING CHAMBER:

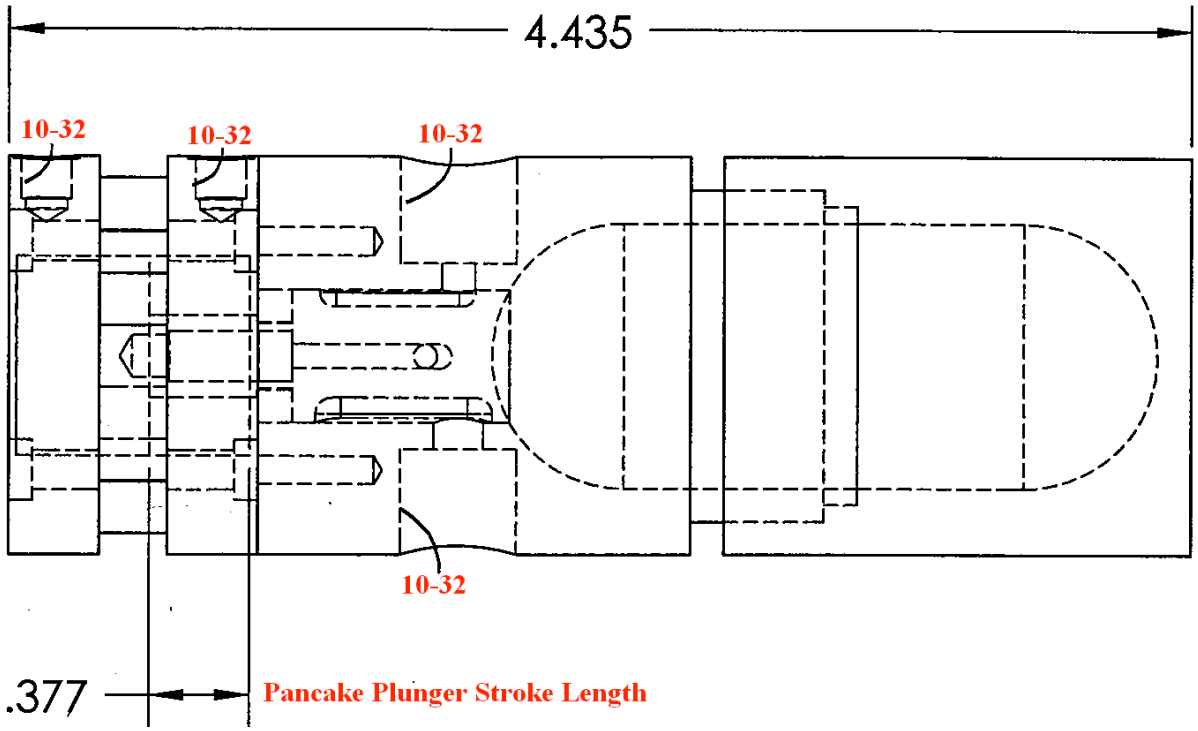

This is the original schematic drawn by the Physics Department Machine Shop. The inlet and outlet pores to the milling chamber body need to be changed so that both accept 10-32 male threaded quick-disconnect couplings.

The pancake cylinder can be purchased from McMaster-Carr, part number 1691T12, shown below:

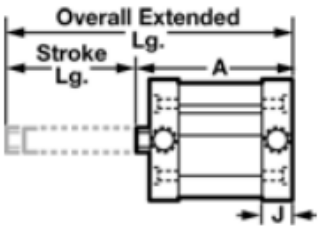

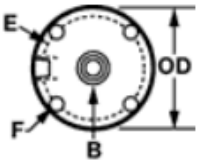

Bore Size	Force @ 100 psi, lbs.	Port Pipe Size, Female	Rod, Thread Size (B)	OD	(E)	Mounting Holes (F)	(J)
3/4"	36	10-32	10-32	1.50"	1.22"	0.15"	0.34"

1/8"-1"

Bore Size	Retracted Lg. (A)	Stroke Lengths	Each
1/2"	0.69"+ Stroke Length	1691T11	$40.75
3/4"	0.69"+ Stroke Length	**1691T12**	42.05

Milling Chamber Cap:

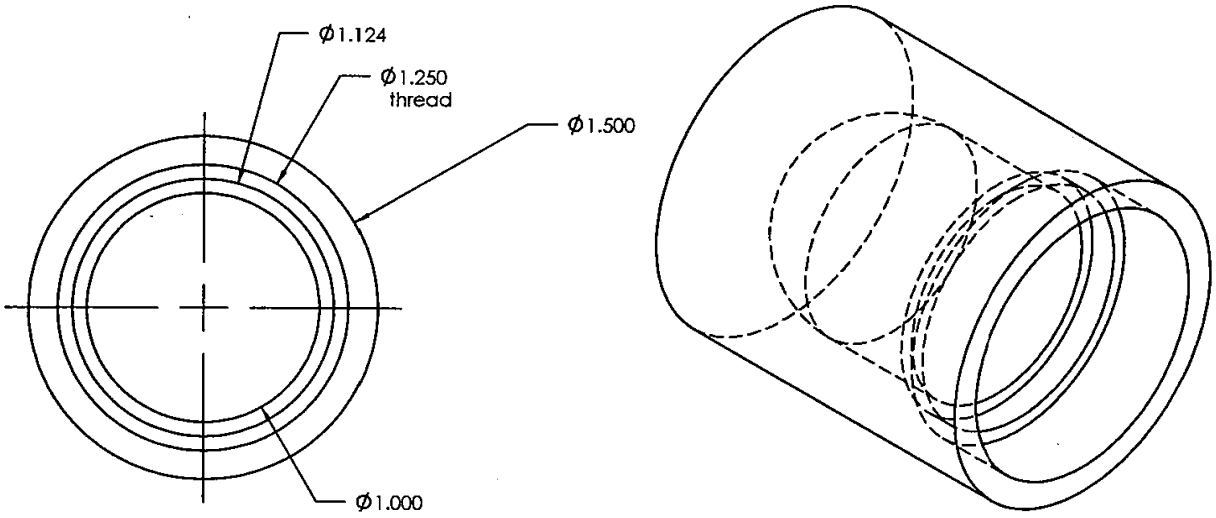

Shown above is the original design that the Physics Department from UW-Madison designed on the computer. In order to reduce weight, a large amount of material can be milled out of the milling chamber cap. Also, we can make four grooves at the base of the cap, instead of three. We can also make these grooves slightly deeper, maybe 1/16" deep. After shaving off excess metal, it will look something like this:

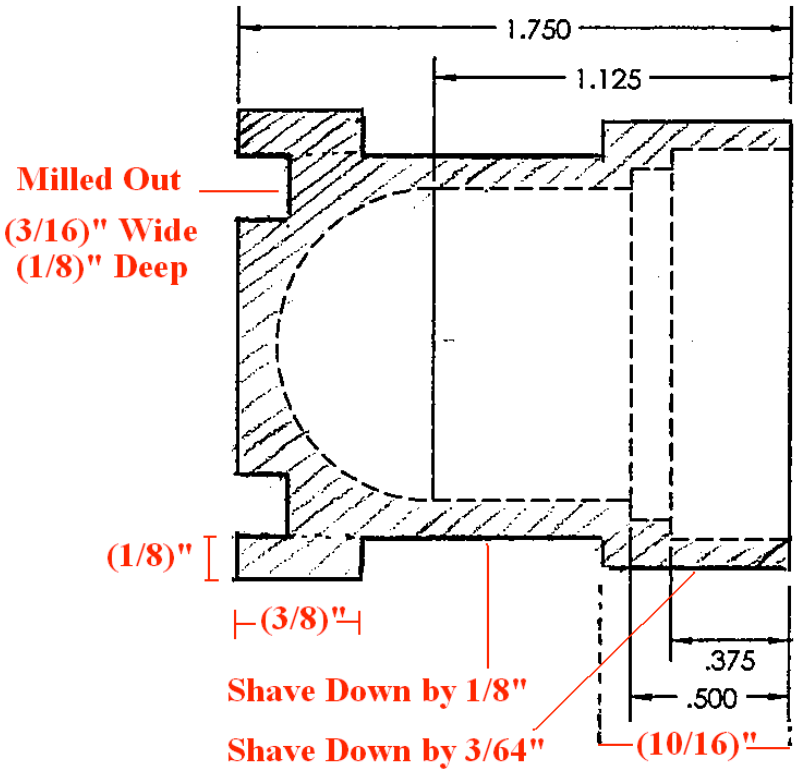
1.750
1.125
Milled Out
(3/16)" Wide
(1/8)" Deep
(1/8)"
(3/8)"
Shave Down by 1/8"
Shave Down by 3/64"
.375
.500
(10/16)"

Milling Chamber Body:

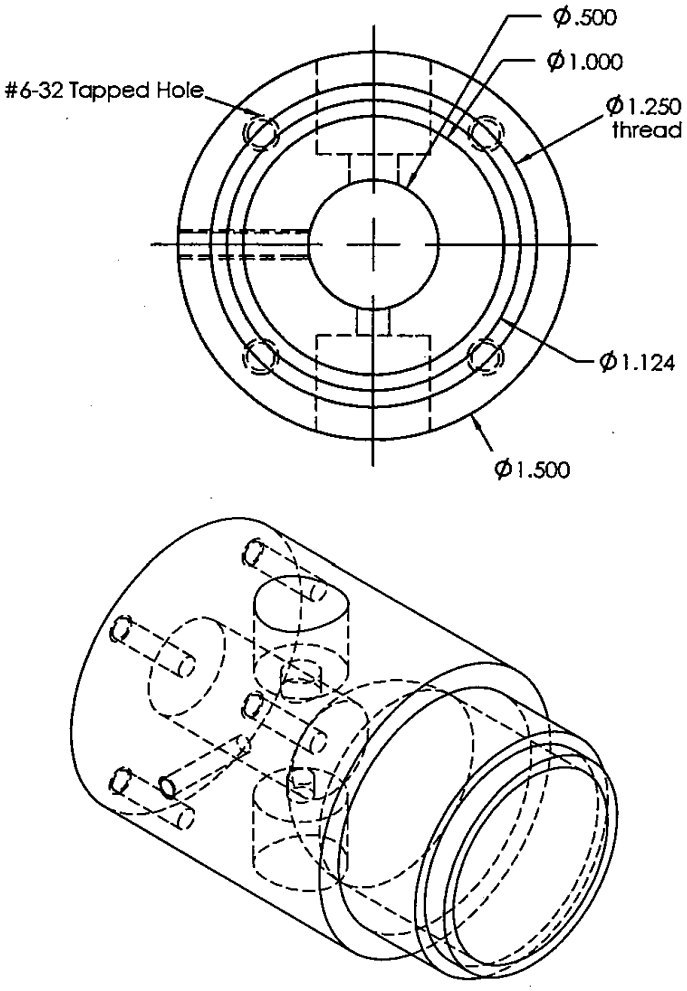

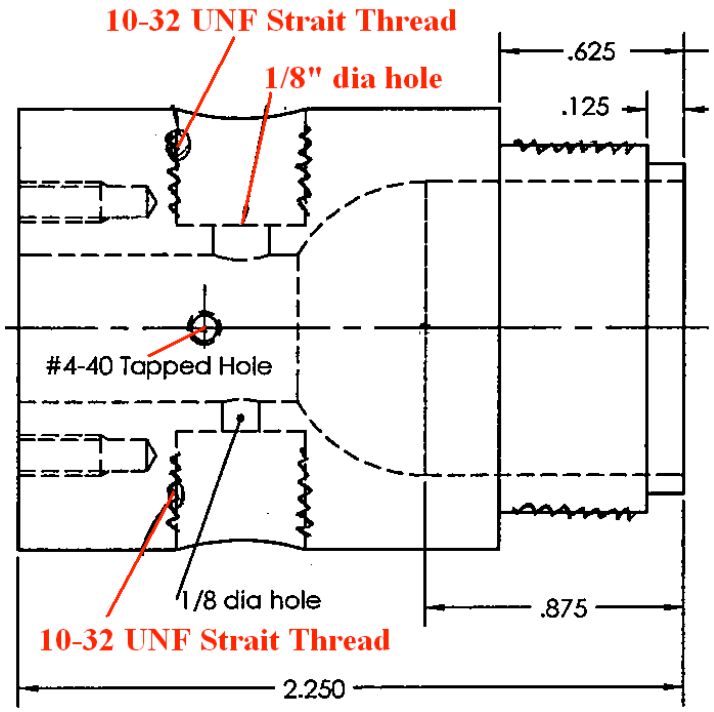

Shown above is what the Physics Department put together. The Inlet/ Outlet pores should both be the same size (1/8" diameter) and be compatible with the 10-32 quick-disconnect hose couplings. The mounting holes in the bottom of the chamber body need to be re-aligned so that the quick-disconnect couplings that supply air to the pancake cylinder are perfectly aligned with the inlet pore (shown as the smaller of the two pores) of the milling chamber body, like we talked about earlier today. Also, some weight can also be saved by shaving off some of the medal, especially in the base of the milling chamber body, as well as making four grooves in the base fo the milling chamber body and making them deeper, as in the milling chamber cap. A rough sketch of what the reduced weight milling chamber body will look like is shown below:

Milling Chamber Body (Continued):

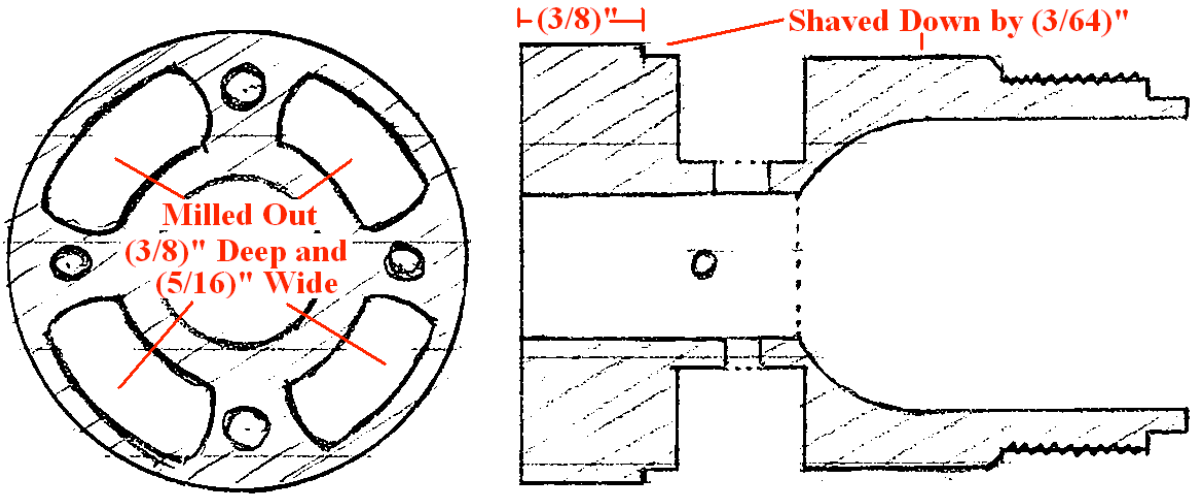

Shown below are the fittings that will be threaded into the milling chamber Inlet/ Outlet and pancake cylinder. Also, the sleeve valve, which will be connected to the outlet pore prior to the coupling so that I can manually shut off air/ liquid flow leaving the outlet pore of the milling chamber body. The threading is in metric for some reason for that part.

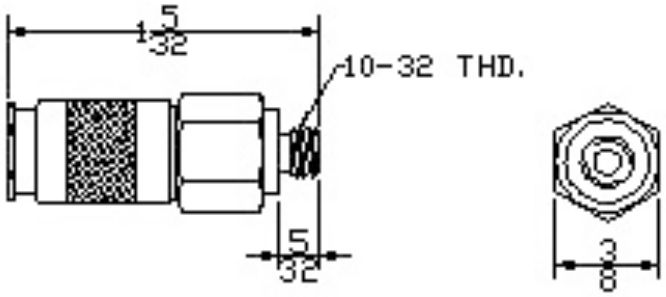

Sleeve Valve (shown below):

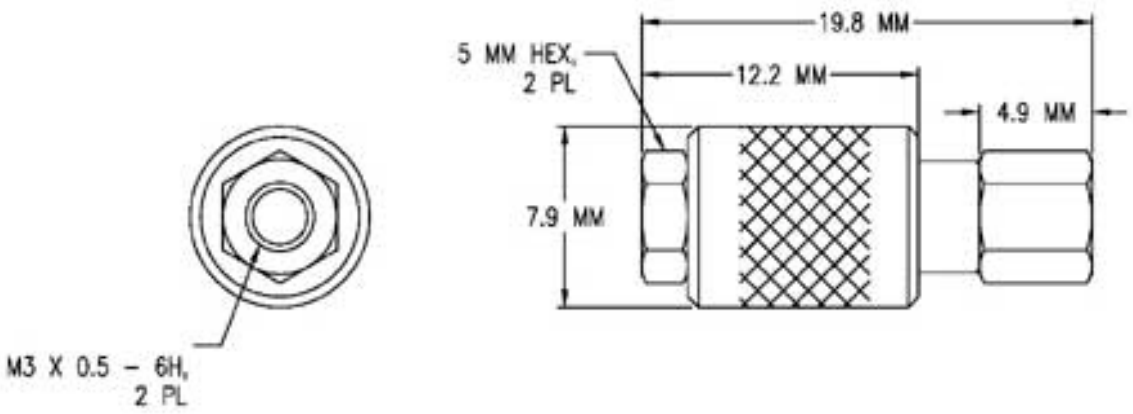

Plunger Valve:

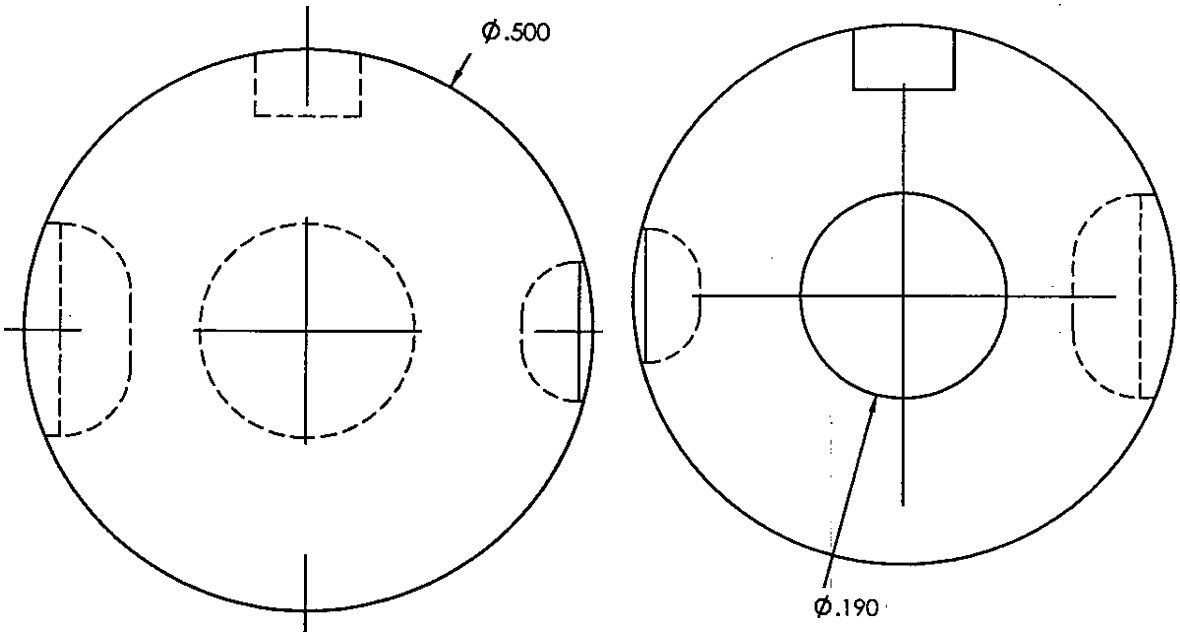

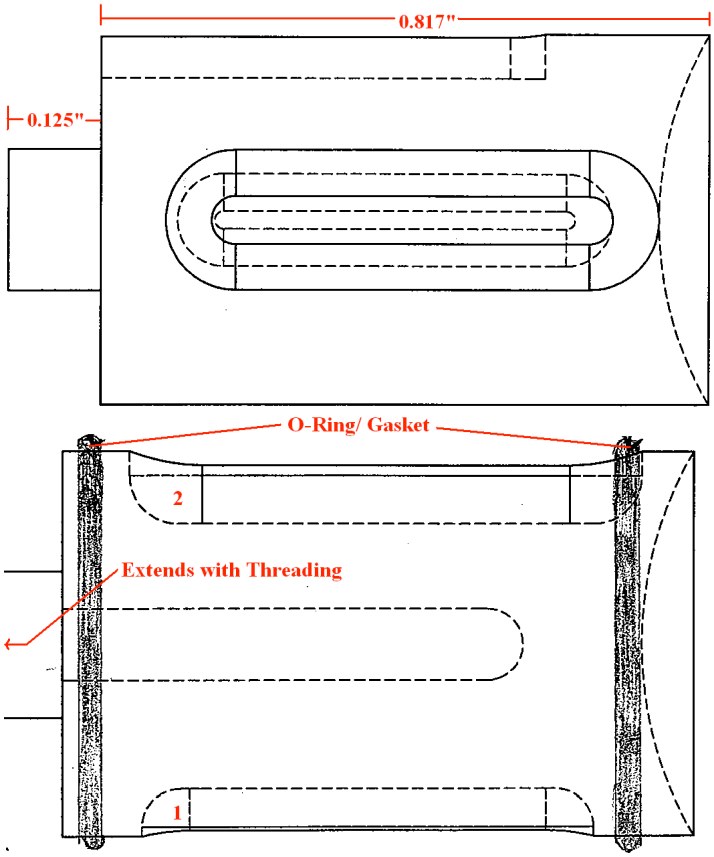

In addition to including the o-ring/ gasket for a tight seal, the two channels (1 and 2 shown in red) need to be the same size to make room for the o-ring. If we can include another o-ring at the base of the plunger, it will ensure that no solvent leaks out while the plunger is raised and solvents flow through the two channels. I'm not sure how long the stem of the plunger is, or what threading it has. It needs to be screwed into the pancake cylinder so that it is almost completely flush with the interior of the milling chamber body.

Milling Chamber Cartridge:

There will be 10 milling chambers per cartridge. The orientation for one of the milling chambers is shown below:

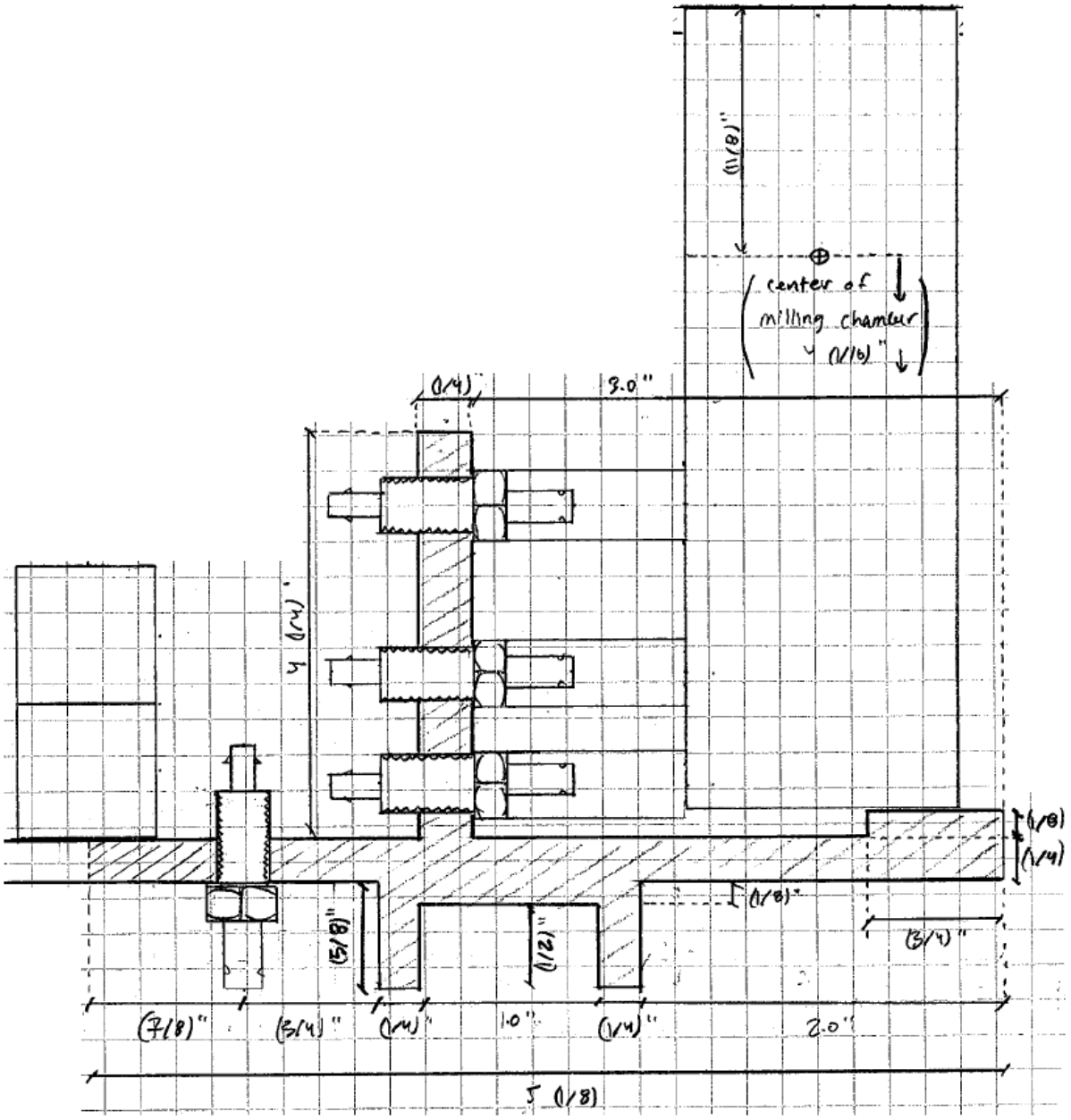

In reality, there will be an identical reflection of the above schematic so the two milling chambers oppose each other and the entire platform is 10.25” long. The two squares shown left most are air manifolds that are .75” wide and tall. We will have to mount these into the platform, however I am still waiting on the schematics for them. An additional platform will be lowered onto the above platform, to keep the milling chambers in place.

Milling Chamber Cartridge (Continued):

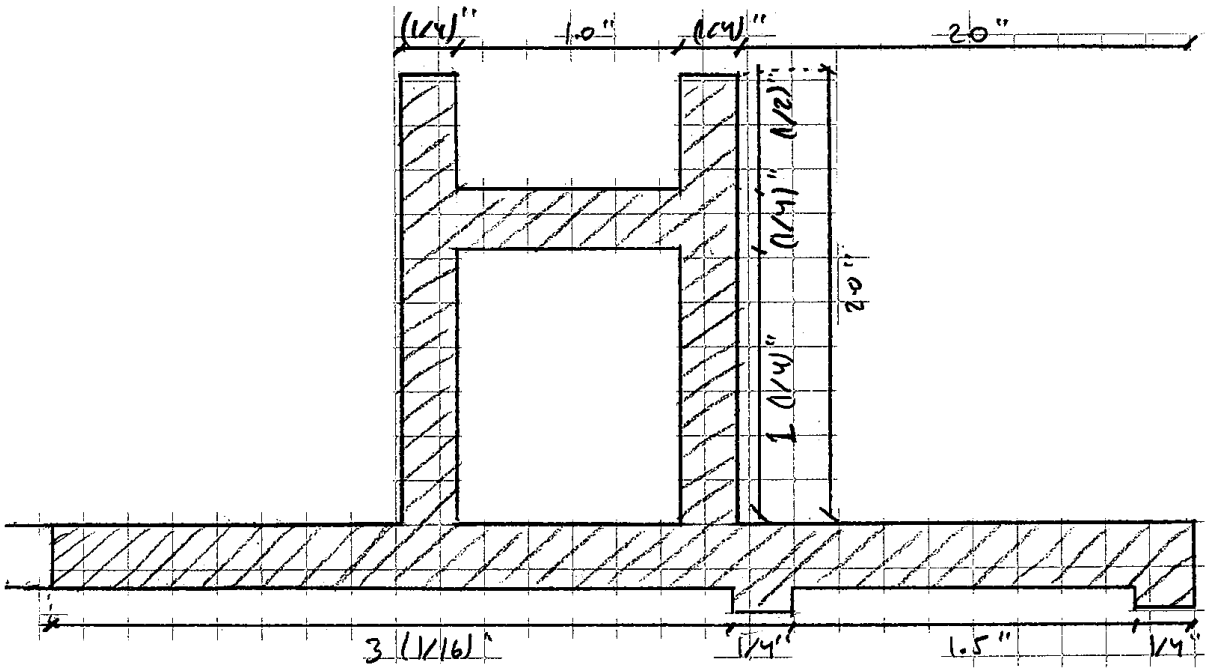

Shown above is the top plate that is lowered onto the top of the milling chambers. Like the figure on the previous page, this schematic needs to be reflected onto itself to represent the full side view of the plate. We will also have to make holes for a skewer to go through both plates in several areas to lock the plates together, with the milling chambers sandwiched between them.

Shown on the following pate is a top view of the bottom plate of the milling chamber cartridge. It is kind of hard to see clearly because of the graph paper and the poorly scanned image. I will give you a better copy at another time.

The couplings that need to be threaded into the top plate are shown below:

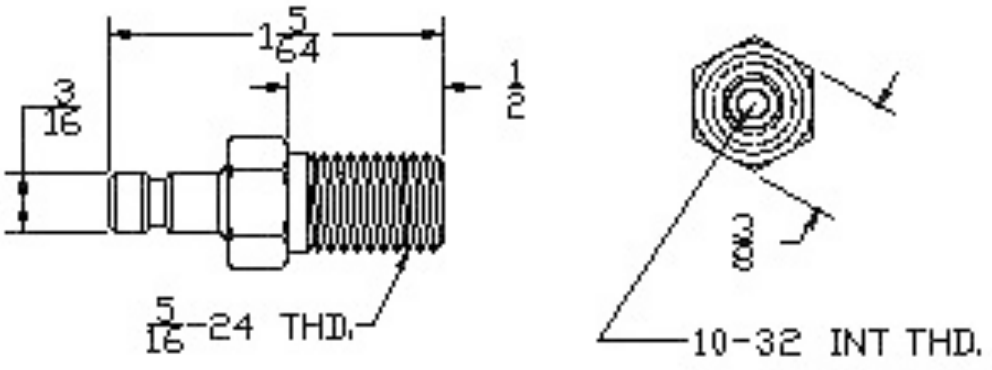

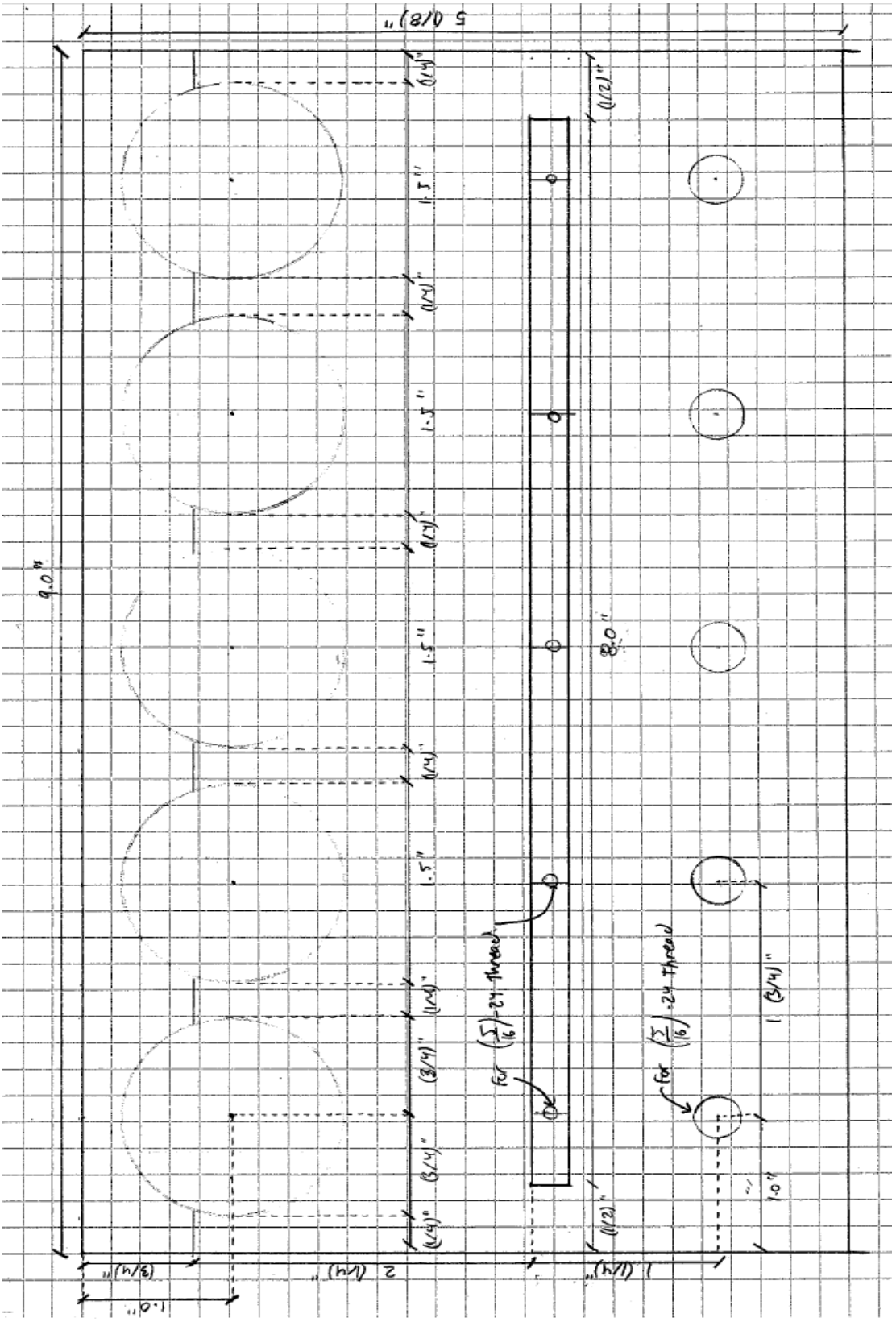
5 (1/8)"
9.0"
(1/4)"
1.5"
1.5"
1.5"
1.5"
(1/4)"
(1/4)"
(3/4)"
(3/4)"
(1/4)"
(1/4)"
(1/2)"
8.0"
(1/2)"
for (5/16)-24 thread
for (5/16)-24 thread
1 (3/4)"
1.0"
1 (1/4)"
2 (1/4)"
(3/4)"
1.0"

Filter Chamber:

Shown left is the filtration chamber body and shown right is the filtration chamber cap. The inlet to the filtration chamber body needs to be compatible with a 1/8 NPT thread. I will be threading a 90 degree elbow male connector into the top of the chamber body. Into that, an additional quick-disconnect coupling will be threaded, so that it can be easily connected to the milling chamber outlet.

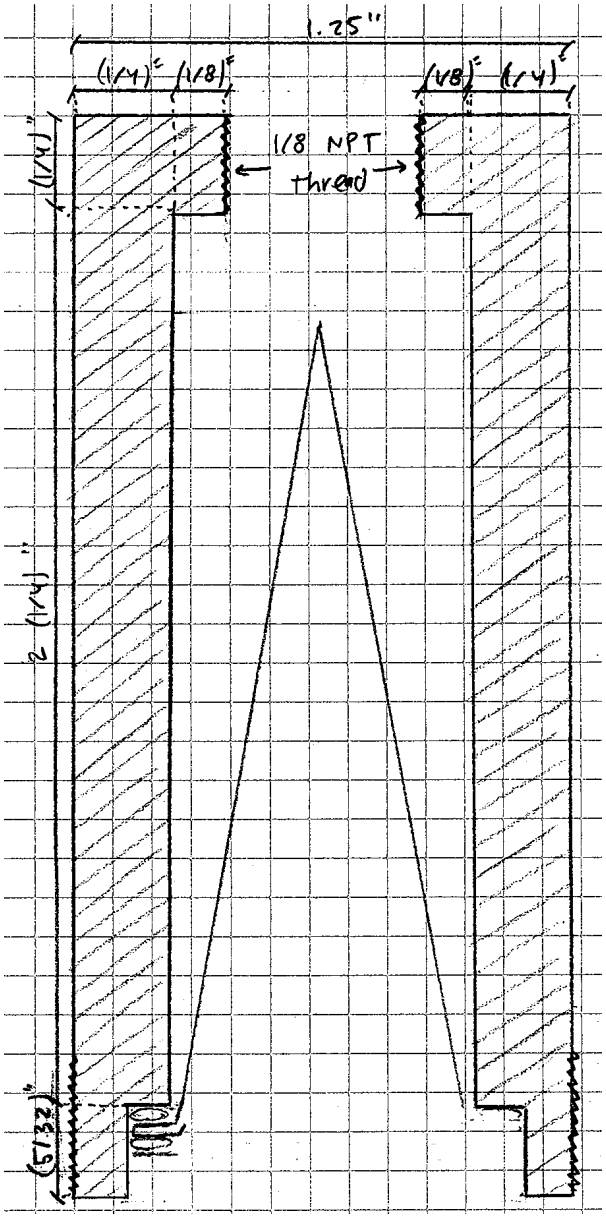

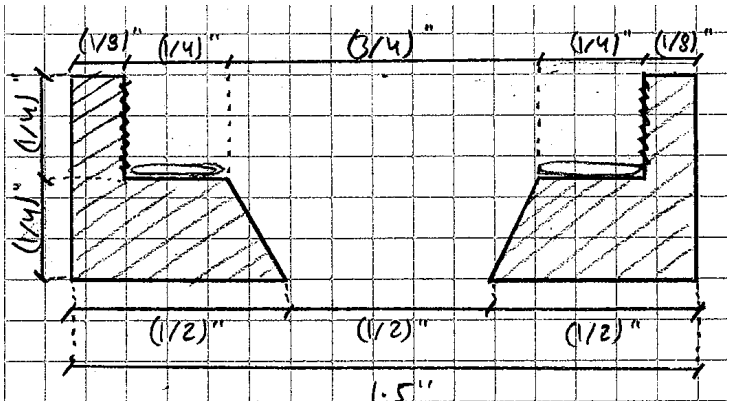

The threading between the filtration chamber cap and body is up to you. It needs to be air tight though. I would prefer to have this part done first so that I can test its ability to properly filter the solvent sample.

MILLING CHAMBER

Beswick Engineering:

Item Number	*Description*
CKV-13-10M-303-V-X	SS303 Check Valve with Viton Seals, 1/8" ID Barb Inlet, 10-32 Ext. Thd. Outlet, Low Back Pressure X-opt.
QDC-101-E-1810-V	Quick Disconnect Plug with 1/8" NPT Ext. Th. and Viton Seals, SS303

McMaster-Carr Supply:

Item Number	*Description*
1691T12	Pancake Composite Tie Rod Air Cylinder; 3/4" Bore, 1/8" to 1" Stroke Length
92196A753	18-8 Stainless Steel Socket Head Cap Screw 5-40 Thread, 7/8" Length, Pack of 50 for $3.45
5058K221	Aluminum Single-Barbed Tube Fittings Adapter for 1/8" Tube ID X 10-32 Unf Male, Silver

Mercer Gasket & Shim:

Item Number	*Description*
(00000000000)8391	Viton (75D, Brown) O-Ring; 3/8" ID, 1/16" Cross Section
(0000000000)44965	Viton (75D-) Gasket Soft Ring, 1-1/8" OD x 1" ID x 1/32" Thk

Cate Machine and Welding:

Item Number	*Description*
N/A	Round Body Milling Chamber Including Single Cap, Body, and Plunger; SS303

CIC Ball Company:

Item Number	*Description*
SS30207500N	3/4" SS 302 Grinding Ball, Grade 1000, Pack of 5 for $37.50

FILTRATION CHAMBER

Beswick Engineering:

Item Number	*Description*
QDC-101-I-1810-NS-303-V	Quick Disconnect Socket with 1/8" NPT Ext. Thd and Viton Seals, No Shut-Off Poppet, SS303

McMaster-Carr Supply:

Item Number	*Description*
48805K18	Precision Threaded Type 316 SS Pipe Fitting 1/8" Pipe Sz, 90 Deg Female X Male Elbow, 5500 PSI
9263K163	Metric Viton® Fluoroelastomer O-Ring 2 mm Width, 4 mm ID, Pack of 25 for $6.44
91251A106	Black-Oxide Alloy Steel Socket Head Cap Screw 4-40 Thread, 1/4" Length, Pack of 100 for $9.27
9317T663	Corrosion-Resistant 304 SS Wire Cloth Disc 60 X 60 Mesh, 1-1/2" Diameter, .0075" Wire Dia, Pack of 25 for $5.37

Mercer Gasket & Shim:

Item Number	*Description*
(0000000000)44967	Viton (75D-) Gasket Soft Ring, 2-1/16" OD x 1-1/2" ID x 1/16" Thk

Cate Machine and Welding:

Item Number	*Description*
N/A	Filtration Chamber v3.0 Including Body, Cap, and Ultrafiltration Membrane Holder, SS303 Body/ Cap, Delrin Holder

Stemmerich Inc.:

Item Number	*Description*
N/A	Duran Tubing; 46 +/- 0.7mm OD x 3.2 +/- 0.3mm Wall x 40 +/- 0.127mm Length, Ground and Chamfered Edges

HOMOGENIZATION PLATFORM

Beswick Engineering:

Item Number	*Description*
MH-1332-303-V	SS 303 Strait Fitting with Viton Seal, 10-32 Ext. Thd. and 1/8" ID Barb
QDC-101-I-DS-1810-303-V	Quick Disconnect Socket with 1/8" NPT Ext. Thd and Viton Seals, Double Shut-Off, SS303
QDC-101-I-1810-303-V	Quick Disconnect Socket with 1/8" NPT Ext. Thd and Viton Seals, SS303
QDC-102-E-1332	Quick Disconnect Plug with (1/8)" ID Barbed Tube Connection, SS 303

McMaster-Carr Supply:

Item Number	*Description*
6541K67	Straight-Jaw Pinch Clamp Pincer
5058K221	Aluminum Single-Barbed Tube Fittings Adapter for 1/8" Tube ID X 10-32 Unf Male, Silver
3861T81	Med-Pressure Anodized Alum Thread Pipe Fitting 1/8" Pipe Size, Hex Nipple, 31/32" Length
44705K382	Low-Pressure Aluminum Threaded Pipe Fitting 1/8" Pipe Size, Square Head Plug
92220A171	Alloy Steel Low Head Socket Cap Screw 10-32 Thread, 1/4" Length, Pack of 25 for $6.88
91771A122	18-8 SS Flat Head Phillips Machine Screw 4-40 Thread, 1-3/4" Length, Pack of 100 for $10.14
54105K34	Double Pinch SS Hose & Tube Clamp 13/64" to 9/32" Clamp Diameter Range, Pack of 25 for $8.86
9334T23	Antimicrobial Blue Polyethylene Tubing 1/8" ID, 1/4" OD, 1/16" Wall, 10 Foot Length for $13.10
5119K48	High-Temp Viton® Fluoroelastomer Tubing Soft, 1/8" ID, 3/8" OD, 1/8" Wall, Black. 5 Foot Length for $10.17
53175K82	Miniature Bolt Hose & Tube Clamp Galvanized Steel, 5/16" to 3/8" Clamp Dia Range, Pack of 10 for $9.01
91251A209	Black-Oxide Alloy Steel Socket Head Cap Screw 4-40 Thread, 1-1/8" Length, Pack of 25 for $7.50

93615A420	18-8 Stainless Steel Low Head Sckt Cap Screw 1/4"-20 Thread, 1" Length, Pack of 10 for $8.41
92510A067	Aluminum Unthreaded Round Spacer 1/4" OD, 13/16" Length, #6 Screw Size
91251A546	Black-Oxide Alloy Steel Socket Head Cap Screw 1/4"-20 Thread, 1-1/2" Length, Pack of 50 for $7.92
91251A110	Black-Oxide Alloy Steel Socket Head Cap Screw 4-40 Thread, 1/2" Length, Pack fo 100 for $7.85
62475K53	Hand-Operated Miniature Air Control Valve Manual Return, 4-Way, 10-32 Female Inlet, Toggle

The Manifold Center:

Item Number	*Description*
D 32-4	Double Row Manifold (4 Ports), Aluminum with 10-32 UNF Port and 1/8 NPT Inlet. Dimensions: 0.75” x 0.75”

FILTRATION PLATFORM

Beswick Engineering:

Item Number	*Description*
QDC-101-E-DS-2PM-V	Quick Disconnect Panel-Mount Plug with Double Shutt-Off, 10-32 Int. Thd and Viton Seals, SS303

McMaster-Carr:

Item Number	*Description*
5058K221	Aluminum Single-Barbed Tube Fittings Adapter for 1/8" Tube ID X 10-32 Unf Male, Silver
5454K67	Miniature Brass Tube Fitting Swivel Adapter for 1/8" NPT Male to 1/8" ID Hose, Pack of 5 for $9.62
44555K149	Brass Double-Barbed Vacuum Tube Fitting 90 Deg Elbow for 1/4" Tube X 1/8" NPTF Male Pipe
5670K86	Type 303 SS Multi-Barbed Tube Fitting Adapter for 1/4" Tube ID X 1/8" NPT Male Pipe
50785K113	Med-Pressure Brass Thrd Pipe Fitting 1/4" Pipe Size, Hex Socket Plug, 1/4" Hex
5085K21	Nickel-Plated Aluminum Manifold 3 Outlets, 1/4" NPT Inlet X 1/8" NPT Outlet
55425K31	High-Pressure Clear Tygon PVC Tubing 1/4" ID, 7/16" OD, 3/32" Wall Thickness, 5' Length Available
55485K52	Long-Flex-Life Clear Tygon PVC Tubing 1/8" ID, 1/4" OD, 1/16" Wall Thickness, 2' Length Available
53175K84	Miniature Bolt Hose & Tube Clamp Galvanized Steel, 3/8" to 29/64" Clamp Dia Range, Pack of 10 for &9.59
93615A420	18-8 Stainless Steel Low Head Sckt Cap Screw 1/4"-20 Thread, 1" Length, Pack of 10 for $8.41
92196A117	18-8 Stainless Steel Socket Head Cap Screw 4-40 Thread, 1-1/8" Length, Pack of 50 for $3.93

93310A106	Self-Locking Button Head Socket Cap Screw 18-8 Stainless Steel, 4-40 Thread, 1/4" Length, Pack of 50 for $11.50
93310A264	Self-Locking Button Head Socket Cap Screw 18-8 Stainless Steel, 10-32 Thread, 1/2" Length, Pack of 25 for $8.60
6718K72	Stainless Stl Industrial-Shape Hose Coupling Plug, for 1/4" Hose ID, 1/4 Coupling Size

Doig Corporation:

Item Number	*Description*
850-ADN	Miniature, Non-Relieving Pressure Regulator - 1/8" NPT Port, 0-100 psig
446-725-008	0-160 psi gauge, 1/8" NPT Back Mounted

Pneumayne Inc.:

Item Number	*Description*
C04240X	3-Way, 3-Position Miniature Toggle Valve, Panel Mount

SOLVENT RESERVOIR

Beswick Engineering:

Item Number	*Description*
QDC-101-E-DS-1810-V	Quick Disconnect Plug with 1/8" NPT Ext. Thd and Viton Seals, Double Shut-Off, SS303

McMaster-Carr:

Item Number	*Description*
55485K52	Long-Flex-Life Clear Tygon PVC Tubing 1/8" ID, 1/4" OD, 1/16" Wall Thickness, 2' Length Available
5454K67	Miniature Brass Tube Fitting Swivel Adapter for 1/8" NPT Male to 1/8" ID Hose, Pack of 5 for $9.62
5058K221	Aluminum Single-Barbed Tube Fittings Adapter for 1/8" Tube ID X 10-32 Unf Male, Silver
3861T81	Med-Pressure Anodized Alum Thread Pipe Fitting 1/8" Pipe Size, Hex Nipple, 31/32" Length
44705K382	Low-Pressure Aluminum Threaded Pipe Fitting 1/8" Pipe Size, Square Head Plug
92220A171	Alloy Steel Low Head Socket Cap Screw 10-32 Thread, 1/4" Length, Pack of 25 for $6.88

Mercer Gasket & Shim:

Item Number	*Description*
(0000000000)42545	Viton (75D-) Gasket Soft Ring, 1-1/4" OD x 3/4" ID x 1/16" Thick

Cate Machine and Welding:

Item Number	*Description*
N/A	Fabrication of Filtration Chamber v1.0, Pack of 20 for $1,620.00

N/A	Modification of Filtration Chamber v1.0 into Solvent Reservoir

The Mannifold Center:

Item Number	*Description*
D 32-4	Double Row Manifold (4 Ports), Aluminum with 10-32 UNF Port and 1/8 NPT Inlet. Dimensions: 0.75” x 0.75”

MISCELLANIOUS PARTS

Air Compressor Direct:

Item Number	*Description*
ACP4406	All-Power QuietZone® 4.6-Gallon Aluminum Twin Stack Air Compressor; Model Number ACP4406

Astro Pneumatic Tool Company:

Item Number	*Description*
N/A	Astro Pneumatic Model # 4550, Air Oprated Vibrational Paint Shaker

References Cited

Akiyama, K., Chikayama, E., Yuasa, H., Shimada, Y., Tohge, T., Shinozaki, K., et al. (2008). PRIMe: A web site that assembles tools for metabolomics and transcriptomics. *In Silico Biology, 8*(3-4), 339-345.

Asiago, V., Nagana Gowda, G., Zhang, S., Shanaiah, N., Clark, J., & Raftery, D. (2008). Use of EDTA to minimize ionic strength dependent frequency shifts in the ^{1}H NMR spectra of urine. *Metabolomics, 4*(4), 328-336.

Atsumi, S., Hanai, T., & Liao, J. C. (2008). Non-fermentative pathways for synthesis of branched-chain higher alcohols as biofuels. *Nature, 451*(7174), 86-89.

Beckonert, O., Keun, H. C., Ebbels, T. M. D., Bundy, J., Holmes, E., Lindon, J. C., et al. (2007). Metabolic profiling, metabolomic and metabonomic procedures for NMR spectroscopy of urine, plasma, serum and tissue extracts. *Nat.Protocols, 2*(11), 2692-2703.

Belle, J. E. L., Harris, N. G., Williams, S. R., & Bhakoo, K. K. (2002). A comparison of cell and tissue extraction techniques using high-resolution 1H-NMR spectroscopy. *NMR in Biomedicine, 15*(1), 37-44.

Bennett, B. D., Kimball, E. H., Gao, M., Osterhout, R., Van Dien, S.,J., & Rabinowitz, J. D. (2009). Absolute metabolite concentrations and implied enzyme active site occupancy in escherichia coli. *Nat Chem Biol, 5*(8), 593-599.

Bloch, F., Hansen, W. W., & Packard, M. (1946). The nuclear induction experiment. *Physical Review, 70*(7-8), 474-485.

Brey, W. W., Edison, A. S., Nast, R. E., Rocca, J. R., Saha, S., & Withers, R. S. (2006). Design, construction, and validation of a 1-mm triple-resonance high-temperature-superconducting probe for NMR. *Journal of Magnetic Resonance, 179*(2), 290-293.

Brynildsen, M. P., & Liao, J. C. (2009). An integrated network approach identifies the isobutanol response network of escherichia coli. *Molecular Systems Biology, 5*, 277.

Chae, Y. K., Kang, W., Kim, S. H., Joo, J. E., Han, J. K., & Hong, B. W. (2010). Metabolic profiling of urine samples from colorectal cancer patients before and after surgical treatment. *Journal of Korean Magnetic Resonance Society, 14*(1), 28-37.

Charlton, A., Allnutt, T., Holmes, S., Chisholm, J., Bean, S., Ellis, N., et al. (2004). NMR profiling of transgenic peas. *Plant Biotechnology Journal, 2*(1), 27-35.

Chignola, F., Mari, S., Stevens, T. J., Fogh, R. H., Mannella, V., Boucher, W., et al. (2011). The CCPN metabolomics project: A fast protocol for metabolite identification by 2D-NMR. *Bioinformatics, 27*(6), 885-886.

Chikayama, E., Sekiyama, Y., Okamoto, M., Nakanishi, Y., Tsuboi, Y., Akiyama, K., et al. (2010). Statistical indices for simultaneous large-scale metabolite detections for a single NMR spectrum. *Analytical Chemistry, 82*(5), 1653-1658.

Chong, W. P. K., Reddy, S. G., Yusufi, F. N. K., Lee, D., Wong, N. S. C., Heng, C. K., et al. (2010). Metabolomics-driven approach for the improvement of chinese hamster ovary cell growth: Overexpression of malate dehydrogenase II. *Journal of Biotechnology, 147*(2), 116-121.

Chylla, R. A., Hu, K., Ellinger, J. J., & Markley, J. L. (2011). Deconvolution of two-dimensional NMR spectra by fast maximum likelihood reconstruction: Application to quantitative metabolomics. *Analytical Chemistry, 83* , 4871-4880.

Cohen, L. (2012, 02/21). Xiao-ke: “Wasting and thirsting” disease and the TCM treatment of diabetes. *Decoded Science, http://www.decodedscience.com/xiao-ke-wasting-and-thirsting-disease-and-the-tcm-treatment-of-diabetes/10828*

Cui, Q., Lewis, I. A., Hegeman, A. D., Anderson, M. E., Li, J., Schulte, C. F., et al. (2008). Metabolite identification via the madison metabolomics consortium database. *Nat Biotech, 26*(2), 162-164.

Dang, L., White, D. W., Gross, S., Bennett, B. D., Bittinger, M. A., Driggers, E. M., et al. (2009). Cancer-associated IDH1 mutations produce 2-hydroxyglutarate. *Nature, 462*(7274), 739-744.

Delaglio, F., Grzesiek, S., Vuister, G. W., Zhu, G., Pfeifer, J., & Bax, A. (1995). NMRPipe: A multidimensional spectral processing system based on UNIX pipes. *Journal of Biomolecular NMR, 6*(3), 277-293.

DeSilva, M. A., Shanaiah, N., Nagana Gowda, G. A., Rosa-Pérez, K., Hanson, B. A., & Raftery, D. (2009). Application of 31P NMR spectroscopy and chemical derivatization for metabolite profiling of lipophilic compounds in human serum. *Magnetic Resonance in Chemistry, 47*, S74-S80.

Dombek, K. M., & Ingram, L. O. (1984). Effects of ethanol on the Escherichia coli plasma membrane. *Journal of Bacteriology, 157*(1), 233-239.

Ellis, D.,I., & Goodacre, R. (2012). Metabolomics-assisted synthetic biology. *Current Opinion in Biotechnology, 23*(1), 22-28.

Ellory, J. C., Preston, R. L., Osotimehin, B., & Young, J. D. (1983). Transport of amino acids for glutathione biosynthesis in human and dog red cells. *Biomedica Biochimica Acta, 42*(11-12), S48-52.

Fiehn, O. (2002). Metabolomics--the link between genotypes and phenotypes. *Plant Molecular Biology, 48*(1-2), 155-171.

Fincham, D. A., Mason, D. K., Paterson, J. Y., & Young, J. D. (1987). Heterogeneity of amino acid transport in horse erythrocytes: A detailed kinetic analysis of inherited transport variation. *The Journal of Physiology, 389*, 385-409.

Fukuda, S., Toh, H., Hase, K., Oshima, K., Nakanishi, Y., Yoshimura, K., et al. (2011). Bifidobacteria can protect from enteropathogenic infection through production of acetate. *Nature, 469*(7331), 543-547.

Gasko, O., & Danon, D. (1972). The metabolism of maturing reticulocytes. *British Journal of Haematology, 23*(5), 525-533.

Geier, F. M., Want, E. J., Leroi, A. M., & Bundy, J. G. (2011). Cross-platform comparison of caenorhabditis elegans tissue extraction strategies for comprehensive metabolome coverage. *Analytical Chemistry, 83*(10), 3730-3736.

Godejohann, M. (2007). Hydrophilic interaction chromatography coupled to nuclear magnetic resonance spectroscopy and mass spectroscopy–A new approach for the

separation and identification of extremely polar analytes in bodyfluids. *Journal of Chromatography A, 1156*(1), 87-93.

Gonzalez, R., Tao, H., Purvis, J. E., York, S. W., Shanmugam, K. T., & Ingram, L. O. (2003). Gene array-based identification of changes that contribute to ethanol tolerance in ethanologenic *escherichia coli*: Comparison of KO11 (parent) to LY01 (resistant mutant). *Biotechnology Progress, 19*(2), 612-623.

Griffith, O. W. (1981). Glutathione turnover in human erythrocytes. inhibition by buthionine sulfoximine and incorporation of glycine by exchange. *The Journal of Biological Chemistry, 256*(10), 4900-4904.

Grimes, J., & O'Connell, T. (2011). The application of micro-coil NMR probe technology to metabolomics of urine and serum. *Journal of Biomolecular NMR, 49*(3), 297-305.

Gromova, M., & Roby, C. (2010). Toward arabidopsis thaliana hydrophilic metabolome: Assessment of extraction methods and quantitative 1H NMR. *Physiologia Plantarum, 140*(2), 111-127.

Gronwald, W., Klein, M. S., Kaspar, H., Fagerer, S. R., Nürnberger, N., Dettmer, K., et al. (2008). Urinary metabolite quantification employing 2D NMR spectroscopy. *Analytical Chemistry, 80*(23), 9288-9297.

Hallows, W. C., Yu, W., Smith, B. C., Devires, M. K., Ellinger, J. J., Someya, S., et al. (2011). Sirt3 promotes the urea cycle and fatty acid oxidation during dietary restriction. *Molecular Cell, 41*(2), 139-149.

Hanai, T., Atsumi, S., & Liao, J. C. (2007). Engineered synthetic pathway for isopropanol production in escherichia coli. *Applied and Environmental Microbiology, 73*(24), 7814-7818.

Harvey, C. M., & Clive Ellory, J. (1989). Identification of amino acid transporters in the red blood cell. In Sidney Fleischer and Becca Fleischer (Ed.), *Methods in enzymology* (pp. 122-160) Academic Press.

Hasunuma, T., Sanda, T., Yamada, R., Yoshimura, K., Ishii, J., & Kondo, A. (2011). Metabolic pathway engineering based on metabolomics confers acetic and formic acid tolerance to a recombinant xylose-fermenting strain of saccharomyces cerevisiae. *Microbial Cell Factories, 10*(1), 2-2.

Hatch, M. D., & Heldt, H. W. (1985). Synthesis, storage, and stability of [4-14C]oxaloacetic acid. *Analytical Biochemistry, 145*(2), 393-397.

Hirayama, T., & Kikuchi, J. (2007). NMR-based metabomics approach: Top-down phenomics, metabolic flux analysis, insoluble metabolite analysis and stable isotope labeling in plant and animal systems. *PLANT AND CELL PHYSIOLOGY, 48*(Suppl. S), S258.

Hohmann, S. (2002). Osmotic stress signaling and osmoadaptation in yeasts. *Microbiology and Molecular Biology Reviews : MMBR, 66*(2), 300-372.

Hoult, D. I., Busby, S. J. W., Gadian, D. G., Radda, G. K., Richards, R. E., & Seeley, P. J. (1974). Observation of tissue metabolites using 31P nuclear magnetic resonance. *Nature, 252*, 285-287.

Hu, K., Ellinger, J. J., Chylla, R. A., & Markley, J. L. (2011). Measurement of absolute concentrations of individual compounds in metabolite mixtures by gradient-selective time-zero 1H–13C HSQC with two concentration references and fast maximum likelihood reconstruction analysis. *Anal.Chem., 83*(24), 9352-9360.

Hu, K., Westler, W. M., & Markley, J. L. (2011). Simultaneous quantification and identification of individual chemicals in metabolite mixtures by two-dimensional extrapolated time-zero 1H–13C HSQC (HSQC0). *J.Am.Chem.Soc., 133*(6), 1662-1665.

Ingram, L. O. (1990). Ethanol tolerance in bacteria. *Critical Reviews in Biotechnology, 9*(4), 305-319.

Karp, P. D., Riley, M., Saier, M., Paulsen, I. T., Collado-Vides, J., Paley, S. M., et al. (2002). The EcoCyc database. *Nucleic Acids Research, 30*(1), 56-58.

Knoshaug, E. P., & Zhang, M. (2009). Butanol tolerance in a selection of microorganisms. *Applied Biochemistry and Biotechnology, 153*(1-3), 13-20.

Lewis, G. D., Farrell, L., Wood, M. J., Martinovic, M., Arany, Z., Rowe, G. C., et al. (2010). Metabolic signatures of exercise in human plasma. *Science Translational Medicine, 2*(33), 1-13.

Lewis, I. A., Schommer, S. C., Hodis, B., Robb, K. A., Tonelli, M., Westler, W. M., et al. (2007). Method for determining molar concentrations of metabolites in complex solutions from two-dimensional (1)h-(13)c NMR spectra. *Analytical Chemistry, 79*(24), 9385-9390.

Lewis, I. A., Campanella, M. E., Markley, J. L., & Low, P. S. (2009). Role of band 3 in regulating metabolic flux of red blood cells. *Proceedings of the National Academy of Sciences,*

Lewis, I. A., Karsten, R. H., Norton, M. E., Tonelli, M., Westler, W. M., & Markley, J. L. (2010). NMR method for measuring carbon-13 isotopic enrichment of metabolites in complex solutions. *Analytical Chemistry, 82*(11), 4558-4563.

Lewis, I. A., Schommer, S. C., & Markley, J. L. (2009). rNMR: Open source software for identifying and quantifying metabolites in NMR spectra. *Magnetic Resonance in Chemistry, 47(S1),* S123-S126.

Lin, C., Wu, H., Tjeerdema, R., & Viant, M. (2007). Evaluation of metabolite extraction strategies from tissue samples using NMR metabolomics. *Metabolomics,* (1), 55-67.

Liu, S., & Qureshi, N. (2009). How microbes tolerate ethanol and butanol. *New Biotechnology, 26*(3-4), 117-121.

Lu, W., Clasquin, M. F., Melamud, E., Amador-Noguez, D., Caudy, A. A., & Rabinowitz, J. D. (2010). Metabolomic analysis via reversed-phase ion-pairing liquid chromatography coupled to a stand alone orbitrap mass spectrometer. *Analytical Chemistry, 82*(8), 3212-3221.

Ludwig, C., Ward, D. G., Martin, A., Viant, M. R., Ismail, T., Johnson, P. J., et al. (2009). Fast targeted multidimensional NMR metabolomics of colorectal cancer. *Magnetic Resonance in Chemistry, 47*, S68-S73; S68-S73.

Ludwig, C., & Günther, U.,L. (2011). MetaboLab - advanced NMR data processing and analysis for metabolomics. *BMC Bioinformatics, 12*, 366-366.

Lundberg, P., Vogel, T., Malusek, A., Lundquist, P., Cohen, L., & Dahlvqist, O. (2005). MDL - the magnetic resonance metabolomics database (mdl.imv.liu.se). *ESMRMB, Basel, Switzerland,*

Maede, Y., Inaba, M., & Taniguchi, N. (1983). Increase of na-K-ATPase activity, glutamate, and aspartate uptake in dog erythrocytes associated with hereditary high accumulation of GSH, glutamate, glutamine, and aspartate. *Blood, 61*(3), 493-499.

Majerus, P. W., Brauner, M. J., Smith, M. B., & Minnich, V. (1971). Glutathione synthesis in human erythrocytes. II. purification and properties of the enzymes of glutathione biosynthesis. *The Journal of Clinical Investigation, 50*(8), 1637-1643.

Manuel y Keenoy, B., Conget, I., Liemans, V., Malaisse-Lagae, F., Sener, A., & Malaisse, W. J. (1991). Generation of 3HOH from D-[6-3H]glucose by erythrocytes: Role of pyruvate alanine interconversion. *Biochemical Medicine and Metabolic Biology, 46*(1), 59-74.

Markley, J. L., Anderson, M. E., Cui, Q., Eghbalnia, H. R., Lewis, I. A., Hegeman, A. D., et al. (2007). New bioinformatics resources for metabolomics. *Pacific Symposium on Biocomputing,* 157-168.

Massou, S., Nicolas, C., Letisse, F., & Portais, J. (2007a). Application of 2D-TOCSY NMR to the measurement of specific 13C-enrichments in complex mixtures of 13C-labeled metabolites. *Metabolic Engineering, 9*(3), 252-257.

Massou, S., Nicolas, C., Letisse, F., & Portais, J. (2007b). NMR-based fluxomics: Quantitative 2D NMR methods for isotopomers analysis. *Phytochemistry, 68*(16), 2330-2340.

Mercier, P., Lewis, M., Chang, D., Baker, D., & Wishart, D. (2011). Towards automatic metabolomic profiling of high-resolution one-dimensional proton NMR spectra. *Journal of Biomolecular NMR,* (3), 307-323.

Minnich, V., Smith, M. B., Brauner, M. J., & Majerus, P. W. (1971). Glutathione biosynthesis in human erythrocytes. I. identification of the enzymes of glutathione synthesis in hemolysates. *The Journal of Clinical Investigation, 50*(3), 507-513.

Morris, C. R., Suh, J. H., Hagar, W., Larkin, S., Bland, D. A., Steinberg, M. H., et al. (2008). Erythrocyte glutamine depletion, altered redox environment, and pulmonary hypertension in sickle cell disease. *Blood, 111*(1), 402-410.

Nakanishi, Y., Fukuda, S., Chikayama, E., Kimura, Y., Ohno, H., & Kikuchi, J. (2010). Dynamic omics approach identifies nutrition-mediated microbial interactions. *J.Proteome Res., 10*(2), 824-836.

Newgard, C. B., An, J., Bain, J. R., Muehlbauer, M. J., Stevens, R. D., Lien, L. F., et al. (2009). A branched-chain amino acid-related metabolic signature that differentiates obese and lean humans and contributes to insulin resistance. *Cell Metabolism, 9*(4), 311-326.

Newgard, C. (2012). Interplay between lipids and branched-chain amino acids in development of insulin resistance. *Cell Metabolism, 15*(5), 606-614.

Nichter, M. (1981). Negotiation of the illness experience: Ayurvedic therapy and the psychosocial dimension of illness. *Culture, Medicine and Psychiatry, 5*(1), 5-24.

Niihara, Y., Zerez, C. R., Akiyama, D. S., & Tanaka, K. R. (1997). Increased red cell glutamine availability in sickle cell anemia: Demonstration of increased active transport, affinity, and increased glutamate level in intact red cells. *The Journal of Laboratory and Clinical Medicine, 130*(1), 83-90.

Oliver, S. G., Winson, M. K., Kell, D. B., & Baganz, F. (1998). Systematic functional analysis of the yeast genome. *Trends in Biotechnology, 16*(9), 373-378.

Olson, D. L., Norcross, J. A., O'Neil-Johnson, M., Molitor, P. F., Detlefsen, D. J., Wilson, A. G., et al. (2004). Microflow NMR: concepts and capabilities. *Anal.Chem., 76*(10), 2966-2974.

Pan, Z., & Raftery, D. (2007). *Comparing and combining NMR spectroscopy and mass spectrometry in metabolomics. Analytical and Bioanalytical Chemistry, 387(2)*, 525-527.

Patti, G. J., Shriver, L. P., Wassif, C. A., Woo, H., Uritboonthai, W., Apon, J., et al. (2010). Nanostructure-initiator mass spectrometry (NIMS) imaging of brain cholesterol metabolites in smith-lemli-opitz syndrome. *Neuroscience, 170*(3), 858-864.

Patti, G. J., Yanes, O., & Siuzdak, G. (2012). Innovation: Metabolomics: The apogee of the omics trilogy. *Nature Reviews Molecular Cell Biology, 13*(4), 263-269.

Pauling, L., Robinson, A. B., Teranishi, R., & Cary, P. (1971). Quantitative analysis of urine vapor and breath by gas-liquid partition chromatography. *Proceedings of the National Academy of Sciences, 68*(10), 2374-2376.

Purcell, E. M., Torrey, H. C., & Pound, R. V. (1946). Resonance absorption by nuclear magnetic moments in a solid. *Physical Review, 69*(1-2), 37-38.

Rabi, I. I., Zacharias, J. R., Millman, S., & Kusch, P. (1938). A new method of measuring nuclear magnetic moment. *Physical Review, 53*(4), 318-318.

Rabinowitz, J. D., & Kimball, E. (2007). Acidic acetonitrile for cellular metabolome extraction from escherichia coli. *Analytical Chemistry, 79*(16), 6167-6173.

Rai, R. K., Tripathi, P., & Sinha, N. (2009). Quantification of metabolites from two-dimensional nuclear magnetic resonance spectroscopy: Application to human urine samples. *Anal.Chem., 81*(24), 10232-10238.

Robinette, S. L., Zhang, F., Bruschweiler-Li, L., & Bruschweiler, R. (2008). Web server based complex mixture analysis by NMR. *Analytical Chemistry, 80*(10), 3606-3611.

Robinette, S. L., Ajredini, R., Rasheed, H., Zeinomar, A., Schroeder, F. C., Dossey, A. T., et al. (2011). Hierarchical alignment and full resolution pattern recognition of 2D NMR spectra: Application to nematode chemical ecology. *Anal.Chem., 83*(5), 1649-1657.

Rod, M. L., Alam, K. Y., Cunningham, P. R., & Clark, D. P. (1988). Accumulation of trehalose by escherichia coli K-12 at high osmotic pressure depends on the presence of amber suppressors. *Journal of Bacteriology, 170*(8), 3601-3610.

Römisch-Margl, W., Prehn, C., Bogumil, R., Röhring, C., Suhre, K., & Adamski, J. (2011). Procedure for tissue sample preparation and metabolite extraction for high-throughput targeted metabolomics. *Metabolomics,* (1), 133-142.

Rutherford, B. J., Dahl, R. H., Price, R. E., Szmidt, H. L., Benke, P. I., Mukhopadhyay, A., et al. (2010). Functional genomic study of exogenous n-butanol stress in escherichia coli. *Applied and Environmental Microbiology, 76*(6), 1935-1945.

Salehpour, M., Possnert, G., & Bryhni, H. (2008). Subattomole sensitivity in biological accelerator mass spectrometry. *Anal.Chem., 80*(10), 3515-3521.

Sass, M. D. (1968). Glutathione synthesis in cell-free preparations from erythrocytes of different ages. *Clinica Chimica Acta; International Journal of Clinical Chemistry, 22*(2), 207-210.

Sekiyama, Y., Chikayama, E., & Kikuchi, J. (2011). Evaluation of a semipolar solvent system as a step toward heteronuclear multidimensional NMR-based metabolomics for 13C-labeled bacteria, plants, and animals. *Analytical Chemistry, 83*(3), 719-726.

Shanaiah, N., Desilva, M. A., Gowda, N., A, G., Raftery, M. A., Hainline, B. E., et al. (2007). Class selection of amino acid metabolites in body fluids using chemical derivatization and their enhanced 13C NMR. *Proceedings of the National Academy of Sciences, 104*(28), 11540-11544.

Shen, C. R., & Liao, J. C. (2008). Metabolic engineering of escherichia coli for 1-butanol and 1-propanol production via the keto-acid pathways. *Metabolic Engineering, 10*(6), 312-320.

Sobolev, A. P., Brosio, E., Gianferri, R., & Segre, A. L. (2005). Metabolic profile of lettuce leaves by high-field NMR spectra. *Magnetic Resonance in Chemistry, 43*(8), 625-638.

Srikanthamurthy, K. R. (1983). *Clinical methods in Āyurveda*. Varanasi: Chaukhambha Orientalia.

Steinbeck, C., Krause, S., & Kuhn, S. (2003). NMRShiftDBConstructing a free chemical information system with open-source components. *J.Chem.Inf.Comput.Sci., 43*(6), 1733-1739.

Tang, H., Xiao, C., & Wang, Y. (2009). Important roles of the hyphenated HPLC-DAD-MS-SPE-NMR technique in metabonomics. *Magnetic Resonance in Chemistry, 47*, S157-S162; S157-S162.

Teymouri, F., Laureano-Pérez, L., Alizadeh, H., & Dale, B. (2004). Ammonia fiber explosion treatment of corn stover. *Applied Biochemistry and Biotechnology, 115*(1), 951-963.

Tiziani, S., Emwas, A., Lodi, A., Ludwig, C., Bunce, C. M., Viant, M. R., et al. (2008). Optimized metabolite extraction from blood serum for 1H nuclear magnetic resonance spectroscopy. *Analytical Biochemistry, 377*(1), 16-23.

Tulpan, D., Léger, S., Belliveau, L., Culf, A., & Čuperlović-Culf, M. (2011). MetaboHunter: An automatic approach for identification of metabolites from 1H-NMR spectra of complex mixtures. *BMC Bioinformatics, 12*, 400-400.

Verwaest, K. A., Vu, T. N., Laukens, K., Clemens, L. E., Nguyen, H. P., Van Gasse, B., et al. (2011). 1H NMR based metabolomics of CSF and blood serum: A metabolic profile for a transgenic rat model of huntington disease. *Biochimica Et Biophysica Acta (BBA) - Molecular Basis of Disease, 1812*(11), 1371-1379.

Vollherbst-Schneck, K., Sands, J. A., & Montenecourt, B. S. (1984). Effect of butanol on lipid composition and fluidity of clostridium acetobutylicum ATCC 824. *Applied and Environmental Microbiology, 47*(1), 193-194.

Wang, T., Shao, K., Chu, Q., Ren, Y., Mu, Y., Qu, L., et al. (2009). Automics: An integrated platform for NMR-based metabonomics spectral processing and data analysis. *BMC Bioinformatics, 10*, 83-83.

Wang, T. J., Larson, M. G., Vasan, R. S., Cheng, S., Rhee, E. P., McCabe, E., et al. (2011). Metabolite profiles and the risk of developing diabetes. *Nature Medicine, 17*(4), 448-453.

Ward, J., Baker, J., Miller, S., Deborde, C., Maucourt, M., Biais, B., et al. (2010). An inter-laboratory comparison demonstrates that [^{1}H]-NMR metabolite fingerprinting is a robust technique for collaborative plant metabolomic data collection. *Metabolomics,* (2), 263-273.

Ward, P. S., Patel, J., Wise, D. R., Abdel-Wahab, O., Bennett, B. D., Coller, H. A., et al. (2010). The common feature of leukemia-associated IDH1 and IDH2 mutations is a neomorphic enzyme activity converting α-ketoglutarate to 2-hydroxyglutarate. *Cancer Cell, 17*(3), 225-234.

Weckwerth, W. *Metabolomics: Methods and Protocols (Methods in Molecular Biology),* 1st ed.; Humana Press: New Jersey, 2006; pp 233-235.

Weiger, M., Speck, T., & Fey, M. (2006). Gradient shimming with spectrum optimisation. *Journal of Magnetic Resonance, 182*(1), 38-48.

Weljie, A. M., Newton, J., Mercier, P., Carlson, E., & Slupsky, C. M. (2006). Targeted profiling: Quantitative analysis of 1H NMR metabolomics data. *Analytical Chemistry, 78*(13), 4430-4442.

Winter, C. G., & Christensen, H. N. (1964). Migration of amino acids across the membrane of the human erythrocyte. *The Journal of Biological Chemistry, 239*, 872-878.

Wishart, D. S., Tzur, D., Knox, C., Eisner, R., Guo, A. C., Young, N., et al. (2007). HMDB: The human metabolome database. *Nucleic Acids Research, 35*(Database issue), D521-6.

Wu, G., Fang, Y. Z., Yang, S., Lupton, J. R., & Turner, N. D. (2004). Glutathione metabolism and its implications for health. *The Journal of Nutrition, 134*(3), 489-492.

Wu, H., Southam, A. D., Hines, A., & Viant, M. R. (2008). High-throughput tissue extraction protocol for NMR- and MS-based metabolomics. *Analytical Biochemistry, 372*(2), 204-212.

Wu, J., An, Y., Yao, J., Wang, Y., & Tang, H. (2010). An optimised sample preparation method for NMR-based faecal metabonomic analysis. *Analyst, 135*(5), 1023-1030.

Xia, J., Bjorndahl, T. C., Tang, P., & Wishart, D. S. (2008). MetaboMiner--semi-automated identification of metabolites from 2D NMR spectra of complex biofluids. *BMC Bioinformatics, 9*, 507.

Xia, J., Psychogios, N., Young, N., & Wishart, D. S. (2009). MetaboAnalyst: A web server for metabolomic data analysis and interpretation. *Nucleic Acids Research, 37*, W652-W660; W652-W660.

Xia, J., Mandal, R., Sinelnikov, I. V., Broadhurst, D., & Wishart, D. S. (2012). MetaboAnalyst 2.0–a comprehensive server for metabolomic data analysis. *Nucleic Acids Research,*

Ye, T., Mo, H., Shanaiah, N., Gowda, G. A. N., Zhang, S., & Raftery, D. (2009). Chemoselective 15N tag for sensitive and high-resolution nuclear magnetic resonance profiling of the carboxyl-containing metabolome. *Anal.Chem., 81*(12), 4882-4888.

Ye, T., Zhang, S., Mo, H., Tayyari, F., Gowda, G. A. N., & Raftery, D. (2010). 13C-formylation for improved nuclear magnetic resonance profiling of amino metabolites in biofluids. *Anal.Chem., 82*(6), 2303-2309.

Ye, T., Zheng, C., Zhang, S., Gowda, G. A. N., Vitek, O., & Raftery, D. (2011). “Add to subtract”: A simple method to remove complex background signals from the 1H nuclear magnetic resonance spectra of mixtures. *Anal.Chem., 84*(2), 994-1002.

Young, D. J., Wolowyk, M. W., Fincham, D. A., Cheeseman, C. I., Rabenstein, D. L., & Ellory, J. C. (1987). Conflicting evidence regarding the transport of alpha-glutamyl-dipeptides by human erythrocytes. *The Biochemical Journal, 242*(1), 309-311.

Young, J. D., Wolowyk, M. W., Jones, S. M., & Ellory, J. C. (1983). Red-cell amino acid transport. evidence for the presence of system ASC in mature human red blood cells. *The Biochemical Journal, 216*(2), 349-357.

Zhang, F., Dossey, A. T., Zachariah, C., Edison, A. S., & Bruschweiler, R. (2007). Strategy for automated analysis of dynamic metabolic mixtures by NMR. application to an insect venom. *Analytical Chemistry, 79*(20), 7748-7752.

Zhou, J., Ma, Q., Yi, H., Wang, L., Song, H., & Yuan, Y. (2011). Metabolome profiling reveals metabolic cooperation between bacillus megaterium and ketogulonicigenium vulgare during induced swarm motility. *Applied and Environmental Microbiology, 77*(19), 7023-7030.